Holographic reflected entropy and islands in interface CFTs

Jaydeep Kumar Basak [iD],[a,b] **Debarshi Basu** [iD],[c] **Vinay Malvimat** [iD],[d]
Himanshu Parihar [iD][e,f] **and Gautam Sengupta** [iD][c]

[a]*Department of Physics, National Sun Yat-Sen University,*
 Kaohsiung 80424, Taiwan
[b]*Center for Theoretical and Computational Physics,*
 Kaohsiung 80424, Taiwan
[c]*Department of Physics, Indian Institute of Technology Kanpur,*
 Kanpur 208016, India
[d]*Asia Pacific Center for Theoretical Physics,*
 77 Cheongam-ro, Nam-gu, Pohang-si, Gyeongsangbuk-do 37673, Korea
[e]*Center of Theory and Computation, National Tsing-Hua University,*
 Hsinchu 30013, Taiwan
[f]*Physics Division, National Center for Theoretical Sciences,*
 Taipei 10617, Taiwan
 E-mail: jkb.hep@gmail.com, debarshi@iitk.ac.in, vinay.malvimat@apctp.org,
 himansp@phys.ncts.ntu.edu.tw, sengupta@iitk.ac.in

ABSTRACT: We investigate the reflected entropy for various mixed state configurations in the two dimensional holographic conformal field theories sharing a common interface (ICFTs). In the $AdS_3/ICFT_2$ framework, we compute the holographic reflected entropy for the required configurations in the vacuum state of the $ICFT_2$ which is given by twice the entanglement wedge cross section (EWCS) in a spacetime involving two AdS_3 geometries glued along a thin interface brane. Subsequently, we evaluate the EWCS in the bulk geometry involving eternal BTZ black strings with an AdS_2 interface brane, which is dual to an $ICFT_2$ in the thermofield double (TFD) state. We explore the system from a doubly holographic perspective and determine the island contributions to the reflected entropy in the two dimensional semi-classical description involving two CFT_2s coupled to an AdS_2 brane. We demonstrate that the results from the island formula match precisely with the bulk AdS_3 results in the large tension limit of the interface brane. We illustrate that the phase structure of the reflected entropy is quite rich involving many novel induced island phases and demonstrate that it obeys the expected Page curve for the reflected entropy in a radiation bath coupled to the AdS_2 black hole.

Contents

1 Introduction

In recent years, the measure of entanglement entropy has been central to a novel resolution of the black hole information loss puzzle. This new resolution involves the appearance of certain regions termed "islands" in the late time entanglement wedge of a bath collecting the Hawking radiation. This in turn results in a particular formula to obtain the fine grained entropy of the bath by including the contributions from the island regions [1–5]. Furthermore, it has been demonstrated that the island formula leads to the expected Page curve for the entanglement entropy of the bath/radiation subsystem and hence indicates towards the unitarity of black hole evaporation process. The island formula has been demonstrated to naturally arise in the context of doubly holographic models and the holographic duals of conformal field theories with boundaries (AdS/BCFT scenarios) in certain limits. This AdS/BCFT construction involves a d-dimensional strongly coupled conformal field theory with a boundary (BCFT$_d$) which is dual to a bulk AdS$_{d+1}$ spacetime truncated by an end of the world (EOW) brane [6, 7]. The holographic entanglement entropy in the AdS/BCFT scenario was demonstrated to naturally contain the island contributions whenever the RT surfaces end on the EOW brane [8–19].

Another interesting related system consists of two conformal field theories that share a common boundary. If the boundary is also conformally invariant then such a quantum system is termed as Interface Conformal Field Theory (ICFT). Furthermore, as described in [20] the holographic dual of such a two dimensional ICFT is described by two AdS$_3$ geometries sharing a common AdS$_2$ brane at which the Israel junction conditions are satisfied. Considering the bulk to be semi-classical, it is possible to describe the above model in a two dimensional effective field theory picture.

Furthermore, the ratio of central charges of the two CFTs plays a crucial role, and in the limit in which the ratio vanishes, the ICFT reduces to a BCFT.[1] In [20], the authors determined the entanglement entropy of a subsystem described by two semi-infinite intervals (one in each CFT) of such a holographic ICFT$_2$. They obtained the entanglement entropy by computing the length of the appropriate geodesics in the bulk AdS$_3$ geometry and demonstrated that there are various novel phases, such as the one in which the geodesic double crosses the bulk interface and is partially in both the AdS$_3$ geometries. Following this, the authors also obtained the entanglement entropy in the semi-classical picture in two dimensions using the island formalism. In the large tension limit, the results from the 3d bulk computation and the 2d computation from the island formula match precisely.

Furthermore, the entanglement entropy of the semi-infinite intervals in a holographic ICFT in the thermo-field double state obeys the expected Page curve in the context of a 2d black hole on the AdS$_2$ brane induced by an eternal black hole in AdS$_3$. An intriguing feature of this construction involves RT surfaces which cross the interface AdS$_2$ brane and return to the original AdS$_3$ geometry. These RT surfaces unique to the AdS/ICFT correspondence were demonstrated to be derived from novel replica wormhole saddles for the entanglement entropy which results in what are known as *induced islands* in one of the CFT$_2$ [21].

In the context of the above mentioned AdS/ICFT correspondence, it would be quite interesting to probe further aspects of entanglement and correlations in ICFTs through various other measures described in quantum information theory. An interesting measure in this regard is the reflected entropy which characterizes the correlations between subsystems in holographic quantum theories.[2] This quantity, introduced in [26], is holographically dual to the cross-section of the entanglement wedge (EWCS) in the dual bulk AdS geometry. Furthermore, the difference between the reflected entropy and the mutual information known as the Markov gap is expected to contain information about tripartite entanglement in the system [27–29]. Hence, this measure is crucial to understanding the deeper entanglement structure of holographic quantum systems especially in the context of black hole information loss paradox. The island contributions to the reflected entropy and the Markov gap have been studied in various interesting scenarios [30–33]. In the present article, we compute the holographic reflected entropy for various mixed state configurations involving adjacent and disjoint intervals in

---

[1]Note that if the ICFT itself is holographic both the central charges are large c$_I$, c$_{II}$. In this scenario, the BCFT limit is defined by considering c$_I$ ≪ c$_{II}$ or vice versa such that the ratio goes to zero.

[2]Recently in [22, 23] it was shown that the reflected entropy for certain states does not obey a desired property for any correlation measure which is the monotonicity under partial trace. However, for holographic states, it has been demonstrated to obey the above mentioned property through the entanglement wedge nesting of the dual EWCS [24–26]. So although it might not serve as a correlation measure for generic quantum systems, it is still useful to characterize correlations between subsystems in the context of holography.

the vacuum and the TFD state of an $ICFT_2$.[3] Furthermore, we will also compute the island contributions to the reflected entropies of the above mentioned configurations in the two dimensional semi-classical effective field theory picture and demonstrate that the results obtained match exactly with the corresponding bulk computation in the large tension limit of the interface brane. We will demonstrate that the phase structure of reflected entropy is much richer than that of the entanglement entropy of the corresponding subsystems. Quite interestingly, we will see that in the 3d bulk geometry whenever the RT surfaces cross the interface brane to the second side and then return back to the original AdS_3 geometry it leads to induced reflected entropy islands for one of the CFT, similar to the induced entanglement entropy islands resulting from the novel saddles mentioned earlier. In the two dimensional effective theory, we will show that these induced reflected entropy islands always correspond to certain asymetric factorizations of the twist correlation functions. Finally, for the configurations involving the TFD state we determine the analogues of the Page curves for the reflected entropy of the bath coupled to the AdS_2 black hole induced by the eternal black hole in the three dimensional bulk.

The paper is organized as follows: in section 2.1 we present a short review of the holographic $ICFT_2$ model considered in this article. Following this, in section 3 we compute the holographic reflected entropy for the adjacent and disjoint intervals in the vacuum state of an $ICFT_2$ by determining the entanglement wedge cross section (EWCS) in the dual bulk pure AdS_3 geometries glued at the interface. Subsequently, in section 4 we obtain the reflected entropy of various configurations explained above in effective two dimensional island perspective and demonstrate that the results from the bulk and the island formulation match precisely in the large brane tension limit. In section 5 we compute the holographic reflected entropy of adjacent intervals by analyzing the EWCS in the geometry involving two eternal black hole geometries sharing an AdS_2 brane dual to the TFD state of an ICFT. Subsequently we obtain the analogues of the Page curves of the reflected entropy for mixed states in the bath collecting the Hawking radiation from the AdS_2 black hole. Furthermore, in section 6 we determine the island contributions for the reflected entropy of the above mentioned subsystems which match exactly with the results from the bulk computations in the large brane tension limit. Finally in section 7 we summarize and present our conclusions.

2 Review of earlier literature

2.1 Holographic $ICFT_2$

As described in [20], the vacuum state of an interface CFT_2 ($ICFT_2$) is dual to two pure AdS_3 geometries that are smoothly glued along a thin interface brane (figure 1). Here we briefly review the details of the bulk AdS_3 geometry. The bulk action in this scenario is given by

$$I = \frac{1}{16\pi G_N} \left[\int_{\mathcal{B}_I} d^3x \sqrt{-g_I} \left(R_I + \frac{2}{L_I^2} \right) + \int_{\mathcal{B}_{II}} d^3x \sqrt{-g_{II}} \left(R_{II} + \frac{2}{L_{II}^2} \right) \right]$$
$$+ \frac{1}{8\pi G_N} \left[\int_\Sigma d^2y \sqrt{-h} \left(K_I - K_{II} \right) - T \int_\Sigma d^2y \sqrt{-h} \right] \tag{2.1}$$

---

[3]Note that recently reflected entropy of various configurations has been investigated for interface CFTs in a slightly different context in [34, 35].
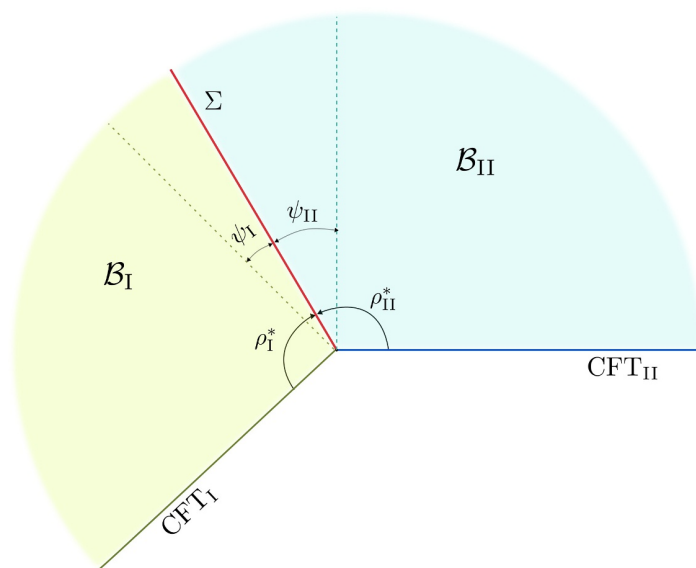
Figure 1. Holographic dual of an interface CFT$_2$. Figure modified from [20].

where G_N corresponds to the AdS$_3$ Newton's constant, $\mathcal{B}_{I,II}$ denote the bulk AdS$_3$ geometries and Σ denotes the EOW brane with tension T. Note that in the above equation g$_{I,II}$ are the metric determinants of the two AdS$_3^{I,II}$ geometries with AdS length scales given by L$_{I,II}$ and R$_{I,II}$ are the corresponding Ricci scalars. The determinant of the induced metric on the interface brane is denoted by h and K$_{I,II}$ correspond to the extrinsic curvature on either side of the brane. The two AdS$_3$ geometries have to be joined smoothly at the interface. This is imposed through the standard Israel junction conditions given by

$$(K_{I,ab} - K_{II,ab}) - h_{ab}(K_I - K_{II}) = -T\, h_{ab}. \tag{2.2}$$

The second Israel junction condition ensures that the metric h_{ab} on the interface brane induced from the two AdS$_3$ geometries to be the same. The AdS$_3$ geometries on either side may be expressed as foliation of AdS$_2$ metrics as described below

$$ds^2_{\mathcal{B}_i} = d\rho_i^2 + L_i^2 \cosh^2\left(\frac{\rho_i}{L_i}\right)\left(\frac{dy_i^2 + d\tau_i^2}{y_i^2}\right), \qquad i = I, II. \tag{2.3}$$

It may then be shown that the locations of the brane $\rho_{I,II}^*$ in the two geometries, are related to the tension by the junction condition (2.2) as follows [20]

$$\tanh\left(\frac{\rho_I^*}{L_I}\right) = \frac{L_I}{2T}\left(T^2 + \frac{1}{L_I^2} - \frac{1}{L_{II}^2}\right), \qquad \tanh\left(\frac{\rho_{II}^*}{L_{II}}\right) = \frac{L_{II}}{2T}\left(T^2 + \frac{1}{L_{II}^2} - \frac{1}{L_I^2}\right). \tag{2.4}$$

From the above expression, it is clear that the tension is bounded from above and below,

$$T_{min} = \left|\frac{1}{L_I} - \frac{1}{L_{II}}\right| < T < \frac{1}{L_I} + \frac{1}{L_{II}} = T_{max}. \tag{2.5}$$

The brane location $\rho_{I,II}^*$ may alternatively be parametrized through the (trigonometric) angles made by the brane with the verticals to the two boundaries as

$$\sin\psi_{I,II} = \tanh\left(\frac{\rho_{I,II}^*}{L_{I,II}}\right). \tag{2.6}$$

As described in [20], the holographic dual of the bulk geometry described above is given by two CFT₂s (referred to as CFT$_\text{I}$ and CFT$_\text{II}$ henceforth) with large central charges $c_\text{I,II} \gg 1$, interacting via a quantum dot (holographically dual to the gravity theory on brane). The central charges are related to the bulk Newton's constant via the standard Brown Henneaux formula [36]

$$c_i = \frac{3 L_i}{2 G_\text{N}}, \qquad i = \text{I}, \text{II}. \tag{2.7}$$

Remarkably, in the limit of a large tension the EOW brane is pushed towards the asymptotic boundary and one may obtain an effective intermediate picture by integrating out the bulk degrees of freedom [20]. In such an effective picture, two non-gravitating CFT reservoirs are coupled to a gravitating theory on the brane and the entanglement entropy of a subsystem is described by the island formalism. The large tension limit discussed above is significant because it is in this limit the holographic entanglement entropy of any subsystem computed from the bulk geometry precisely matches with the corresponding result obtained from the island formula in the two dimensional effective field theory involving two CFTs coupled to the brane. In order to take the large tension limit of the brane appropriately, T is parametrized by δ as described below

$$T^2 = \frac{1}{L_\text{I}^2} + \frac{1}{L_\text{II}^2} + \frac{2 - \delta^2}{L_\text{I} L_\text{II}}. \tag{2.8}$$

It is clear from the above expression that the limit $\delta \to 0$ the tension is maximum $T \to T_\text{max}$. In this limit, the angles $\psi_\text{I,II}$ may be expanded as [20]

$$\psi_\text{I} = \frac{\pi}{2} - \frac{L_\text{I}}{L_\text{I} + L_\text{II}} \delta + \mathcal{O}\left(\delta^2\right), \qquad \psi_\text{II} = \frac{\pi}{2} - \frac{L_\text{II}}{L_\text{I} + L_\text{II}} \delta + \mathcal{O}\left(\delta^2\right). \tag{2.9}$$

2.2 Reflected entropy

In this subsection, we provide a brief review the mixed state entanglement measure known as the reflected entropy which involves both classical and quantum correlations [26]. To this end it is required to consider a bipartite quantum system $A \cup B$ in a mixed state ρ_{AB} and its *canonical* purification $|\sqrt{\rho_{AB}}\rangle$ in a doubled Hilbert space $\mathcal{H}_A \otimes \mathcal{H}_B \otimes \mathcal{H}_{A^\star} \otimes \mathcal{H}_{B^\star}$, where $A^\star$ and $B^\star$ represent the CPT conjugates of the subsystems A and B respectively [37, 38]. The reflected entropy $S_R(A : B)$ between the two parties may then be defined as the von Neumann entropy of the reduced density matrix $\rho_{AA^\star} = \text{Tr}_{\mathcal{H}_B \otimes \mathcal{H}_B^\star} |\sqrt{\rho_{AB}}\rangle \langle \sqrt{\rho_{AB}}|$ [26] as follows

$$S_R(A : B) \equiv S_{vN}(\rho_{AA^\star})_{\sqrt{\rho_{AB}}}. \tag{2.10}$$

It satisfies several interesting properties including suitable upper and lower bounds, monogamy, polygamy while the monotonicity property holds only in certain (holographic) states. Furthermore, in separable states involving classical mixtures, the reflected entropy reduces to the *Shannon entropy* indicating its affinity towards classical correlations.

Interestingly the authors in [26] developed a novel replica technique to compute the reflected entropy between two subsystems A and B which we briefly review below. To begin with, one constructs the state $|\rho_{AB}^{m/2}\rangle \equiv |\psi_m\rangle$ as the canonical purification of the state ρ_{AB}^m

by considering an m-fold replication of the original manifold where $m \in 2\mathbb{Z}^+$. Subsequently the Rényi reflected entropy for this state $|\psi_m\rangle$ is obtained as the Rényi entropy $S_n (AA^\star)_{\psi_m}$ of the reduced density matrix

$$\rho_{AA^\star}^{(m)} = \mathrm{Tr}_{\mathcal{H}_B \otimes \mathcal{H}_B^\star} |\rho_{AB}^{m/2}\rangle \langle \rho_{AB}^{m/2}|, \tag{2.11}$$

which involves yet another replication in the Rényi index n and results in a nm-sheeted replica manifold.[4] Similar to the case of EE, one introduces branch cuts $A(\mu,\nu)^\pm$ and $B(\mu,\nu)^\pm$ on each replica labeled by $(\mu,\nu) \in \mathbb{Z}_m \times \mathbb{Z}_n$, where the $\pm$ denotes the bra and kets of ρ_{AB}. These branch cuts are subsequently sewed under certain elements g_A and g_B of the group $\mathcal{S}_{mn}$ preserving the replica permutation symmetry. The actions of the permutation group elements are as follows [26, 30]

$$\begin{aligned} g_A: & \quad (\mu,\nu) \to (\mu+1, \nu + \delta_{\mu,m/2-1} - \delta_{\mu,m-1}), \\ g_B: & \quad (\mu,\nu) \to (\mu+1, \nu). \end{aligned} \tag{2.12}$$

The Rényi reflected entropy is then given in terms of a properly weighted partition function $Z_{n,m}$ on the above replica manifold which may, in turn, be obtained as the correlation functions of twist operators[5] σ_{g_A} and σ_{g_B} inserted at the endpoints of the subsystems $A \equiv [z_1, z_2]$ and $B \equiv [z_3, z_4]$ in the orbifold theory $\mathrm{CFT}^{\otimes mn}/\mathcal{S}_{mn}$ (obtained via quotienting by the replica symmetry group $\mathcal{S}_{mn}$) as follows [26]

$$\begin{aligned} S_n (AA^\star)_{\psi_m} &= \frac{1}{1-n} \log \frac{Z_{n,m}}{(Z_{1,m})^n} \\ &= \frac{1}{1-n} \log \frac{\left\langle \sigma_{g_A}(z_1) \sigma_{g_A^{-1}}(z_2) \sigma_{g_B}(z_3) \sigma_{g_B^{-1}}(z_4) \right\rangle_{\mathrm{CFT}^{\otimes mn}/\mathcal{S}_{mn}}}{\left(\left\langle \sigma_{g_m}(z_1) \sigma_{g_m^{-1}}(z_2) \sigma_{g_m}(z_3) \sigma_{g_m^{-1}}(z_4) \right\rangle_{\mathrm{CFT}^{\otimes m}/\mathcal{S}_m} \right)^n}. \end{aligned} \tag{2.13}$$

In the denominator of the above equation the partition function $Z_{1,m}$ arises from the normalization of the state $|\rho_{AB}^{m/2}\rangle$ and σ_{g_m} are the twist fields at the endpoints of the intervals in m-replicated manifold. Subsequently, the reflected entropy for the bipartite state may be computed in the replica limit, where both replica parameters are analytically continued along the real line and finally taken to unity.[6]

Remarkably, in [26], the authors also established that in holographic theories (with two derivative gravity duals), the reflected entropy is given by twice the minimal cross-section of the bulk entanglement wedge, which we will briefly review below.

---

[4]See [26, 39] for details about replica construction of the state $|\rho_{AB}^{m/2}\rangle$ and the sewing mechanism of such replica sheets.

[5]Although the elements g_A and g_B are conjugate to each other, the twist operators are not strictly local due to their sensitivity to the homology with the subsystem that defines them. As a result, the dominant operator exchanged between $\sigma_{g_A^{-1}}$ and σ_{g_B} is not identity:

$$\sigma_{g_A^{-1}} \sigma_{g_B} \to \sigma_{g_A^{-1} g_B} + \ldots.$$

[6]The two replica limits $m \to 1$ and $n \to 1$ do not always commute [40, 41]. However, for the cases considered here, these two limits may be implemented interchangeably without affecting the final result.
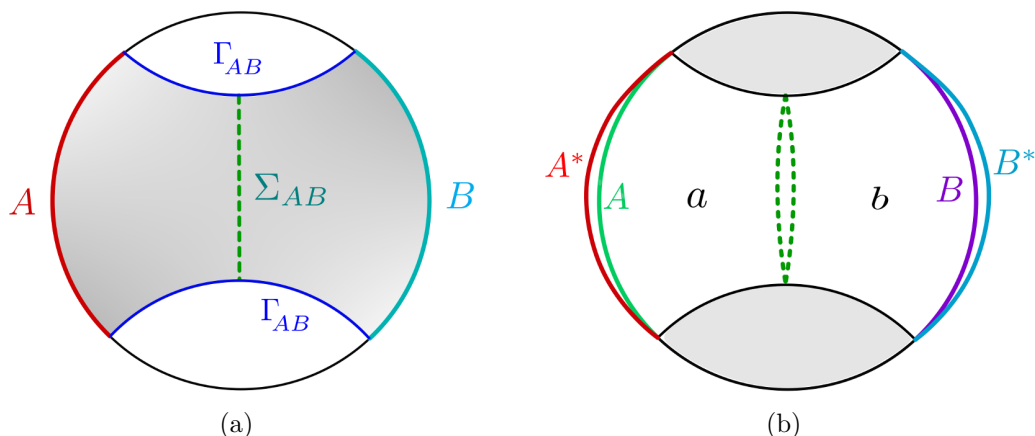
Figure 2. Schematics of the bulk entanglement wedge corresponding to two disjoint subsystems A and B in the dual CFT. Figure modified from [26].

2.3 Entanglement wedge cross section

In the context of AdS/CFT correspondence, for a subsystem A in the dual CFT, the codimension-one bulk region Ξ_A bounded by A and the corresponding (H)RT surface Γ_A is referred to as the entanglement wedge dual to the reduced density matrix ρ_A [24, 42, 43]. For a bipartite system described by ρ_{AB}, the minimal cross-section of the entanglement wedge (EWCS) quantifies the quantum entanglement and correlation between the two parties. When the subsystems A and B are large enough so that the entanglement entropy is obtained through the extremal surface Γ_{AB} as depicted in figure 2(a), one obtains a connected entanglement wedge Ξ_{AB} bounded by the union of the hypersurfaces $A \cup B \cup \Gamma_{AB}$ [25, 44], namely[7]

$$\partial \Xi_{AB} \equiv A \cup B \cup \Gamma_{AB} \,. \tag{2.14}$$

As described in [25, 44], to obtain the minimal EWCS, one first divides Γ_{AB} in two segments as $\Gamma_{AB} = \Gamma_{(A)} \cup \Gamma_{(B)}$ and subsequently constructs the extremal curve Σ_{AB} homologous to $A \cup \Gamma_{(A)}$ in the entanglement wedge. The EWCS is then defined as the minimal area of the curve sought out from all the candidate Σ_{AB}s, where the minimization is performed over all possible partitions (cf. figure 2(a)):

$$E_W(A:B) = \min_{\Gamma_{AB}^{(A)} \subset \Gamma_{AB}} \text{ext} \left[\frac{\text{Area}\,(\Sigma_{AB})}{4G_{\mathrm{N}}} \right] \,. \tag{2.15}$$

We now briefly sketch the derivation of the holographic prescription for the reflected entropy, following the Lewkowycz-Maldacena procedure for EE [45]. The bulk dual description of the canonical purification $|\sqrt{\rho_{AB}}\rangle$ features two copies of the entanglement wedge dual to ρ_{AB} glued along the (H)RT surfaces Γ_{AB} [37, 38] in the form of a wormhole geometry. From figure 2(b), the EE for the subsystem $AA^\star$ may be computed through the area of a *cosmic*

---

[7]For small subsystems A and B, if they are separated enough, the entanglement entropy is computed through the combination of two disconnected HRT surfaces and consequently the entanglement wedge is disconnected with a trivial cross-section.

brane homologous to $AA^\star$ [46] (in the replica limit, this cosmic brane reduces to the reflected minimal surface [26]) as follows

$$S(AA^\star) = \frac{\mathrm{Area}\,(\Gamma_{AA^\star})}{4G_\mathrm{N}} + \mathcal{O}\left(G_\mathrm{N}^0\right)\,, \tag{2.16}$$

where $\Gamma_{AA^\star}$ is the RT surface homologous to $AA^\star$ in this wormhole geometry. The holographic duality is then established through the remnant $\mathbb{Z}_2$ symmetry which dictates that $\mathrm{Area}\,(\Gamma_{AA^\star}) = 2\,\mathrm{Area}(\partial a \cap \partial b)$, where a and b denote the two portions of the bulk entanglement wedge through the minimal cross-section.

3 EWCS in Poincaré AdS$_3$ dual to vacuum state of ICFT$_2$

In this section, we determine the minimal (extremal) entanglement wedge cross section (EWCS) in the above described bulk AdS$_3$ geometry dual to half of the reflected entropy of mixed state configurations involving adjacent and disjoint subsystems in an ICFT$_2$.[8] Furthermore, we will determine the corresponding expressions for EWCS in the large tension limit of the interface brane. In the subsequent sections we will demonstrate that the results derived from the island formula for the reflected entropy match precisely with the corresponding expressions for twice the area of EWCS obtained in the large tension limit.

3.1 Adjacent subsystems

In this section, we compute the minimal (extremal) entanglement wedge cross section corresponding to two adjacent subsystems in a holographic ICFT$_2$. Consider the bipartite mixed state configuration of two adjacent subsystems A and B at a constant time slice $\tau = \tau_0$, described by

$$A = \left[\tilde{b}_1, \tilde{b}_2\right]_\mathrm{I} \cup [b_1, b_2]_\mathrm{II} \qquad \text{and} \qquad B = \left[\tilde{b}_2, \tilde{b}_3\right]_\mathrm{I} \cup [b_2, b_3]_\mathrm{II}\,,$$

where the subscripts I, II denote whether the subsystem resides in the CFT$_\mathrm{I}$ or CFT$_\mathrm{II}$. The schematics of this configuration is depicted in figure 3. The computation of the minimal EWCS for $A \cup B$ consists of two parts. As there are many choices for the RT surface corresponding to a subsystems $A \cup B$, the first step involves determining all such RT saddles and their corresponding entanglement wedges. Now, depending on the size of the subsystems and their distances from the interface, EWCS can have many different phases within each RT saddle or the entanglement wedge of $A \cup B$. In the following, we will divide the possible configurations of RT saddles into two sub-classes, namely those corresponding to the RT surfaces crossing the EOW brane once and those where multiple crossovers are possible [20]. For each phase of the RT saddle we will construct the bulk entanglement wedge and subsequently compute the corresponding minimal (extremal) cross-section dual to the reflected entropy $S_R(A : B)$.

---

[8]Note that for a different set of mixed state configurations, quite recently EWCS dual to the vacuum state of an ICFT$_2$ on a circle has been determined in [35].
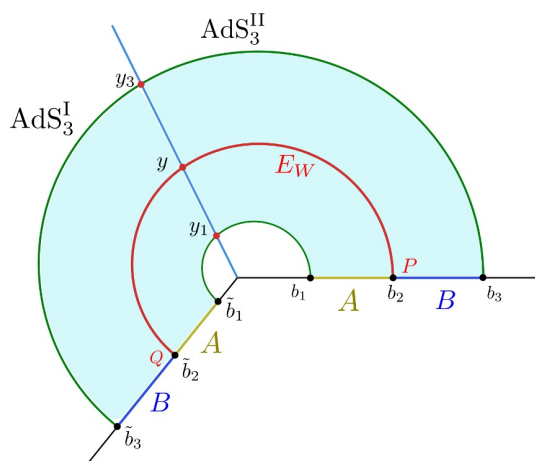
Figure 3. Configuration of single crossing RT saddles for adjacent subsystems in the boundary CFT$_2$s.

3.1.1 Configurations involving single crossover of RT surfaces

In this subsection, we consider the cases where the RT surface crosses the EOW brane once and subsequently compute the minimal EWCS for various phases in that RT saddle. In particular, the RT surfaces connecting the ends points of the subsystems on both CFTs consists of circular segments[9] which cross the EOW brane at the points y_1 and y_3. The entanglement wedge and the RT surfaces are depicted by the shaded region and the green curves respectively in figure 3. Note that, according to the Israel junction conditions [20], the distances $y_{1,3}$ along the EOW brane are identical as seen from either AdS$_3$ geometry.

To find to the length of the RT surface, we utilize the fact that the length of a geodesic connecting two bulk points (τ_1, x_1, z_1) and (τ_2, x_2, z_2) in the Poincaré AdS$_3$ geometry is given by

$$d = L \cosh^{-1}\left[\frac{(x_1 - x_2)^2 + (\tau_1 - \tau_2)^2 + z_1^2 + z_2^2}{2 z_1 z_2} \right], \tag{3.1}$$

where L is the AdS$_3$ length scale. The Poincaré coordinates of the points y_i on the EOW brane as seen from the AdS$_3^{\mathrm{II}}$ and AdS$_3^{\mathrm{I}}$ geometry respectively, are given by

$$\begin{aligned} (\tau_0, y_i \sin\psi_{\mathrm{II}}, y_i \cos\psi_{\mathrm{II}}) && \text{from AdS}_3^{\mathrm{II}}, \\ (\tau_0, y_i \sin\psi_{\mathrm{I}}, y_i \cos\psi_{\mathrm{I}}) && \text{from AdS}_3^{\mathrm{I}}, \end{aligned} \tag{3.2}$$

where $\psi_{\mathrm{I,II}}$ are the angles made by the EOW brane with the holographic directions z_i in each AdS$_3$ geometry. Therefore, the total length of the geodesic segments connecting the

---

[9]Such RT saddles have already been considered in [20], where the authors utilized techniques from hyperbolic geometry to obtain the lengths of these surfaces. In the following, however, we will use an alternative method more suited to our purpose and find agreement with earlier results.

points $\tilde{b}_{1,3}$ and $b_{1,3}$ may be obtained using eq. (3.1) as

$$
d = L_{\mathrm{I}} \log \left[\frac{\left(\tilde{b}_1 + y_1 \sin\psi_{\mathrm{I}}\right)^2 + (y_1 \cos\psi_{\mathrm{I}})^2}{y_1 \cos\psi_{\mathrm{I}}} \right] + L_{\mathrm{II}} \log \left[\frac{(b_1 + y_1 \sin\psi_{\mathrm{II}})^2 + (y_1 \cos\psi_{\mathrm{II}})^2}{y_1 \cos\psi_{\mathrm{II}}} \right]
$$
$$
+ L_{\mathrm{I}} \log \left[\frac{\left(\tilde{b}_2 + y_2 \sin\psi_{\mathrm{I}}\right)^2 + (y_2 \cos\psi_{\mathrm{I}})^2}{y_2 \cos\psi_{\mathrm{I}}} \right] + L_{\mathrm{II}} \log \left[\frac{(b_2 + y_2 \sin\psi_{\mathrm{II}})^2 + (y_2 \cos\psi_{\mathrm{II}})^2}{y_2 \cos\psi_{\mathrm{II}}} \right] .
$$
(3.3)

Extremizing with respect to $y_{1,3}$, the locations of the crossing points may be expressed as[10]

$$
y_i^* = \frac{\left(b_i - \tilde{b}_i\right) \sin\left(\frac{\psi_{\mathrm{I}} - \psi_{\mathrm{II}}}{2}\right) + \sqrt{(b_i - \tilde{b}_i)^2 \sin^2\left(\frac{\psi_{\mathrm{I}} - \psi_{\mathrm{II}}}{2}\right) + 4 b_i \tilde{b}_i \cos^2\left(\frac{\psi_{\mathrm{I}} + \psi_{\mathrm{II}}}{2}\right)}}{2 \cos\left(\frac{\psi_{\mathrm{I}} + \psi_{\mathrm{II}}}{2}\right)} ,
$$
(3.4)

where $i = 1, 3$. Substituting the above extremal values in eq. (3.3) and subsequently utilizing the Ryu-Takayanagi prescription [47], we may obtain the entanglement entropy for $A \cup B$ when the single crossing RT saddles dominate.

Phase-I

In phase-I the subsystems A and B are comparable and close to the interface. The candidate for the minimal EWCS depicted by the red curve in figure 3, is given by two circular geodesic segments connecting the points $P = (\tau_0, b_2)$ and $Q = (\tau_0, \tilde{b}_2)$ on both sides of the interface which meet smoothly[11] at the EOW brane at the point which is at a distance y from the interface. The total length of the geodesic segments connecting the points P and Q may now be obtained using eq. (3.1) and eq. (3.2) as

$$
d_{PQ} = L_{\mathrm{I}} \log \left[\frac{\left(\tilde{b}_2 + y \sin\psi_{\mathrm{I}}\right)^2 + (y \cos\psi_{\mathrm{I}})^2}{\epsilon\, y \cos\psi_{\mathrm{I}}} \right] + L_{\mathrm{II}} \log \left[\frac{(b_2 + y \sin\psi_{\mathrm{II}})^2 + (y \cos\psi_{\mathrm{II}})^2}{\epsilon\, y \cos\psi_{\mathrm{II}}} \right] .
$$
(3.5)

Extremizing the total length with respect to y, the location of the crossing point is given by eq. (3.4) with $i = 2$. We now consider the large tension limit $T \to T_{\max}$ described in eq. (2.8) where the EOW brane is pushed towards the asymptotic boundary. We may now utilize eq. (2.9) to obtain the minimal EWCS in the large tension limit $\delta \to 0$, for this phase as follows

$$
E_W(A : B) = \frac{L_I}{4G_{\mathrm{N}}} \log \left[\frac{(y^* + \tilde{b}_2)^2}{2 y^* \epsilon} \right] + \frac{L_{\mathrm{II}}}{4G_{\mathrm{N}}} \log \left[\frac{(y^* + b_2)^2}{2 y^* \epsilon} \right] + S_{\mathrm{int}}^{(\delta)} ,
$$
(3.6)

where the location of the intersection point y^* is now given by

$$
y^* = \frac{(L_{\mathrm{II}} - L_{\mathrm{I}})\left(b_2 - \tilde{b}_2\right) + \sqrt{(L_{\mathrm{II}} - L_{\mathrm{I}})^2 \left(b_2 - \tilde{b}_2\right)^2 + 4 b_2 \tilde{b}_2 \left(L_{\mathrm{I}} + L_{\mathrm{II}}\right)^2}}{2 \left(L_{\mathrm{I}} + L_{\mathrm{II}}\right)} ,
$$
(3.7)

---

[10]To extremize the above expression, we are required to impose the Israel-Lanczos junction condition [20] $L_{\mathrm{I}} \sec\psi_{\mathrm{I}} = L_{\mathrm{II}} \sec\psi_{\mathrm{II}}$.

[11]The smoothness of the geodesics segments across the EOW brane is a consequence of the Israel-Lanczos gluing conditions [20].
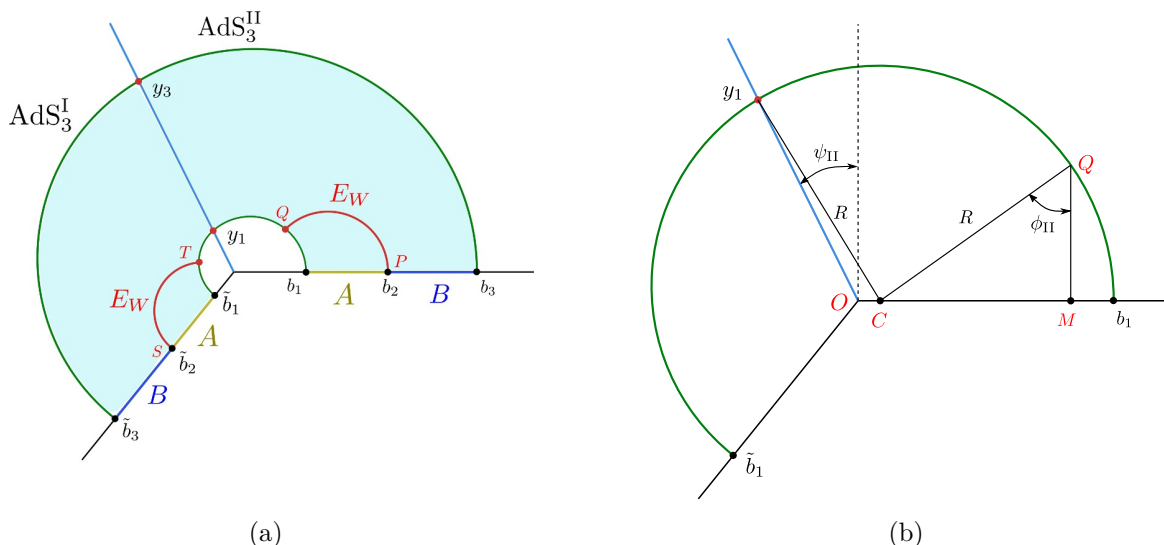
Figure 4. Adjacent subsystems: phase-II.

and $S_{\mathrm{int}}^{(\delta)}$ is the large tension limit of the interface entropy $S_{\mathrm{int}} = \frac{\rho_{\mathrm{I}}^* + \rho_{\mathrm{II}}^*}{4G_{\mathrm{N}}}$, defined as

$$S_{\mathrm{int}}^{(\delta)} = \frac{c_{\mathrm{I}}}{6} \log \left[\frac{2(L_{\mathrm{I}} + L_{\mathrm{II}})}{L_{\mathrm{I}}\, \delta} \right] + \frac{c_{\mathrm{II}}}{6} \log \left[\frac{2(L_{\mathrm{I}} + L_{\mathrm{II}})}{L_{\mathrm{II}}\, \delta} \right] + \mathcal{O}\left(\delta \right) . \tag{3.8}$$

Phase-II

In phase-II, we consider the subsystem A to be smaller compared to B. The minimal EWCS in this phase depicted by red curve in figure 4(a), consists of two circular arcs each connecting the common boundary of A and B and the smaller RT surface joining b_1 and $\tilde{b}_1$ on either side of the EOW brane. The coordinates of the end point Q of the geodesic segment PQ in the $\mathrm{AdS}_3^{\mathrm{II}}$ may be parametrized by an angle ϕ_{II} as follows

$$Q : (\tau_{\mathrm{II}}, x_{\mathrm{II}}, z_{\mathrm{II}}) = (\tau_0, \overline{OM}, \overline{MQ}) = (\tau_0, b_1 - R + R \sin \phi_{\mathrm{II}}, R \cos \phi_{\mathrm{II}}) , \tag{3.9}$$

where the overline in OM and MQ simply denote that they are Euclidean distances (here we have followed the notation in [20]), R is the radius of the circular arc joining the points b_1 and y_1^* on the $\mathrm{AdS}_3^{\mathrm{II}}$ side as shown in figure 4(b). Note that, as described earlier, the location of the point y_1^* is given in eq. (3.4).

Similarly for the $\mathrm{AdS}_3^{\mathrm{I}}$ region, the coordinates of the point T may be parametrized by an arbitrary angle ϕ_{I} as

$$T : (\tau_{\mathrm{I}}, x_{\mathrm{I}}, z_{\mathrm{I}}) = \left(\tau_0, \tilde{b}_1 - r + r \sin \phi_{\mathrm{I}}, r \cos \phi_{\mathrm{I}} \right) , \tag{3.10}$$

where, r is the radius of the circular arc joining the points $\tilde{b}_1$ and y_1^* on the $\mathrm{AdS}_3^{\mathrm{II}}$ side. To compute the radii R and r, we utilize the equations of the circular arc as follows

$$\begin{aligned} R^2 &= (b_1 - R)^2 - 2y_1^*(b_1 - R) \cos \left(\psi_{\mathrm{II}} + \frac{\pi}{2} \right) + y_1^{*2} , \\ r^2 &= \left(r - \tilde{b}_1 \right)^2 - 2y_1^* \left(r - \tilde{b}_1 \right) \cos \left(\frac{\pi}{2} - \psi_{\mathrm{I}} \right) + y_1^{*2} , \end{aligned} \tag{3.11}$$

which may be solved to obtain

$$R = b_1 + \frac{y_1^{*2} - b_1^2}{2(b_1 + y_1 \sin \psi_{\mathrm{II}})}, \qquad r = \tilde{b}_1 + \frac{y_1^{*2} - \tilde{b}_1^2}{2(\tilde{b}_1 + y_1 \sin \psi_{\mathrm{I}})}. \tag{3.12}$$

Now using eq. (3.1), the total length of the circular arcs is obtained to be

$$\begin{aligned} d &= d_{PQ} + d_{ST} \\ &= L_{\mathrm{I}} \log \left[\frac{\left(\tilde{b}_2 - \left(\tilde{b}_1 + r \sin \phi_{\mathrm{I}} - r \right) \right)^2 + (r \cos \phi_{\mathrm{I}})^2}{r \epsilon \cos \phi_{\mathrm{I}}} \right] \\ &\quad + L_{\mathrm{II}} \log \left[\frac{(b_2 - (b_1 + R \sin \phi_{\mathrm{II}} - R))^2 + (R \cos \phi_{\mathrm{II}})^2}{R \epsilon \cos \phi_{\mathrm{II}}} \right]. \end{aligned} \tag{3.13}$$

Extremizing the above length with respect to the arbitrary angles ϕ_{I} and ϕ_{II}, we have

$$\phi_{\mathrm{I}} = \tan^{-1} \left[\frac{2r \left(r + \tilde{b}_2 - \tilde{b}_1 \right)}{\left(\tilde{b}_2 - \tilde{b}_1 \right) \left(2r + \tilde{b}_2 - \tilde{b}_1 \right)} \right], \qquad \phi_{\mathrm{II}} = \tan^{-1} \left[\frac{2R \left(R - b_1 + b_2 \right)}{(b_2 - b_1) \left(2R + b_2 - b_1 \right)} \right]. \tag{3.14}$$

Substituting the above extremal values, the total minimal EWCS may be obtained as

$$\begin{aligned} E_W(A:B) &= \frac{L_{\mathrm{I}}}{4G_{\mathrm{N}}} \log \left[\frac{\left(\tilde{b}_2 - \tilde{b}_1 \right) \left(2r + \tilde{b}_2 - \tilde{b}_1 \right)}{\epsilon\, r} \right] + \frac{L_{\mathrm{II}}}{4G_{\mathrm{N}}} \log \left[\frac{(b_2 - b_1) \left(2R + b_2 - b_1 \right)}{\epsilon\, R} \right] \\ &= \frac{L_{\mathrm{I}}}{4G_{\mathrm{N}}} \log \left[\frac{2 \left(\tilde{b}_2 - \tilde{b}_1 \right) \left(y_1^{*2} + \tilde{b}_1 \tilde{b}_2 + y_1^* \left(\tilde{b}_1 + \tilde{b}_2 \right) \sin \psi_{\mathrm{I}} \right)}{\epsilon \left(y_1^{*2} + \tilde{b}_1^2 + 2 y_1^* \tilde{b}_1 \sin \psi_{\mathrm{I}} \right)} \right] \\ &\quad + \frac{L_{\mathrm{II}}}{4G_{\mathrm{N}}} \log \left[\frac{2 (b_2 - b_1) \left(y_1^{*2} + b_1 b_2 + y_1^* (b_1 + b_2) \sin \psi_{\mathrm{II}} \right)}{\epsilon \left(y_1^{*2} + b_1^2 + 2 b_1 y_1^* \sin \psi_{\mathrm{II}} \right)} \right]. \end{aligned} \tag{3.15}$$

We now utilize eq. (2.9) to obtain the minimal EWCS in the large tension limit $\delta \to 0$, as follows

$$E_W(A:B) = \frac{L_{\mathrm{I}}}{4G_{\mathrm{N}}} \log \left[\frac{2 \left(\tilde{b}_2 - \tilde{b}_1 \right) \left(\tilde{b}_2 + y_1^* \right)}{\epsilon \left(\tilde{b}_1 + y_1^* \right)} \right] + \frac{L_{\mathrm{II}}}{4G_{\mathrm{N}}} \log \left[\frac{2 (b_2 - b_1)(b_2 + y_1^*)}{\epsilon (b_1 + y_1^*)} \right]. \tag{3.16}$$

Phase-III

In phase III, the subsystem B is small compared to A and the minimal EWCS lands on the outer RT surface on both AdS_3 regions as depicted in figure 5. The computation of the minimal EWCS for this phase follows a procedure similar to the previous subsection. The total length of the candidate EWCS in this case is given by

$$\begin{aligned} d &= L_{\mathrm{I}} \log \left[\frac{\left(\tilde{b}_2 - \left(\tilde{b}_3 + r \sin \phi_{\mathrm{I}} - r \right) \right)^2 + (r \cos \phi_{\mathrm{I}})^2}{\epsilon\, r \cos \phi_{\mathrm{I}}} \right] \\ &\quad + L_{\mathrm{II}} \log \left[\frac{(b_2 - (b_3 + R \sin \phi_{\mathrm{II}} - R))^2 + (R \cos \phi_{\mathrm{II}})^2}{\epsilon\, R \cos \phi_{\mathrm{II}}} \right]. \end{aligned} \tag{3.17}$$
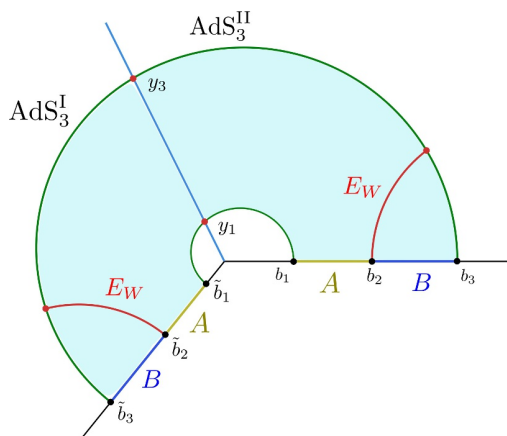
Figure 5. Adjacent subsystems: phase-III.

In the above expression, we have parametrized two arbitrary points on the RT surface connecting $\tilde{b}_3$ and b_3 on the asymptotic boundary. As earlier, r and R denote the radii of the circular geodesic segments joining the set of points $(\tilde{b}_3, y_3^*)$ and (b_3, y_3^*) respectively. These radii may be obtained by utilizing the equations of the respective circular segments, similar to the previous subsection (cf. eq. (3.12)).

Now extremizing eq. (3.17) with respect to the arbitrary angles ϕ_{I} and ϕ_{II}, the minimal EWCS in phase III may be obtained by the following replacements: y_1^* with y_3^*, and b_1, $\tilde{b}_1$ with b_3, $\tilde{b}_3$ in eq. (3.15). In the large tension limit, the EWCS reduces to

$$E_W(A:B) = \frac{L_{\mathrm{I}}}{4G_{\mathrm{N}}} \log\left[\frac{2(\tilde{b}_3 - \tilde{b}_2)(\tilde{b}_2 + y_3^*)}{\epsilon(\tilde{b}_3 + y_3^*)}\right] + \frac{L_{\mathrm{II}}}{4G_{\mathrm{N}}} \log\left[\frac{2(b_3 - b_2)(b_2 + y_3^*)}{\epsilon(b_3 + y_3^*)}\right]. \tag{3.18}$$

3.1.2 Configurations involving double crossing of RT surfaces

We now consider the RT saddles homologous to $A \cup B$ which cross the EOW brane multiple times before ending on either of the asymptotic boundaries. Recall that, following the convention in [20], we have set $c_{\mathrm{I}} < c_{\mathrm{II}}$. With this convention, it was demonstrated in [20] that for a sufficiently large subsystem in the $\mathrm{CFT}_2^{\mathrm{II}}$, there exists at least one such geodesic homologous to the subsystem which finds it more efficient to cross the EOW brane, traverse a finite distance in the $\mathrm{AdS}_3^{\mathrm{I}}$ geometry and then returns to the $\mathrm{AdS}_3^{\mathrm{II}}$ geometry.[12] The computation of the length of such "double-crossing" geodesics was outlined in the appendix of [20] utilizing purely geometrical methods. In the following, however, we pursue a different route more suited to our purpose and find agreement with their result.

Consider a subsystem $D = [b_i, b_j]_{\mathrm{II}}$ entirely in the $\mathrm{CFT}_2^{\mathrm{II}}$. The double crossing RT saddle homologous to D consists of three semi-circular geodesic arcs as sketched in figure 6; two of them connect $b_{i,j}$ with arbitrary bulk points $\bar{y}_{i,j}$ on the brane[13] and the third arc connecting

---

[12]Note that, it was further argued in [20] that the RT saddles crossing the brane more than twice always have greater length and hence do not contribute to the correlation functions or the entanglement entropy at the leading order.

[13]We have denoted the locations of the points where the geodesics cross the brane by $\bar{y}_k$ to emphasize that these points are, in principle, different than those corresponding to a pair of single crossing geodesics emanating from b_k.
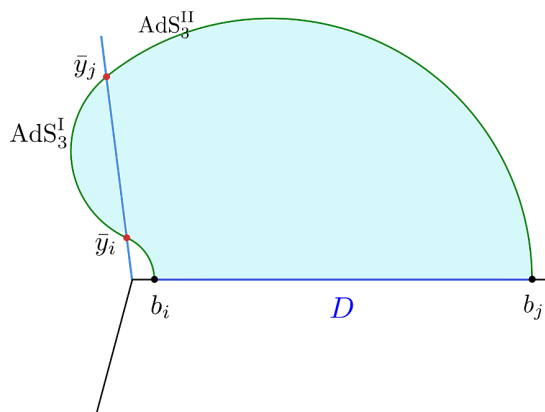
Figure 6. Schematics of the (double-crossing) bulk geodesic homologous to the subsystem D described by a finite subsystem $[b_i, b_j]$ in dual CFT$_{\text{II}}$.

$\bar{y}_i$ with $\bar{y}_j$ residing entirely in the AdS$_3^{\text{I}}$ geometry. The Poincaré coordinates of the bulk points are same as given in eq. (3.2). Using the geodesic length formula in eq. (3.1), we may obtain the total length of these three circular arcs as follows

$$
d_{PQ} = L_{\text{II}} \log\left[\frac{(b_j + \bar{y}_j \sin\psi_{\text{II}})^2 + (\bar{y}_j \cos\psi_{\text{II}})^2}{\epsilon_2\, \bar{y}_j \cos\psi_{\text{II}}}\right] + L_{\text{II}} \log\left[\frac{(b_i + \bar{y}_i \sin\psi_{\text{II}})^2 + (\bar{y}_i \cos\psi_{\text{II}})^2}{\epsilon_2\, \bar{y}_i \cos\psi_{\text{II}}}\right]
$$
$$
+ L_{\text{I}} \cosh^{-1}\left[\frac{(\bar{y}_j - \bar{y}_i)^2 \sin^2\psi_{\text{I}} + \left(\bar{y}_i^2 + \bar{y}_j^2\right)\cos^2\psi_{\text{I}}}{2\bar{y}_i\bar{y}_j \cos^2\psi_{\text{I}}}\right]. \tag{3.19}
$$

We are required to extremize the above length over the arbitrary locations $\bar{y}_{i,j}$. To this end, we make the following change of variables b_j, $\bar{y}_j$ to Θ_D, k_D:

$$
b_j = \Theta_D b_i\,, \qquad \bar{y}_j = k_D^2 \Theta_D \bar{y}_i\,. \tag{3.20}
$$

Extremization of the length with respect to $\bar{y}_i$ leads to

$$
\left(k_D^2 \bar{y}_i^2 - b_i^2\right)\left(\left(k_D^2 + 1\right) \bar{y}_i b_i \sin\psi_{\text{II}} + k_D^2 \bar{y}_i^2 + b_i^2\right) = 0\,, \tag{3.21}
$$

and the only real non-negative solution is given by $\bar{y}_i = \frac{b_i}{k_D}$. Substituting this in eq. (3.19) and furthermore extremizing over the remaining variable k_D, we obtain the following algebraic equation

$$
\cos\psi_{\text{I}} \sec\psi_{\text{II}} \left(1 + k_D^2 \Theta_D\right) \frac{\left(1 + k_D^2 + 2k_D \sin\psi_{\text{II}}\right)}{\sqrt{1 + k_D^4 \Theta_D^2 + 2k_D^2 \Theta_D \cos 2\psi_{\text{I}}}} = 1 - k_D^2\,. \tag{3.22}
$$

The above eighth order polynomial equation may be readily solved for k_D. However, the solutions are not very illuminating and we will omit the details here. Substituting the extremal value $k_D = k_D^*$ (corresponding to the extremal locations $\bar{y}_{i,j}^*$ on the brane) in eq. (3.19) we may now obtain the length of the RT saddle connecting b_i and b_j on the right boundary as sketched in figure 6. Utilizing the RT prescription [47], the holographic entanglement entropy
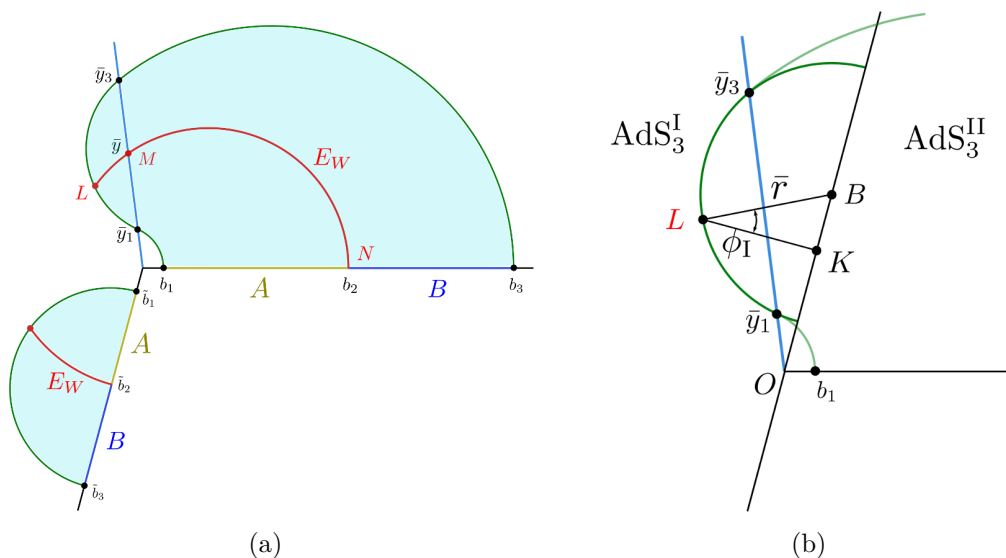
Figure 7. (a) Schematics of the EWCS in phase-I when the RT surface crosses the brane twice. (b) Schematic of circular arc joining y_1 and y_3 in the AdS$_I$ geometry.

of subsystem D for the double crossing configuration is given by

$$S(\rho_D) \equiv S_{\text{double}}\left([b_i, b_j]\right) = \frac{L_{\text{I}}}{4G_{\text{N}}} \cosh^{-1}\left[\frac{1 + k_D^{*2}\Theta_D \cos(2\psi_{\text{I}}) + k_D^{*2}\Theta_D\left(k_D^{*2}\Theta_D - 1\right)}{2k_D^{*2}\Theta_D \cos^2\psi_{\text{I}}}\right]$$
$$+ \frac{L_{\text{II}}}{2G_{\text{N}}} \log\left[\frac{\sqrt{b_i b_j}\left(1 + k_D^{*2} + 2k_D^* \sin\psi_{\text{II}}\right)}{k_D^* \cos\psi_{\text{II}}}\right]. \qquad (3.23)$$

Large tension limit: in the large tension limit, the extremal value of $\bar{y}_1$ remains the same while the extremization conditions in eq. (3.22) reduce to the cubic equation

$$L_{\text{II}}(k_D - 1)\left(k_D^2\Theta_D - 1\right) + L_{\text{I}}(k_D + 1)\left(k_D^2\Theta_D + 1\right) = 0. \qquad (3.24)$$

In the following, we will consider various phases for the entanglement entropy of $A \cup B$ such that the corresponding RT surface homologous to $[b_1, b_3]$ in AdS$_{\text{II}}$ geometry crosses the EOW brane twice at the points $\bar{y}_1^*$ and $\bar{y}_3^*$. It consists of three semi-circular arcs, one of which resides solely in the AdS$_{\text{I}}$ geometry. Note that, the extremal values of the locations $\bar{y}_{1,2}$ may be obtained from eq. (3.22) (or, from eq. (3.24) in the large tension limit). On the other hand, the RT surface on the AdS$_{\text{I}}$ side is a semi-circle depicted in figure 7(a) by the green curve which connects $\tilde{b}_1$ and $\tilde{b}_3$, that does not cross the brane. The bulk entanglement wedge is now the region bounded by these geodesics and the corresponding subsystems as depicted by the shaded regions in figure 7(a). Furthermore, we will systematically investigate the phase transitions of the minimal EWCS for different subsystem sizes and geometry.

Phase-I

We begin with the phase where the subsystems in CFT$_2^{\text{II}}$ are comparable in size and the minimal EWCS consists of two extremal curves as shown by the red curves in figure 7(a).

The minimal EWCS E_W^{I} residing entirely in the AdS$_{\mathrm{I}}$ geometry may be computed using standard AdS$_3$/CFT$_2$ techniques [25, 44] as

$$E_W^{\mathrm{I}}(A:B) = \frac{L_{\mathrm{I}}}{4G_{\mathrm{N}}} \log \left[\frac{2(\tilde{b}_2 - \tilde{b}_1)(\tilde{b}_3 - \tilde{b}_2)}{\epsilon_1(\tilde{b}_3 - \tilde{b}_1)} \right]. \tag{3.25}$$

The minimal EWCS E_W^{II} in the AdS$_{\mathrm{I}}$ geometry consists of two circular geodesic segments NM and ML as shown by the red curve in figure 7(a). The segment NM starts from the point b_2 and ends at the point M on the EOW brane which is at a distance $\bar{y}$ from the interface O. The other circular arc ML connects the point $\bar{y}$ on the EOW brane and ends on the geodesic segment connecting $\bar{y}_1^*$ and $\bar{y}_3^*$ in the AdS$_{\mathrm{I}}$ region. Hence, the total length of these curves is given by $d_{NL} = d_{NM} + d_{ML}$. The Poincaré coordinates of the point L are similar to that given in eq. (3.9). From figure 7(b), the coordinates of L can be parametrized as

$$L : (x_{\mathrm{I}}, z_{\mathrm{I}}) = \left(\overline{OK}, \overline{LK} \right) = \left(\overline{OB} - \overline{BK}, \overline{LK} \right) = (x_0 - \bar{r}\sin\phi_{\mathrm{I}}, \bar{r}\cos\phi_{\mathrm{I}}) \tag{3.26}$$

where overline on OK, LK once again denote that they are Euclidean distances, $\overline{BL} = \bar{r}$ corresponds to the radius of the circular arc connecting $\bar{y}_1^*$ and $\bar{y}_3^*$ and K is a point where the perpendicular dropped from L intersects $\overline{OB}$. x_0 is the center coordinate of the circular arc, and the arbitrary angle ϕ_{I} parametrizes the position of L on this circular arc. The center and the radius of the circular arc are given by

$$\bar{r} = \frac{\sqrt{\bar{y}_1^{*2} + \bar{y}_3^{*2} + 2\bar{y}_1^*\bar{y}_3^*\cos(2\psi_{\mathrm{I}})}}{2\sin\psi_{\mathrm{I}}}, \qquad x_0 = \frac{\bar{y}_1^* + \bar{y}_3^*}{2\sin\psi_{\mathrm{I}}}. \tag{3.27}$$

We may now obtain the total length of the two circular geodesic arcs using eq. (3.1) as

$$d_{NL} = L_{\mathrm{I}} \cosh^{-1} \left[\frac{(x_0 - \bar{r}\sin\phi_{\mathrm{I}} + \bar{y}\sin\psi_{\mathrm{I}})^2 + (\bar{y}\cos\psi_{\mathrm{I}})^2 + (\bar{r}\cos\phi_{\mathrm{I}})^2}{2\bar{y}\cos\psi_{\mathrm{I}}\,\bar{r}\cos\phi_{\mathrm{I}}} \right]$$
$$+ L_{\mathrm{II}} \log \left[\frac{(b_2 + \bar{y}\sin\psi_{\mathrm{II}})^2 + (\bar{y}\cos\psi_{\mathrm{II}})^2}{\bar{y}\epsilon_2\cos\psi_{\mathrm{II}}} \right]. \tag{3.28}$$

On extremizing with respect to ϕ_{I}, we obtain

$$\phi_{\mathrm{I}} = \sin^{-1} \left[\frac{2\bar{r}(x_0 + \bar{y}\sin\psi_{\mathrm{I}})}{\bar{r}^2 + x_0^2 + 2x_0\bar{y}\sin\psi_{\mathrm{I}} + \bar{y}^2} \right]. \tag{3.29}$$

Now, substituting the value of ϕ_{I} in eq. (3.28) followed by extremizing over $\bar{y}$, we obtain a polynomial equation in $\bar{y}$ whose physical solution leads to the minimal EWCS

$$E_W^{\mathrm{II}}(A:B) = L_{\mathrm{I}} \cosh^{-1} \left[\frac{\sqrt{\left(\bar{r}^2 + x_0^2 + 2x_0\bar{y}^*\sin\psi_{\mathrm{I}} + \bar{y}^{*2}\right)^2 - 4\bar{r}^2(x_0 + \bar{y}^*\sin\psi_{\mathrm{I}})^2}}{2\bar{r}\bar{y}^*\cos\psi_{\mathrm{I}}} \right]$$
$$+ L_{\mathrm{II}} \log \left[\frac{b_2^2 + \bar{y}^{*2} + 2b_2\bar{y}^*\sin\psi_{\mathrm{II}}}{\epsilon\,\bar{y}^*\cos\psi_{\mathrm{II}}} \right]. \tag{3.30}$$

In the large tension limit $\delta \to 0$, using eq. (3.27), the result simplifies to

$$E_W^{\mathrm{II}}(A:B) = \frac{L_{\mathrm{I}}}{4G_{\mathrm{N}}} \log \left[\frac{(\bar{y}^* - \bar{y}_1^*)(\bar{y}^* - \bar{y}_3^*)}{\bar{y}^*(\bar{y}_1^* - \bar{y}_3^*)} \right] + \frac{L_{\mathrm{II}}}{4G_{\mathrm{N}}} \log \left[\frac{(b_2 + \bar{y}^*)^2}{2\bar{y}^*\epsilon} \right] + S_{\mathrm{int}}^{(\delta)}, \tag{3.31}$$
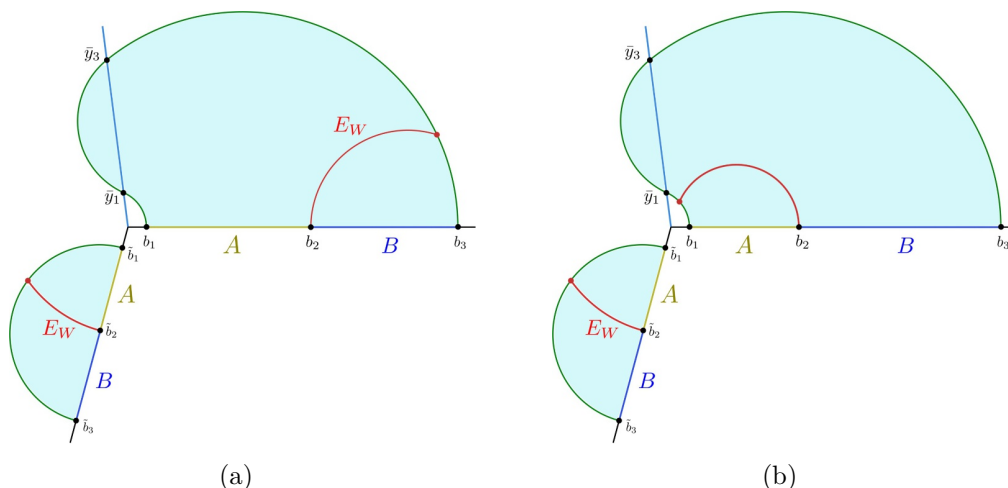
Figure 8. Adjacent subsystems: double-crossing phase-II and III.

where $\bar{y}^*$ corresponds to the solution of the extremization condition in the $\delta \to 0$ limit which is given by

$$L_{\mathrm{I}} \left(\frac{\bar{y}_1^*}{\bar{y} - \bar{y}_1^*} + \frac{\bar{y}}{\bar{y} - \bar{y}_2^*} \right) + L_{\mathrm{II}} \frac{\bar{y} - b_2}{\bar{y} + b_2} = 0 \,. \tag{3.32}$$

Note that, in eq. (3.31), $S_{\mathrm{int}}^{(\delta)}$ denotes the large tension limit of the interface entropy given in eq. (3.8).

Phase-II

In phase-II, the subsystem B is smaller compared to A in $\mathrm{CFT}_2^{\mathrm{II}}$ and the minimal EWCS consists of two circular geodesic segments, one of which is similar to the previous subsection. The other geodesic starts from b_2 and ends on the outer RT surface in $\mathrm{AdS}_{\mathrm{II}}$ geometry. Both the segments are depicted by the red curves in figure 8(a). The portion of the minimal EWCS in $\mathrm{AdS}_3^{\mathrm{I}}$ geometry is again given by eq. (3.25). The endpoint of the other portion in $\mathrm{AdS}_3^{\mathrm{II}}$ on the outer RT surface may be parametrized by an arbitrary angle ϕ_{II}, similar to eq. (3.9). Using eq. (3.1) the length of this geodesic segment may be expressed as

$$d_{\mathrm{II}} = L_{\mathrm{II}} \log \left[\frac{\left(b_2 - \left(b_3 + \bar{R} \sin \phi_{\mathrm{II}} - \bar{R} \right) \right)^2 + (\bar{R} \cos \phi_{\mathrm{II}})^2}{\bar{R} \epsilon_2 \cos \phi_{\mathrm{II}}} \right] \tag{3.33}$$

where $\bar{R}$ is the radius of the outer RT surface,

$$\bar{R} = b_3 + \frac{\bar{y}_3^{*2} - b_3^2}{2(b_3 + \bar{y}_3^* \sin \psi_{\mathrm{II}})} \,. \tag{3.34}$$

After extremizing over ϕ_2, we may readily obtain the minimal EWCS for this phase, with $\bar{y}_3^*$ obtained from eq. (3.22). In the limit of large brane tension $\delta \to 0$, the minimal EWCS reduces to

$$E_W(A:B) = \frac{L_{\mathrm{I}}}{4G_{\mathrm{N}}} \log \left[\frac{2(\tilde{b}_2 - \tilde{b}_1)(\tilde{b}_3 - \tilde{b}_2)}{\epsilon_1 (\tilde{b}_3 - \tilde{b}_1)} \right] + \frac{L_{\mathrm{II}}}{4G_{\mathrm{N}}} \log \left[\frac{2(b_3 - b_2)(b_2 + \bar{y}_3^*)}{\epsilon_2 (b_3 + \bar{y}_3^*)} \right], \tag{3.35}$$

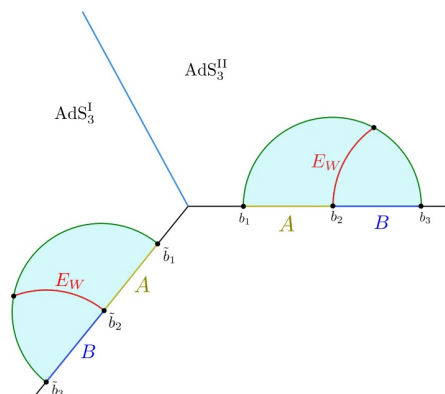with $\bar{y}_3^*$ now given by the physical solution to eq. (3.24).

Figure 9. Adjacent subsystems: no crossing.

Phase-III

For phase-III, we consider the subsystem A in CFT_2^{II} to be smaller than B such the minimal EWCS lands on the smaller RT surface crossing the brane at $\bar{y}_1$ as depicted in figure 8(b).

The computation for the EWCS in this phase is similar to the previous subsection and in the large tension limit, it reduces to the following expression

$$E_W(A:B) = \frac{L_{\text{I}}}{4G_{\text{N}}} \log\left[\frac{2(\tilde{b}_2 - \tilde{b}_1)(\tilde{b}_3 - \tilde{b}_2)}{\epsilon_1(\tilde{b}_3 - \tilde{b}_1)} \right] + \frac{L_{\text{II}}}{4G_{\text{N}}} \log\left[\frac{2(b_2 - b_1)(b_2 + \bar{y}_1^*)}{\epsilon_2(b_1 + \bar{y}_1^*)} \right], \quad (3.36)$$

where $\bar{y}_1^* = \frac{b_1}{k_D^*}$, k_D^* being the solution of the extremization equation in eq. (3.24).

3.1.3 RT saddles with no brane crossing

When the total system $A \cup B$ is small compared to their distance from the interface, the corresponding RT surface becomes disconnected as shown in figure 9. The minimal EWCS consist of two circular arcs which correspond to the EWCS of two adjacent subsystems in AdS_3^{I} and AdS_3^{II} regions respectively. So, the minimal EWCS for this phase may be expressed as [25, 44]

$$E_W(A:B) = \frac{L_{\text{I}}}{4G_{\text{N}}} \log\left[\frac{2\left(\tilde{b}_2 - \tilde{b}_1\right)\left(\tilde{b}_3 - \tilde{b}_2\right)}{\epsilon\left(\tilde{b}_3 - \tilde{b}_1\right)} \right] + \frac{L_{\text{II}}}{4G_{\text{N}}} \log\left[\frac{2(b_2 - b_1)(b_3 - b_2)}{\epsilon(b_3 - b_1)} \right]. \quad (3.37)$$

3.2 Disjoint subsystems

In this section, we consider the bipartite mixed state configuration ρ_{AB} described by unions of two disjoint intervals $[b_1, b_2]$ and $[b_3, b_4]$ on the two CFT_2 s at a constant time slice $\tau = \tau_0$ on either side of the interface. In particular, we take the bipartition of ρ_{AB} as follows:

$$A = [b_1, b_2]_{\text{I}} \cup [b_1, b_2]_{\text{II}} \qquad \text{and} \qquad B = [b_3, b_4]_{\text{I}} \cup [b_3, b_4]_{\text{II}} .$$

The schematics of this configuration is sketched in figure 10. The computation of the holographic entanglement entropy for ρ_{AB} consists of different saddles of the bulk Ryu-Takayanagi (RT) surfaces homologous to $A \cup B$ which we investigate systematically in the following. For each phase of the RT saddle we will construct the bulk entanglement wedge

and subsequently compute the corresponding minimal (extremal) cross-section which is dual to the reflected entropy $S_{\mathrm{R}}(A : B)$. Note that, within each phase of the entanglement entropy for $A \cup B$, the minimal cross section dividing the entanglement wedge of $A \cup B$ experiences phase transitions depending upon the subsystem sizes as well as their distances from the interface. Besides we will disregard all possible RT saddles for which the bulk entanglement wedge is disconnected and consequently the EWCS is vanishing. In the following, we will further divide the possible configurations of RT saddles into two sub-classes, namely those corresponding to the RT surfaces crossing the EOW brane once and those where multiple crossovers are possible for a single RT surface as described in [20].

3.2.1 Configurations involving single crossover of RT surfaces

We begin by considering the configurations of bulk extremal surfaces Γ_{AB} homologous to $A \cup B$ which cross the EOW brane at the points y_1 and y_4 along with two usual dome shaped geodesics connecting b_2 and b_3 in each of the AdS_3 geometries as sketched in figure 10. The Poincaré coordinates of the points on the brane are given as

$$
\begin{aligned}
(\tau_0, y_k \sin \psi_{\mathrm{I}}, y_k \cos \psi_{\mathrm{I}}) \,, && \text{from } \mathrm{AdS}_3^{\mathrm{I}} \\
(\tau_0, y_k \sin \psi_{\mathrm{II}}, y_k \cos \psi_{\mathrm{II}}) \,, && \text{from } \mathrm{AdS}_3^{\mathrm{II}}
\end{aligned}
\tag{3.38}
$$

with $k = \mathrm{I}, \mathrm{II}$. In the above parametrization, we have used the fact that the Israel junction conditions enforce the distances y_k along the EOW brane to be identical as seen from either side of the geometry. Note that the locations y_k of the bulk points along the EOW brane are chosen arbitrarily. The total length of the geodesics homologous to $A \cup B$ may now be computed[14] using eq. (3.1) as follows

$$
\begin{aligned}
d = {} & L_{\mathrm{I}} \log \left[\frac{(b_1 + y_1 \sin \psi_{\mathrm{I}})^2 + (y_1 \cos \psi_{\mathrm{I}})^2}{\epsilon \, y_1 \cos \psi_{\mathrm{I}}} \right] + L_{\mathrm{II}} \log \left[\frac{(b_1 + y_1 \sin \psi_{\mathrm{II}})^2 + (y_1 \cos \psi_{\mathrm{II}})^2}{\epsilon \, y_1 \cos \psi_{\mathrm{II}}} \right] \\
& + L_{\mathrm{I}} \log \left[\frac{(b_4 + y_4 \sin \psi_{\mathrm{I}})^2 + (y_4 \cos \psi_{\mathrm{I}})^2}{\epsilon \, y_4 \cos \psi_{\mathrm{I}}} \right] + L_{\mathrm{II}} \log \left[\frac{(b_4 + y_4 \sin \psi_{\mathrm{II}})^2 + (y_4 \cos \psi_{\mathrm{II}})^2}{\epsilon \, y_4 \cos \psi_{\mathrm{II}}} \right] \\
& + 2 \left(L_{\mathrm{I}} + L_{\mathrm{II}} \right) \log \left(\frac{b_3 - b_2}{\epsilon} \right) .
\end{aligned}
\tag{3.39}
$$

Extremizing eq. (3.39) over the bulk points y_1 and y_4, we obtain the extremal values to be

$$
y_1^* = b_1 \,, \qquad y_4^* = b_4 \,.
\tag{3.40}
$$

Substituting these in the expression for the geodesic length and subsequently using the RT formula, the entanglement entropy for the mixed state ρ_{AB} reads

$$
S \left(A \cup B \right) = \frac{L_{\mathrm{I}} + L_{\mathrm{II}}}{4 G_{\mathrm{N}}} \left[\log \left(\frac{2 b_1}{\epsilon} \right) + \log \left(\frac{2 b_4}{\epsilon} \right) + 2 \log \left(\frac{b_3 - b_2}{\epsilon} \right) \right] + \frac{\rho_{\mathrm{I}}^* + \rho_{\mathrm{II}}^*}{2 G_{\mathrm{N}}} \,,
\tag{3.41}
$$

where we have utilized the following relation between the angles ψ_k and the brane location ρ_k^* in the Poincaré slicing coordinates [20],

$$
\sec \psi_k = \cosh \left(\frac{\rho_k^*}{L_k} \right) , \qquad (k = \mathrm{I}, \mathrm{II}) .
\tag{3.42}
$$

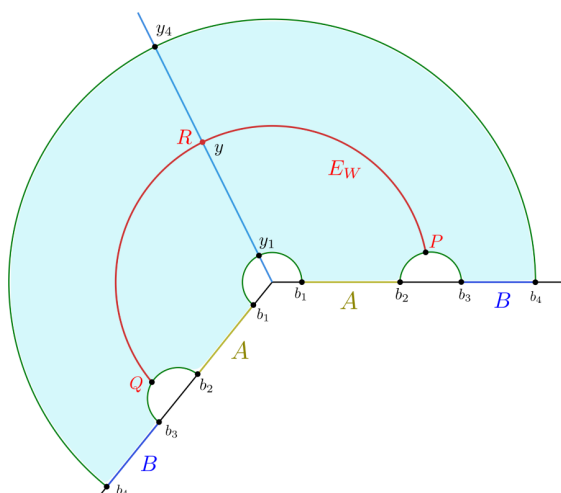[14]Here we are using the same technique described in section 3.1.1.

Figure 10. Configurations of single crossing RT saddles for two disjoint subsystems in the boundary CFT_2s.

Once we have obtained the RT saddles corresponding to the configuration of disjoint intervals, the entanglement wedge dual to the reduced density matrix can be constructed as the codimension one bulk region bounded by the RT surfaces and the subsystems on the boundary. This is shown by the shaded region in figure 10. As we shall see below, there are three possible phases of the minimal EWCS for this configuration of the RT saddles corresponding to ρ_{AB}. In the following, we will investigate the phase transition of the minimal EWCS for different sizes of A and B.

Phase-I

The first phase of EWCS corresponds to sufficiently small separations between rather large subsystems A and B in both CFT_2s (recall that, we have considered configurations of A and B to be symmetric with respect to the interface). In this case, as depicted in figure 10, the minimal EWCS connects the dome-shaped geodesics joining b_2 and b_3 on both sides of the interface by crossing the EOW brane once at the point R. The candidate EWCS depicted by the red curve in figure 10, consists of two circular geodesic arcs emanating respectively from the points P and Q on the geodesic connecting b_2 and b_3 on the $CFT_2^{II/I}$ and landing on the EOW brane at the common[15] location denoted by R. Therefore, the total length of the red curve is given by the sum of geodesic lengths as $d_{PQ} = d_{PR} + d_{QR}$. Note that the points P and Q are only constrained to be on the geodesics connecting b_2 and b_3 and hence possess a degree of arbitrariness. We set the location of P by introducing the (arbitrary) angle ϕ_{II} as sketched in figure 11 and a similar parametrization of the point Q on the other geodesic is dependent on an angle ϕ_{I}. Therefore, in the Poincaré AdS_3^{II} geometry on the right

---

[15]Note that the two geodesic segments on either sides of the brane must join smoothly at the location of the brane as discussed in [20]. We observed that the smoothness of the geodesic crossing the EOW brane is achieved naturally through the extremization of the total geodesic length with respect to the point R.
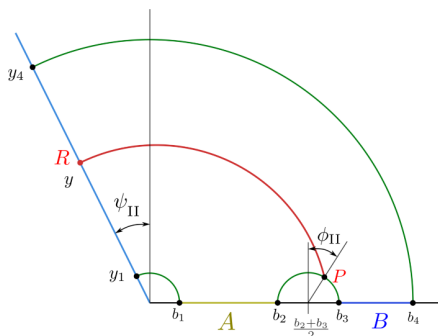
Figure 11. Disjoint intervals: phase-I.

side of the brane, the coordinate of P are obtained as

$$P : (\tau_{\mathrm{II}}, x_{\mathrm{II}}, z_{\mathrm{II}}) = \left(\tau_0, \frac{b_3 + b_2}{2} + \frac{b_3 - b_2}{2}\sin\phi_{\mathrm{II}}, \frac{b_3 - b_2}{2}\cos\phi_{\mathrm{II}}\right). \tag{3.43}$$

The coordinates of Q in $\mathrm{AdS}_3^{\mathrm{I}}$ may be found similarly. Furthermore, the Poincaré coordinates of the point R on the brane may be written as

$$\begin{aligned} R : (\tau_0, y\sin\psi_{\mathrm{I}}, y\cos\psi_{\mathrm{I}}), & \qquad\qquad \text{from } \mathrm{AdS}_3^{\mathrm{I}} \\ (\tau_0, y\sin\psi_{\mathrm{II}}, y\cos\psi_{\mathrm{II}}), & \qquad\qquad \text{from } \mathrm{AdS}_3^{\mathrm{II}} \end{aligned} \tag{3.44}$$

Therefore, utilizing eq. (3.1), we obtain the length of the candidate EWCS as follows

$$\begin{aligned} d_{PQ} = {} & L_{\mathrm{I}}\cosh^{-1}\left[\frac{\left(\frac{b_3+b_2}{2} + \frac{b_3-b_2}{2}\sin\phi_{\mathrm{I}} + y\sin\psi_{\mathrm{I}}\right)^2 + \left(\frac{b_3-b_2}{2}\cos\phi_{\mathrm{I}}\right)^2 + (y\cos\psi_{\mathrm{I}})^2}{2\left(\frac{b_3-b_2}{2}\cos\phi_{\mathrm{I}}\right)y\cos\psi_{\mathrm{I}}}\right] \\ & + L_{\mathrm{II}}\cosh^{-1}\left[\frac{\left(\frac{b_3+b_2}{2} + \frac{b_3-b_2}{2}\sin\phi_{\mathrm{II}} + y\sin\psi_{\mathrm{II}}\right)^2 + \left(\frac{b_3-b_2}{2}\cos\phi_{\mathrm{II}}\right)^2 + (y\cos\psi_{\mathrm{II}})^2}{2\left(\frac{b_3-b_2}{2}\cos\phi_{\mathrm{II}}\right)y\cos\psi_{\mathrm{II}}}\right]. \end{aligned} \tag{3.45}$$

Extremizing the above expression over the arbitrary angles ϕ_{I} and ϕ_{II}, we obtain

$$\begin{aligned} \phi_{\mathrm{I}} &= \sin^{-1}\left[\frac{(b_2 - b_3)(b_2 + b_3 + 2y\sin\psi_{\mathrm{I}})}{b_2^2 + b_3^2 + 2y^2 + 2y(b_2 + b_3)\sin\psi_{\mathrm{I}}}\right], \\ \phi_{\mathrm{II}} &= \sin^{-1}\left[\frac{(b_2 - b_3)(b_2 + b_3 + 2y\sin\psi_{\mathrm{II}})}{b_2^2 + b_3^2 + 2y^2 + 2y(b_2 + b_3)\sin\psi_{\mathrm{II}}}\right]. \end{aligned} \tag{3.46}$$

Substituting these values back and subsequently extremizing over the location y along the EOW brane, we obtain

$$\partial_y\, d_{PQ} = 0 \implies y = \sqrt{b_2 b_3}. \tag{3.47}$$

– 21 –

Finally, the minimal EWCS is obtained using eq. (3.47) as follows

$$E_W(A:B) = \frac{L_I}{4G_N} \cosh^{-1}\left[\frac{(b_2 + b_3 + 2\sqrt{b_2 b_3}\sin\psi_I)}{(b_3 - b_2)\cos\psi_I}\right]$$
$$+ \frac{L_{II}}{4G_N}\cosh^{-1}\left[\frac{(b_2 + b_3 + 2\sqrt{b_2 b_3}\sin\psi_{II})}{(b_3 - b_2)\cos\psi_{II}}\right]. \tag{3.48}$$

Using standard trigonometric identities, the above result may be re-expressed as

$$E_W(A:B) = \frac{L_I + L_{II}}{4G_N}\log\left(\frac{b_2 + b_3 + 2\sqrt{b_2 b_3}}{b_3 - b_2}\right) + \frac{L_I}{4G_N}\cosh^{-1}\left(\frac{1}{\cos\psi_I}\right)$$
$$+ \frac{L_{II}}{4G_N}\cosh^{-1}\left(\frac{1}{\cos\psi_{II}}\right). \tag{3.49}$$

Utilizing the relation between the angles ψ_k and the location of the brane ρ_k^* given in eq. (3.42), the above minimal EWCS may be written in the following instructive form

$$E_W(A:B) = \frac{L_I + L_{II}}{4G_N}\log\left(\frac{b_2 + b_3 + 2\sqrt{b_2 b_3}}{b_3 - b_2}\right) + \frac{\rho_I^* + \rho_{II}^*}{4G_N}$$
$$= \frac{c_I + c_{II}}{6}\log\left(\frac{\sqrt{b_3} + \sqrt{b_2}}{\sqrt{b_3} - \sqrt{b_2}}\right) + S_{int}, \tag{3.50}$$

where $S_{int} = \frac{\rho_I^* + \rho_{II}^*}{4G_N}$ is termed the interface entropy [20].

We now take the large tension limit, $T \to T_{max}$, and expand around $\delta \to 0$ as described in eq. (2.9). Consequently the leading order term in the interface entropy S_{int} is given by eq. (3.8).

Phase-II

Next we consider the situation when the subsystem B is small compared to both A and the separation between A and B. In this case, the minimal EWCS comprises of two separate semi-circular arcs emanating from the geodesics connecting b_2 and b_3 which lands on the RT surface connecting b_4 on either side. The schematics of the configuration is sketched in figure 12.

As seen from figure 13, the Poincaré coordinates of the points P and Q are given in eq. (3.43) while those for the point R in the AdS$_3^{II}$ geometry are parametrized by the angle ϕ_R as follows

$$R : (\tau_{II}, x_{II}, z_{II}) = (\tau_0, b_4\sin\phi_R, b_4\cos\phi_R)\ , \tag{3.51}$$

where we have utilized the fact that the radius of the circular geodesic connecting b_4 from either side is $R = b_4$, as seen from eq. (3.40). Similarly, the Poincaré coordinates of the point S on the AdS$_3^I$ geometry is given in terms of the angle ϕ_S as

$$S : (\tau_I, x_I, z_I) = (\tau_0, b_4\sin\phi_S, b_4\cos\phi_S)\ . \tag{3.52}$$
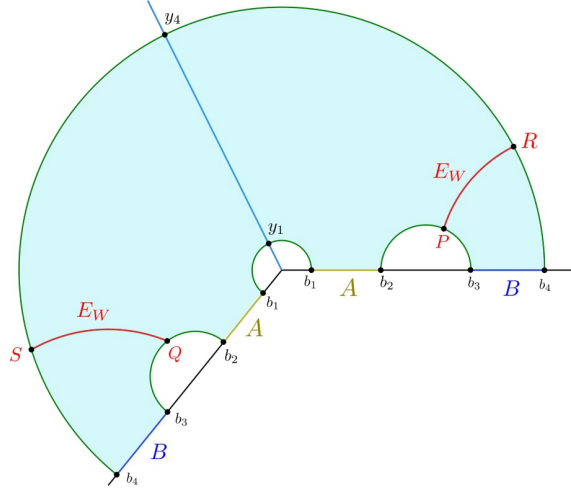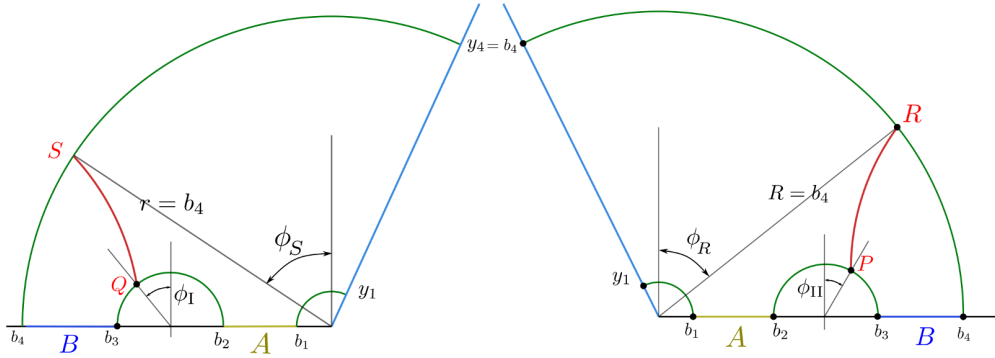
Figure 12. Disjoint intervals: phase-II.

Figure 13. Calculation of the minimal EWCS in phase-II.

Now utilizing eq. (3.1), the total length of the geodesics may be obtained as follows

$$
d_{\mathrm{II}} = d_{PR} + d_{QS}
$$

$$
= L_{\mathrm{I}} \cosh^{-1} \left[\frac{\left(b_4 \sin \phi_S - \left(\frac{b_2 + b_3}{2} + \frac{b_3 - b_2}{2} \sin \phi_{\mathrm{I}} \right) \right)^2 + \left(\frac{b_3 - b_2}{2} \cos \phi_{\mathrm{I}} \right)^2 + \left(b_4 \cos \phi_S \right)^2}{2 \left(\frac{b_3 - b_2}{2} \cos \phi_{\mathrm{I}} \right) b_4 \cos \phi_S} \right]
$$

$$
+ L_{\mathrm{II}} \cosh^{-1} \left[\frac{\left(b_4 \sin \phi_R - \left(\frac{b_2 + b_3}{2} + \frac{b_3 - b_2}{2} \sin \phi_{\mathrm{II}} \right) \right)^2 + \left(\frac{b_3 - b_2}{2} \cos \phi_{\mathrm{II}} \right)^2 + \left(b_4 \cos \phi_R \right)^2}{2 \left(\frac{b_3 - b_2}{2} \cos \phi_{\mathrm{II}} \right) b_4 \cos \phi_R} \right].
$$

(3.53)

Extremizing over the arbitrary angles ϕ_{I}, ϕ_{II}, ϕ_R, ϕ_S we obtain

$$
\phi_{\mathrm{I}} = \phi_{\mathrm{II}} = \sin^{-1} \left[\frac{b_2^2 - b_3^2}{b_2^2 + b_3^2 - 2b_4^2} \right], \qquad \phi_R = \phi_S = \sin^{-1} \left[\frac{(b_2 + b_3) b_4}{b_4^2 + b_2 b_3} \right].
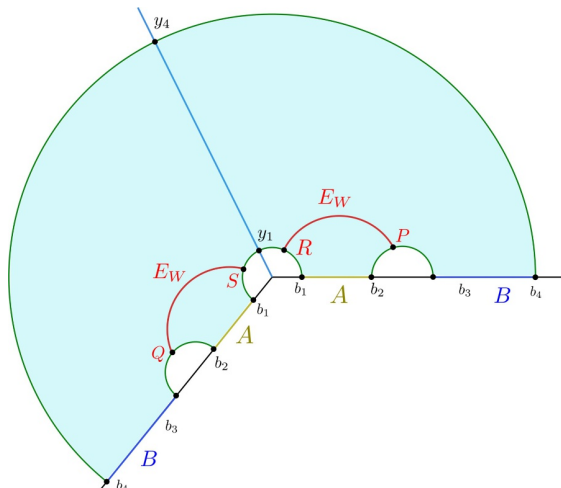$$

(3.54)

Figure 14. Disjoint intervals: phase-III.

Substituting the above extremal values in eq. (3.53), we obtain the minimal EWCS to be

$$
\begin{aligned}
E_W(A:B) &= \frac{L_\mathrm{I} + L_\mathrm{II}}{4G_\mathrm{N}} \cosh^{-1}\left[\frac{b_4^2 - b_2 b_3}{b_4(b_3 - b_2)}\right] \\
&= \frac{L_\mathrm{I} + L_\mathrm{II}}{4G_\mathrm{N}} \log\left[\frac{b_4^2 - b_2 b_3 + \sqrt{(b_4^2 - b_2^2)(b_4^2 - b_3^2)}}{b_4(b_3 - b_2)}\right].
\end{aligned}
\tag{3.55}
$$

Note that the above expression does not contain any contribution from the brane as the EWCS land on the RT surface (R and S in figure 12) connecting the b_4 points. As a result we observe the absence of any δ dependent term in the expression of minimal EWCS.

Phase-III

The last phase concerns small A and large B with a small separation between them. In this phase, the minimal EWCS is anchored on the RT surface connecting b_1 on either side as depicted in figure 14. Once again, we consider two arbitrary points R and S parametrized by the angles ϕ_R and ϕ_S, now on the smaller single crossing RT surface. The Poincaré coordinates of these points may be read off from eqs. (3.51) and (3.52) with b_4 replaced by b_1. Utilizing eq. (3.1), the total length of the candidate EWCS may be computed as follows t

$$
\begin{aligned}
d_\mathrm{III} &= d_{PR} + d_{QS} \\
&= L_\mathrm{I} \cosh^{-1}\left[\frac{\left(b_1 \sin\phi_S - \left(\frac{b_2+b_3}{2} + \frac{b_3-b_2}{2}\sin\phi_\mathrm{I}\right)\right)^2 + \left(\frac{b_3-b_2}{2}\cos\phi_\mathrm{I}\right)^2 + (b_1\cos\phi_S)^2}{2\left(\frac{b_3-b_2}{2}\cos\phi_\mathrm{I}\right)b_1\cos\phi_S}\right] \\
&\quad + L_\mathrm{II} \cosh^{-1}\left[\frac{\left(b_1 \sin\phi_R - \left(\frac{b_2+b_3}{2} + \frac{b_3-b_2}{2}\sin\phi_\mathrm{II}\right)\right)^2 + \left(\frac{b_3-b_2}{2}\cos\phi_\mathrm{II}\right)^2 + (b_1\cos\phi_R)^2}{2\left(\frac{b_3-b_2}{2}\cos\phi_\mathrm{II}\right)b_1\cos\phi_R}\right].
\end{aligned}
\tag{3.56}
$$

Extremizing over the arbitrary angles ϕ_{I}, ϕ_{II}, ϕ_R, ϕ_S we obtain

$$\phi_{\mathrm{I}} = \phi_{\mathrm{II}} = \sin^{-1}\left[\frac{b_2^2 - b_3^2}{b_2^2 + b_3^2 - 2b_1^2}\right], \qquad \phi_R = \phi_S = \sin^{-1}\left[\frac{(b_2 + b_3)\,b_1}{b_1^2 + b_2 b_3}\right]. \qquad (3.57)$$

Substituting the above extremal values in eq. (3.56), we obtain the minimal EWCS to be

$$\begin{aligned} E_W(A:B) &= \frac{L_{\mathrm{I}} + L_{\mathrm{II}}}{4G_{\mathrm{N}}} \cosh^{-1}\left[\frac{b_2 b_3 - b_1^2}{b_1\,(b_3 - b_2)}\right] \\ &= \frac{L_{\mathrm{I}} + L_{\mathrm{II}}}{4G_{\mathrm{N}}} \log\left[\frac{b_2 b_3 - b_1^2 + \sqrt{(b_2^2 - b_1^2)(b_3^2 - b_1^2)}}{b_1\,(b_3 - b_2)}\right]. \qquad (3.58) \end{aligned}$$

3.2.2 Double crossing configurations

Next, we consider configurations of the RT saddles corresponding to the entanglement entropy of $A \cup B$ such that one or more RT surfaces cross the brane twice. Within each such configuration, we will construct the bulk entanglement wedge dual to ρ_{AB} and systematically investigate the phase transitions of the minimal EWCS for different subsystem sizes and the geometry. To proceed, we further divide the possible RT saddles into two sub-classes. First we consider the RT surfaces homologous to $C = [b_2, b_3]_{\mathrm{I}} \cup [b_2, b_3]_{\mathrm{II}}$ which do not cross the brane. In the second case we explore the possibility of C owning an island by considering the RT surfaces homologous to C which crosses the brane and comes back.[16]

A. RT surfaces homologous to C which do not cross the brane

We begin with the configuration where in the $\mathrm{AdS}_3^{\mathrm{II}}$ geometry, the geodesics homologous to the intervals $[b_1, b_2]_{\mathrm{I}} \cup [b_3, b_4]_{\mathrm{II}}$ in the $\mathrm{CFT}_2^{\mathrm{II}}$ have the following topology:

- the geodesic connecting b_1 and b_4 crosses the EOW brane twice at the bulk points distant $\bar{y}_1^*$ and $\bar{y}_4^*$ along the brane from the interface. In other words, the geodesic is made up of three semi-circular segments, one of which resides entirely in the $\mathrm{AdS}_3^{\mathrm{I}}$ geometry. Note that the locations of the points $\bar{y}_1^*$ and $\bar{y}_4^*$ on the EOW brane should be determined by solving the extremization conditions[17] given in eq. (3.22) and $\bar{y}_1 = \frac{b_1}{k_{ABC}}$. We note that such configurations occur when Θ_{ABC} is larger than a critical value [20].

- the geodesic semi-circle connecting b_2 and b_3 never crosses the brane and has a dome like structure.

On the other hand, the geodesics homologous to the subsystems in the $\mathrm{CFT}_2^{\mathrm{I}}$ consist of single semi-circles and have the topology of a dome. The schematics of this configuration is sketched in figure 15. The bulk entanglement wedge is the region of the spacetime bounded

---

[16]There is yet another possibility where both the RT surfaces homologous to C and ABC has a double crossing topology. However, we have checked numerically that this situation fails to arise for a sufficiently large range of parameter values and hence in the following we shall drop this possibility from our discussion.

[17]In this case, as is clear from the context, the parameters Θ_D and k_D in eq. (3.22) should be replaced by $\Theta_{ABC} = \frac{b_4}{b_1}$ and $k_{ABC} = \sqrt{\frac{y_4}{\Theta_{ABC} y_1}}$ respectively.
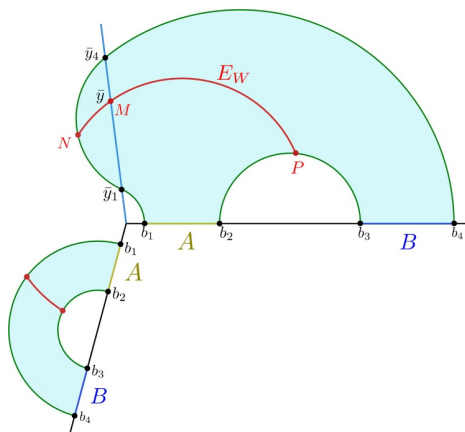
Figure 15. Disjoint intervals: double-crossing phase-I.

by these geodesics and the corresponding subsystems as shown by the shaded regions in figure 15. The entanglement entropy for $A \cup B$ in this phase is given by

$$S(A \cup B) = S_{\text{double}}\left([b_1, b_4]\right) + \frac{L_{\text{I}} + L_{\text{II}}}{2G_{\text{N}}} \log\left(\frac{b_3 - b_2}{\epsilon}\right) + \frac{L_{\text{I}}}{2G_{\text{N}}} \log\left(\frac{b_4 - b_1}{\epsilon}\right), \qquad (3.59)$$

where S_{double} is defined in eq. (3.23).

The minimal EWCS for this configuration consists of two extremal curves, one of which resides entirely in the AdS_3^{I} geometry and corresponds to the usual notion of EWCS in standard $\text{AdS}_3/\text{CFT}_2$ scenario. The minimal EWCS residing entirely in the AdS_3^{I} region may be computed using the standard $\text{AdS}_3/\text{CFT}_2$ techniques [25, 44] and the result reads as

$$E_W^{\text{I}}(A : B) = \frac{L_{\text{I}}}{4G_{\text{N}}} \log\left[1 + 2\eta + 2\sqrt{\eta(\eta + 1)}\right], \qquad (3.60)$$

where the cross-ratio η is given by

$$\eta = \frac{(b_2 - b_1)(b_4 - b_3)}{(b_3 - b_2)(b_4 - b_1)}. \qquad (3.61)$$

On the other hand, there are three possible choices for the other extremal curve which we shall consider below.

Phase-I

In the first phase, we allow the candidate extremal curve for the minimal EWCS originating in the AdS_3^{II} geometry to cross the brane and probe the geometry beyond the "end of the world". This phase occurs when the sizes of the subsystems A and B are comparable. The schematics of this configuration is sketched in figure 15. To compute the length of this candidate extremal curve, note that it consists of two circular geodesic segments joined smoothly at the location of the brane. The segment MP starts from the point P on the dome shaped RT surface connecting b_2 and b_3 and ends on the EOW brane at the point M on the EOW brane which is at a distance $\bar{y}$ from the interface O. The other circular arc MN ends on the geodesic segment which connects the bulk points $\bar{y}_1$ and $\bar{y}_4$. Therefore, the total length of this surface is given
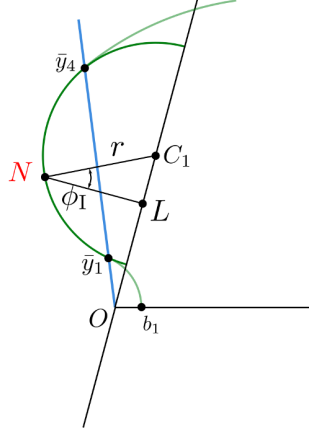
Figure 16. Computation of the minimal EWCS for the disjoint intervals in double-crossing phase-I.

by $d_{NP} = d_{MP} + d_{MN}$. The Poincaré coordinates of the points P and M may be read off from eqs. (3.43) and (3.44). To obtain the coordinates of the point N, consider the diagram in figure 16, where r and x_0 are the radius and center coordinates of the circular arc connecting $\bar{y}_1$ and $\bar{y}_4$, and the arbitrary angle ϕ_{I} parametrizes the position of N on this circular arc.

From figure 16, the Poincaré coordinates of N may be read off as

$$N : (x_{\mathrm{I}}, z_{\mathrm{I}}) = \left(\overline{C_1 L}, \overline{NL}\right) = \left(\overline{OC_1} - \overline{OL}, \overline{NL}\right) = (x_0 - r \sin\phi_{\mathrm{I}}, r \cos\phi_{\mathrm{I}}) , \qquad (3.62)$$

where the center and the radius of the circular arc are given as

$$r = \frac{\sqrt{\bar{y}_1^{*2} + \bar{y}_4^{*2} + 2\bar{y}_1^* \bar{y}_4^* \cos(2\psi_{\mathrm{I}})}}{2 \sin\psi_{\mathrm{I}}} , \qquad x_0 = \frac{\bar{y}_1^* + \bar{y}_4^*}{2 \sin\psi_{\mathrm{I}}} . \qquad (3.63)$$

Now utilizing the length formula in eq. (3.1), we may obtain the length of the candidate EWCS as follows

$$d_{NP} = L_{\mathrm{II}} \cosh^{-1} \left[\frac{\left(\frac{b_3+b_2}{2} + \frac{b_3-b_2}{2} \sin\phi_{\mathrm{II}} + \bar{y} \sin\psi_{\mathrm{II}}\right)^2 + \left(\frac{b_3-b_2}{2} \cos\phi_{\mathrm{II}}\right)^2 + (\bar{y} \cos\psi_{\mathrm{II}})^2}{2 \left(\frac{b_3-b_2}{2} \cos\phi_{\mathrm{II}}\right) \bar{y} \cos\psi_{\mathrm{II}}} \right]$$

$$+ L_{\mathrm{I}} \cosh^{-1} \left[\frac{(x_0 - r \sin\phi_{\mathrm{I}} - \bar{y} \sin\psi_{\mathrm{I}})^2 + (\bar{y} \cos\psi_{\mathrm{I}})^2 + (r \cos\phi_{\mathrm{I}})^2}{2 (\bar{y} \cos\psi_{\mathrm{I}}) (r \cos\phi_{\mathrm{I}})} \right] . \qquad (3.64)$$

Extremizing the above length over ϕ_{I} and ϕ_{II}, we obtain the following extremal values

$$\phi_{\mathrm{I}} = \sin^{-1} \left[\frac{2r(x_0 - \bar{y} \sin\psi_{\mathrm{I}})}{r^2 + x_0^2 - 2x_0 \bar{y} \sin\psi_{\mathrm{I}} + \bar{y}^2} \right]$$

$$\phi_{\mathrm{II}} = \sin^{-1} \left[\frac{(b_2 - b_3)(b_2 + b_3 + 2\bar{y} \sin\psi_{\mathrm{II}})}{b_2^2 + b_3^2 + 2\bar{y}^2 + 2\bar{y}(b_2 + b_3) \sin\psi_{\mathrm{II}}} \right] . \qquad (3.65)$$

Substituting these and subsequently extremizing over the remaining parameter $\bar{y}$, we obtain

$$\frac{L_{\mathrm{I}} \left(r^2 - x_0^2 + \bar{y}^2\right)}{\bar{y} \sqrt{\left(r^2 - 2x_0 \bar{y} \sin\psi_{\mathrm{I}} + x_0^2 + \bar{y}^2\right)^2 - 4r^2 \left(x_0 - \bar{y} \sin\psi_{\mathrm{I}}\right)^2}}$$

$$= \frac{L_{\mathrm{II}} \left(\bar{y}^2 - b_2 b_3\right)}{\bar{y} \sqrt{\left(2b_2 \bar{y} \sin\psi_{\mathrm{II}} + b_2^2 + \bar{y}^2\right) \left(2b_3 \bar{y} \sin\psi_{\mathrm{II}} + b_3^2 + \bar{y}^2\right)}} . \qquad (3.66)$$
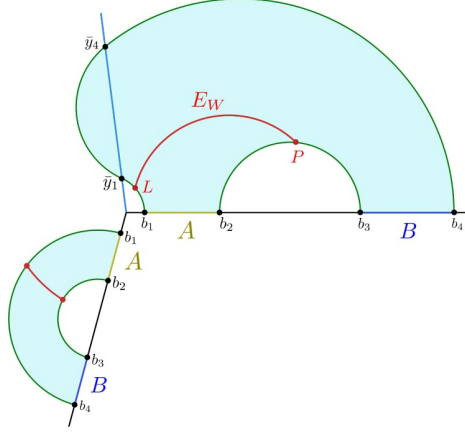
Figure 17. Disjoint intervals: double-crossing phase-II.

The algebraic equation in eq. (3.66) may now be solved for $\bar{y}$ and the corresponding extremal value $\bar{y} = \bar{y}^*$ determines the minimal EWCS to be

$$
\begin{aligned}
E_W(A:B) &= \frac{L_{\text{II}}}{4G_{\text{N}}} \cosh^{-1}\left[\frac{\sqrt{(\bar{y}^{*2} + b_2^2 + 2b_2\bar{y}^*\sin\psi_{\text{II}})(\bar{y}^{*2} + b_3^2 + 2b_3\bar{y}^*\sin\psi_{\text{II}})}}{\bar{y}^*(b_3 - b_2)\cos\psi_{\text{II}}}\right] \\
&+ \frac{L_{\text{I}}}{4G_{\text{N}}} \cosh^{-1}\left[\frac{\sqrt{(r^2 - 2x_0\bar{y}^*\sin\psi_{\text{I}} + x_0^2 + \bar{y}^{*2})^2 - 4r^2(x_0 - \bar{y}^*\sin\psi_{\text{I}})^2}}{2\bar{y}^* r\cos\psi_{\text{I}}}\right] \\
&+ \frac{L_{\text{I}}}{4G_{\text{N}}} \log\left[1 + 2\eta + 2\sqrt{\eta(\eta+1)}\right],
\end{aligned}
\tag{3.67}
$$

where we have included the contribution from the left geometry in the final expression. In the large tension limit $\delta \to 0$, the extremization condition in eq. (3.66) reduces to

$$
\frac{L_{\text{II}}(\bar{y}^2 - b_2 b_3)}{(b_2 + \bar{y})(b_3 + \bar{y})} + L_{\text{I}}\left(\frac{\bar{y}}{\bar{y} - \bar{y}_4^*} + \frac{\bar{y}_1^*}{\bar{y} - \bar{y}_1^*}\right) = 0.
\tag{3.68}
$$

Substituting the extremal value $\bar{y} = \bar{y}^*$, the EWCS may now be obtained in the large tension limit to be

$$
\begin{aligned}
E_W(A:B) &= \frac{L_{\text{I}}}{4G_{\text{N}}} \log\left[\frac{(\bar{y}_4^* - \bar{y}^*)(\bar{y}^* - \bar{y}_1^*)}{\bar{y}^*(\bar{y}_4^* - \bar{y}_1^*)}\right] + \frac{L_{\text{II}}}{4G_{\text{N}}} \log\left[\frac{(\bar{y}^* + b_2)(\bar{y}^* + b_3)}{\bar{y}^*(b_3 - b_2)}\right] + S_{\text{int}}^{(\delta)} \\
&+ \frac{L_{\text{I}}}{4G_{\text{N}}} \log\left[1 + 2\eta + 2\sqrt{\eta(\eta+1)}\right],
\end{aligned}
\tag{3.69}
$$

where $S_{\text{int}}^{(\delta)}$ is the $\delta \to 0$ limit of the interface entropy, defined in eq. (3.8).

Phase-II

In the next phase, when the size of the subsystem A is small compared to that of B, the minimal EWCS ends on the smaller segment of the double crossing RT surface anchored on b_1, as depicted in figure 17.

To compute the length of the minimal EWCS we consider a candidate surface which ends on an arbitrary point K parametrized by an angle ϕ_K, on the segment of the RT surface anchored on b_1. From figure 18, the Poincaré coordinates of the point K may be read off as follows

$$K : (x_{\mathrm{II}}, z_{\mathrm{II}}) = \left(\overline{OT}, \overline{TK}\right) = \left(\overline{C_1 T} - \overline{OC_1}, \overline{TK}\right) = (r_1 \sin \phi_K - x_{C_1}, r_1 \cos \phi_K) , \quad (3.70)$$

where the radius r_1 and the center coordinate $|x_{C_1}|$ of the circular geodesic connecting b_1 and $\bar{y}_1^*$ are given by

$$r_1 = b_1 + x_{C_1} , \qquad x_{C_1} = -\frac{\bar{y}_1^{*2} - b_1^2}{2\left(b_1 + \bar{y}_1^* \sin\left(\psi_{\mathrm{II}}\right)\right)} . \quad (3.71)$$

The other endpoint of the candidate EWCS may be parametrized by another arbitrary angle ϕ_{II} similar to eq. (3.43). Now, utilizing, the general formula for the geodesic length in eq. (3.1), we may obtain the length of the candidate surface as follows

$$d_{PK} = L_{\mathrm{II}} \cosh^{-1} \left[\frac{\left(x_{C_1} - r_1 \sin \phi_K + \frac{b_2 + b_3}{2} + \frac{b_3 - b_2}{2} \sin \phi_{\mathrm{II}}\right)^2 + \left(\frac{b_3 - b_2}{2} \cos \phi_{\mathrm{II}}\right)^2 + (r_1 \cos \phi_K)^2}{2 \left(\frac{b_3 - b_2}{2} \cos \phi_{\mathrm{II}}\right) r_1 \cos \phi_K}\right] . \quad (3.72)$$

Extremizing the above length over the arbitrary angles ϕ_{II} and ϕ_K, we obtain the extremal solutions to be

$$\phi_K = \sin^{-1} \left[\frac{r_1 \left(b_2 + b_3 + 2x_{C_1}\right)}{r_1^2 + \left(b_2 + x_{C_1}\right)\left(b_3 + x_{C_1}\right)}\right]$$

$$\phi_{\mathrm{II}} = \sin^{-1} \left[\frac{\left(b_2 - b_3\right)\left(b_2 + b_3 + 2x_{C_1}\right)}{-2r_1^2 + b_2^2 + b_3^2 + 2\left(b_2 + b_3\right) x_{C_1} + 2x_{C_1}^2}\right] . \quad (3.73)$$

Substituting these in eq. (3.72) the minimal EWCS is obtained as follows

$$\begin{aligned} E_W(A:B) &= \frac{L_{\mathrm{I}}}{4G_{\mathrm{N}}} \log\left[1 + 2\eta + 2\sqrt{\eta(\eta+1)}\right] + \frac{L_{\mathrm{II}}}{4G_{\mathrm{N}}} \cosh^{-1}\left[\frac{r_1^2 - \left(x_{C_1} + b_2\right)\left(x_{C_1} + b_3\right)}{r_1 \left(b_3 - b_2\right)}\right] \\ &= \frac{L_{\mathrm{I}}}{4G_{\mathrm{N}}} \log\left[1 + 2\eta + 2\sqrt{\eta(\eta+1)}\right] \\ &\quad + \frac{L_{\mathrm{II}}}{4G_{\mathrm{N}}} \cosh^{-1}\left[\frac{2\left(b_1^2 - b_2 b_3\right) \bar{y}_1^* \sin \psi_{\mathrm{II}} + b_1 \left(b_1 \left(b_2 + b_3\right) - 2b_2 b_3\right) + \left(2b_1 - b_2 - b_3\right) \bar{y}_1^{*2}}{\left(b_3 - b_2\right)\left(2b_1 \bar{y}_1^* \sin \psi_{\mathrm{II}} + b_1^2 + \bar{y}_1^{*2}\right)}\right] . \end{aligned} \quad (3.74)$$

In the above expression, we have included the contribution from the left geometry as well. In the $\delta \to 0$ limit, the minimal EWCS reduces to

$$E_W(A:B) = \frac{L_{\mathrm{I}}}{4G_{\mathrm{N}}} \log\left[1 + 2\eta + 2\sqrt{\eta(\eta+1)}\right] + \frac{L_{\mathrm{II}}}{4G_{\mathrm{N}}} \cosh^{-1}\left[1 + 2\frac{\left(b_1 - b_2\right)\left(b_3 + \bar{y}_1^*\right)}{\left(b_2 - b_3\right)\left(b_1 + \bar{y}_1^*\right)}\right] . \quad (3.75)$$
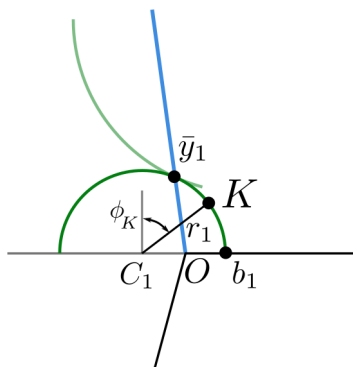
Figure 18. Computation of the minimal EWCS for two disjoint subsystems in double-crossing phase-II.
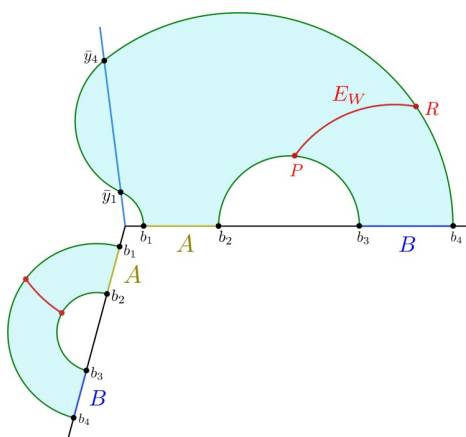

Figure 19. Disjoint intervals: double-crossing phase-III.

Phase-III

The final phase of the EWCS considering the present structure of the entanglement entropy of $A \cup B$ concerns a geodesic in the $\mathrm{AdS}_3^{\mathrm{II}}$ geometry, emanating from the dome connecting b_2 and b_3 and ending on the larger segment of the double crossing RT surface anchored on b_4. The schematics of the configuration is depicted in figure 19.

The radius r_2 and the coordinate of the center of the circular geodesic segment connecting b_4 and $\bar{y}_4^*$ are given by

$$r_2 = b_4 + x_{C_2}, \qquad x_{C_2} = \frac{b_4^2 - \bar{y}_4^{*2}}{2\left(\bar{y}_4^* \sin\left(\psi_{\mathrm{II}}\right) + b_4\right)}. \tag{3.76}$$

The computation of the length of the minimal EWCS follows very closely the analysis in the previous subsection and hence we skip the details here. The minimal EWCS, including the contribution from the left geometry, is then given by

$$E_W(A:B) = \frac{L_{\mathrm{I}}}{4G_{\mathrm{N}}} \cosh^{-1}\left[1 + 2\eta\right] + \frac{L_{\mathrm{II}}}{4G_{\mathrm{N}}} \cosh^{-1}\left[\frac{r_2^2 - (x_{C_2} - b_2)(x_{C_2} - b_3)}{r_2(b_3 - b_2)}\right]. \tag{3.77}$$
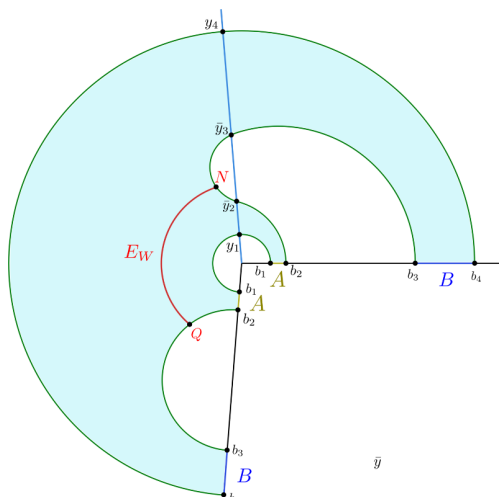
– 30 –

Figure 20. Disjoint intervals: double-crossing phase-IV.

In the large tension limit, the above expression simplifies to

$$E_W(A:B) = \frac{L_\mathrm{I}}{4G_\mathrm{N}} \log\left[1 + 2\eta + 2\sqrt{\eta(\eta+1)}\right] + \frac{L_\mathrm{II}}{4G_\mathrm{N}} \cosh^{-1}\left[1 + 2\frac{(b_3 - b_4)(b_2 + \bar{y}_4^*)}{(b_2 - b_3)(b_4 + \bar{y}_4^*)}\right].$$

(3.78)

B. Double crossing RT surface for subsystem C

Next we consider another phase for the RT saddles corresponding to the entanglement entropy of $A \cup B$ sketched in figure 20. In this phase, there exists a double crossing RT surface homologous to the interval $[b_2, b_3]_\mathrm{II}$ on the $\mathrm{CFT}_2^\mathrm{II}$, which crosses the EOW brane twice at the bulk points $\bar{y}_2^*$ and $\bar{y}_3^*$ respectively. This phase becomes dominant when $\Theta_C = \frac{b_3}{b_2}$ is greater than its critical value. The locations of these bulk points are determined by solving the extremization condition in eq. (3.22) together with $\bar{y}_2 = \frac{b_2}{k_C}$, where $k_C^2 = \frac{\bar{y}_3}{\Theta_C \bar{y}_2}$.

This configuration may be understood from the single-crossing one in figure 10 as the dome shaped geodesic connecting b_2 and b_3 undergoes a phase transition to a double-crossing one. Recall that, as determined earlier, the single crossing geodesics in figure 10 cross the EOW brane at the bulk points $y_1^* = b_1$ and $y_4^* = b_4$ respectively. Therefore, in this phase, the entanglement entropy of $A \cup B$ is given by

$$S(A \cup B) = S_\mathrm{double}([b_2, b_3]) + \frac{L_\mathrm{I} + L_\mathrm{II}}{4G_\mathrm{N}}\left[\log\left(\frac{2b_1}{\epsilon}\right) + \log\left(\frac{2b_4}{\epsilon}\right)\right] + \frac{\rho_\mathrm{I}^* + \rho_\mathrm{II}^*}{2G_\mathrm{N}}.$$

(3.79)

The entanglement wedge dual to the density matrix ρ_{AB} is depicted by the shaded region in figure 20. Within this phase of $S(A \cup B)$, the minimal EWCS can undergo phase transitions depending upon the subsystem sizes and their relative distances from the interface. Note that, in principle, segments of the candidate curves for the EWCS may penetrate into the $\mathrm{AdS}_3^\mathrm{II}$ geometry. However, similar to [20], we may argue that passing through the geometry which is less curved (recall that $L_\mathrm{II} > L_\mathrm{I}$) increases the total length. Hence, we may conclude that the minimal curves reside within the $\mathrm{AdS}_3^\mathrm{I}$ geometry and never probe the $\mathrm{AdS}_3^\mathrm{II}$ as depicted in figures 20 to 22.

Phase-IV

In the first phase sketched in figure 20, the EWCS is given by the minimal geodesic between the double crossing RT surface emanating from the right asymptotic boundary and the dome-shaped RT surface connecting b_2 and b_3 on the left asymptotic boundary. We may parametrize an arbitrary point N on the double-crossing geodesic by the angle ϕ_N, similar to eq. (3.62), with the radius and center coordinate of the semi-circular arc in AdS_3^{I} given as follows

$$r = \frac{\sqrt{\bar{y}_2^{*2} + \bar{y}_3^{*2} + 2\bar{y}_3^*\bar{y}_2^* \cos(2\psi_1)}}{2\sin(\psi_1)}, \qquad x_0 = \frac{\bar{y}_2^* + \bar{y}_3^*}{2\sin(\psi_1)}. \tag{3.80}$$

On the other hand the Poincaré coordinates of the arbitrary point Q on the dome-shaped RT in the left geometry are given in eq. (3.43) with ϕ_{II} replaced by ϕ_Q. Therefore, utilizing the formula in eq. (3.1), the length of this candidate surface may be computed as follows

$$d_{NQ} = L_{\text{I}} \cosh^{-1}\left[\frac{\left(\frac{b_3+b_2}{2} + \frac{b_3-b_2}{2}\sin\phi_Q + x_0 - r\sin\phi_N\right)^2 + \left(\frac{b_3-b_2}{2}\cos\phi_Q\right)^2 + (r\cos\phi_N)^2}{2\left(\frac{b_3-b_2}{2}\cos\phi_Q\right)r\cos\phi_N}\right]. \tag{3.81}$$

Extremizing over the arbitrary angles ϕ_N and ϕ_Q, we obtain the extremal values to be

$$\phi_N = \sin^{-1}\left[\frac{r(b_2 + b_3 + 2x_0)}{(b_2 + x_0)(b_3 + x_0) + r^2}\right]$$

$$\phi_Q = \sin^{-1}\left[\frac{(b_2 - b_3)(b_2 + b_3 + 2x_0)}{2(b_2 + b_3)x_0 + b_2^2 + b_3^2 - 2r^2 + 2x_0^2}\right]. \tag{3.82}$$

Substituting these in the expression for the length, we obtain the minimal EWCS to be

$$E_W(A:B) = \frac{L_{\text{I}}}{4G_{\text{N}}}\cosh^{-1}\left[\frac{(b_2 + x_0)(b_3 + x_0) - r^2}{(b_3 - b_2)r}\right]$$

$$= \frac{L_{\text{I}}}{4G_{\text{N}}}\cosh^{-1}\left[\frac{2(b_2 b_3 + \bar{y}_2^*\bar{y}_3^*)\sin(\psi_1) + (b_2 + b_3)(\bar{y}_2^* + \bar{y}_3^*)}{(b_3 - b_2)\sqrt{\bar{y}_2^{*2} + \bar{y}_3^{*2} + 2\bar{y}_3^*\bar{y}_2^* \cos(2\psi_1)}}\right]. \tag{3.83}$$

In the limit of large brane tension $\delta \to 0$, the above expression reduces to

$$E_W(A:B) = \frac{L_{\text{I}}}{4G_{\text{N}}}\log\left[1 + 2\zeta + 2\sqrt{\zeta(\zeta + 1)}\right], \tag{3.84}$$

where the cross-ratio ζ is given by

$$\zeta = \frac{(b_3 + \bar{y}_2^*)(b_2 + \bar{y}_3^*)}{(b_3 - b_2)(\bar{y}_2^* - \bar{y}_3^*)}. \tag{3.85}$$

Phase-V

Next, we consider the configuration where the candidate EWCS comprises of two disconnected geodesic segments one of which connects the double crossing RT surface and the bigger single crossing one connecting b_4 on either side. On the other hand, the second segment connects the dome shaped RT surface and the bigger single crossing one. The schematics of the configuration is depicted in figure 21.
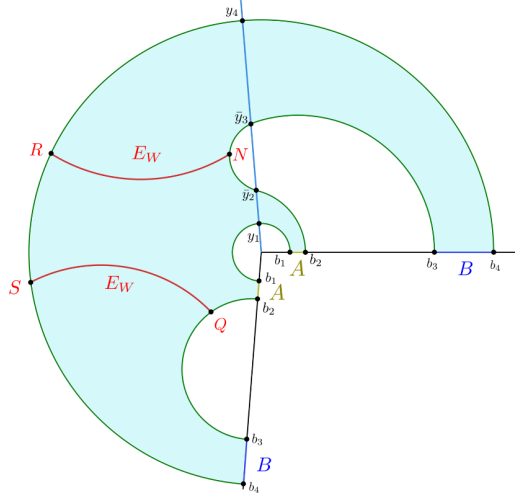
Figure 21. Disjoint intervals: double-crossing phase-V.

As described earlier, we may parametrize the endpoints of these geodesic segments on the double crossing and dome-shaped RT surfaces similar to eqs. (3.43) and (3.62). Furthermore, recall that the single crossing RT surface cross the EOW brane at $y_4^* = b_4$ and hence the endpoints of the geodesic segments on this surface may be parametrized as in eq. (3.52). Therefore, utilizing eq. (3.1), the total length of the two geodesics segments in figure 21 may be computed as follows

$$
\begin{aligned}
d &= d_{NR} + d_{QS} \\
&= L_{\mathrm{I}} \cosh^{-1}\left[\frac{(x_0 - r\sin\phi_{\mathrm{N}} + b_4\sin\phi_R)^2 + (r\cos\phi_{\mathrm{N}})^2 + (b_4\cos\phi_R)^2}{2rb_4\cos\phi_{\mathrm{N}}\cos\phi_R} \right] \\
&\quad + L_{\mathrm{I}} \cosh^{-1}\left[\frac{\left(b_4\sin\phi_S - \left(\frac{b_2+b_3}{2} + \frac{b_3-b_2}{2}\sin\phi_Q\right)\right)^2 + \left(\frac{b_3-b_2}{2}\cos\phi_Q\right)^2 + (b_4\cos\phi_S)^2}{2\left(\frac{b_3-b_2}{2}\cos\phi_Q\right)b_4\cos\phi_S} \right].
\end{aligned}
$$

(3.86)

Extremizing over the arbitrary angles ϕ_{N}, ϕ_Q, ϕ_R and ϕ_S, we obtain

$$
\phi_R = -\sin^{-1}\left[\frac{2b_4x_0}{-r^2+b_4^2+x_0^2}\right], \qquad \phi_{\mathrm{N}} = \sin^{-1}\left[\frac{2rx_0}{r^2-b_4^2+x_0^2}\right]
$$

$$
\phi_Q = \sin^{-1}\left[\frac{b_2^2-b_3^2}{b_2^2+b_3^2-2b_4^2}\right], \qquad \phi_S = \sin^{-1}\left[\frac{(b_2+b_3)b_4}{b_4^2+b_2b_3}\right].
$$

(3.87)

Substituting these extremal values, we obtain the minimal EWCS to be

$$
\begin{aligned}
E_W(A:B) &= \frac{L_{\mathrm{I}}}{4G_{\mathrm{N}}}\left(\cosh^{-1}\left[\frac{b_4^2-b_2b_3}{(b_3-b_2)b_4}\right] + \cosh^{-1}\left[\frac{2rb_4}{r^2+b_4^2-x_0^2}\right]\right) \\
&= \frac{L_{\mathrm{I}}}{4G_{\mathrm{N}}}\left(\cosh^{-1}\left[\frac{b_4^2-b_2b_3}{(b_3-b_2)b_4}\right] + \cosh^{-1}\left[\frac{\sin\psi_{\mathrm{I}}\,(b_4^2-\bar{y}_2^*\bar{y}_3^*)}{b_4\sqrt{2\bar{y}_3^*\bar{y}_2^*\cos(2\psi_{\mathrm{I}})+\bar{y}_2^{*2}+\bar{y}_3^{*2}}}\right]\right).
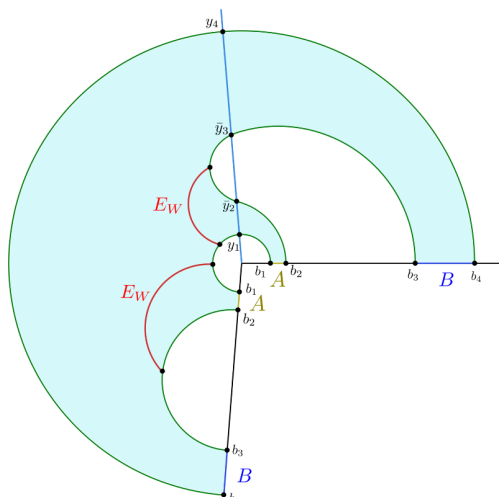\end{aligned}
$$

(3.88)

Figure 22. Disjoint intervals: double-crossing phase-VI.

In the $\delta \to 0$ limit, the above expression reduces to

$$E_W(A:B) = \frac{L_I}{4G_N} \left(\cosh^{-1}\left[\frac{b_4^2 - b_2 b_3}{(b_3 - b_2)\, b_4} \right] + \log\left[1 + 2\xi + 2\sqrt{\xi(\xi+1)} \right] \right) \tag{3.89}$$

where the cross ratio ξ is given by

$$\xi = \frac{(b_4 - \bar{y}_2^*)(b_4 + \bar{y}_3^*)}{2b_4\,(\bar{y}_2^* - \bar{y}_3^*)}. \tag{3.90}$$

Phase-VI

There is one more possibility for the EWCS where two disconnected geodesic segments land on the smaller single crossing RT surface, as depicted in figure 22. The computation of the lengths are similar to that in the previous subsection and we may obtain the expression from eq. (3.88) via the replacement $b_4 \to b_1$ as follows

$$E_W(A:B) = \frac{L_I}{4G_N} \left(\cosh^{-1}\left[\frac{b_2 b_3 - b_1^2}{(b_3 - b_2)\, b_1} \right] + \cosh^{-1}\left[\frac{\sin\psi_I \,(b_1^2 - \bar{y}_2^* \bar{y}_3^*)}{b_1 \sqrt{2\bar{y}_3^* \bar{y}_2^* \cos(2\psi_I) + \bar{y}_2^{*2} + \bar{y}_3^{*2}}} \right] \right). \tag{3.91}$$

In the large tension limit $(\delta \to 0)$, the above expression reduces to

$$E_W(A:B) = \frac{L_I}{4G_N} \left(\cosh^{-1}\left[\frac{b_2 b_3 - b_1^2}{(b_3 - b_2)\, b_1} \right] + \cosh^{-1}\left[\frac{b_1^2 - \bar{y}_2^* \bar{y}_3^*}{b_1\,(\bar{y}_2^* - \bar{y}_3^*)} \right] \right). \tag{3.92}$$

RT saddles with no brane crossing

Finally, we consider the simplest RT saddle homologous to $A \cup B$ which never cross the EOW brane and has dome-shaped structures in each AdS$_3$ geometry as sketched in figure 23. Once again, we only consider the configuration with a connected (though disjoint into two parts in
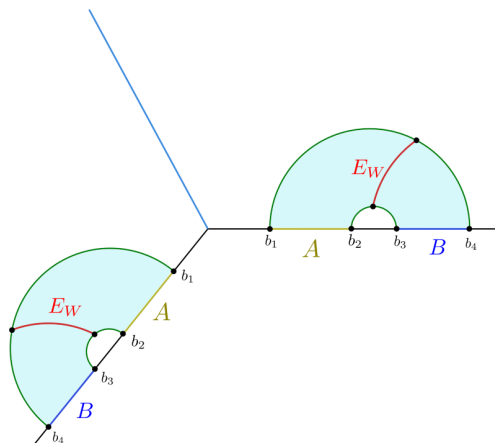
Figure 23. Disjoint intervals: EWCS without brane-crossing.

each spacetime) entanglement wedge. The corresponding entanglement wedge cross-section may be computed utilizing standard AdS_3/CFT_2 techniques as follows [25, 44]

$$E_W(A:B) = \frac{L_{\mathrm{I}} + L_{\mathrm{II}}}{4G_{\mathrm{N}}} \log\left[1 + 2\eta + 2\sqrt{\eta(\eta+1)}\right], \qquad (3.93)$$

where the cross-ratio η is given in eq. (3.61).

4 Reflected entropy from island prescription: vacuum state

In this section, we will discuss the effective lower dimensional perspective of the setup where the gravitational theory on the brane is coupled to two non-gravitating bath CFT_2s. As described in [20], the gravitational theory on the brane in the effective intermediate picture is obtained by integrating out the bulk AdS_3 degrees of freedom on either side of the brane.

In the large tension limit $T \to T_{\max}$, the theory on the brane is given by two CFT_2s coupled to the weakly fluctuating (AdS_2) metric. The nature of the CFTs on the brane also follows from the dimensional reduction of the bulk geometry. In the large tension regime, we obtain a non-local action [8, 48] which may be rewritten in terms of the Polyakov action by introducing two auxiliary fields φ_k ($k = \mathrm{I}, \mathrm{II}$) as follows [20, 21]:

$$I = \sum_{k=\mathrm{I},\mathrm{II}} \frac{L_k}{32\pi G_{\mathrm{N}}} \int_\Sigma \mathrm{d}^2 y \sqrt{-h} \left[-\frac{1}{2} h^{ab} \nabla_a \varphi_k \nabla_b \varphi_k + \varphi_k R^{(2)} - \frac{2}{L_k} e^{-\varphi_k} \right], \qquad (4.1)$$

where h_{ab} is the induced metric on the brane and $R^{(2)}$ is the corresponding Ricci scalar. The above Polyakov action may be interpreted as two CFT_2s with central charges $c_k = \frac{3L_k}{4G_{\mathrm{N}}}$ located on the AdS_2 brane Σ. Hence, as advocated in [20], we have two CFT_2s on the whole real line interacting through the common metric on the AdS_2 brane and decoupled on the other halves as depicted in figure 24. This constitutes the setup of a QFT coupled to gravity on a hybrid manifold, usual in the island paradigm [3, 4, 49, 50].
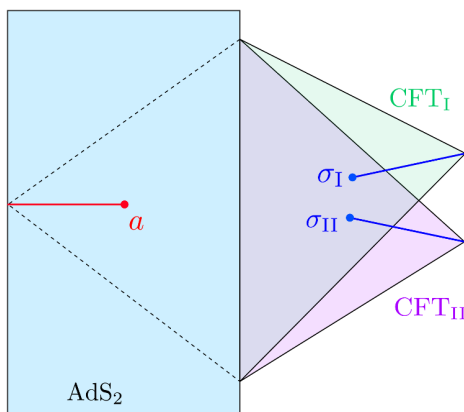
Figure 24. Two-dimensional effective model obtained from integrating out the three-dimensional bulk geometry in the AdS/ICFT model. Figure modified from [20].

From the Polyakov action eq. (4.1), the transverse area term of a co-dimension two surface χ appearing in the island formula may be obtained as follows [21, 48]

$$
\frac{\mathrm{Area}(\chi)}{4G_{\mathrm{N}}^{(2)}} = \frac{1}{8G_{\mathrm{N}}} \sum_{k=\mathrm{I,II}} L_k \, \varphi_k(\chi) = \frac{1}{8G_{\mathrm{N}}} \sum_{k=\mathrm{I,II}} L_k \log\left[-\frac{2}{L_k^2 \, R^{(2)}} \right]
$$
$$
= \frac{c_{\mathrm{I}}}{6} \log\left(\frac{1}{\cos\psi_{\mathrm{I}}} \right) + \frac{c_{\mathrm{II}}}{6} \log\left(\frac{1}{\cos\psi_{\mathrm{II}}} \right) \equiv \Phi_0 \,, \tag{4.2}
$$

where in the last equality, we have used the Brown-Henneaux relations as well as the fact that the Ricci scalar on the brane Σ is given by [20, 21]

$$
R^{(2)} = -\frac{2}{\ell_{\mathrm{eff}}^2} \equiv -\frac{2}{L_k^2} \cos^2\psi_k \,, \qquad k = \mathrm{I, II} \,. \tag{4.3}
$$

Now we discuss the computation of entanglement entropy of subsystems in the bath CFT$_2$s utilizing the concept of generalized entropy and the island formalism. The generalized Rényi entropy for subsystems in the baths is computed through an Euclidean path integral on the replica manifold obtained by sewing n copies of the original manifold along branch cuts present on the subsystems under consideration [49, 51]. As the bath CFT$_2$s couple to the gravitational theory on the brane, in certain saddles to the gravitational part of the path integral, additional smooth branch points may emerge at the replica fixed points on copies of the brane theory. These are the endpoints of the so called *island* region corresponding to the bath subsystems.

However, unlike the usual scenario with a single bath coupled to gravity [3, 4, 49, 50], in the present case, the existence of an additional bath leads to novel saddle points to the gravitational path integral. In [21], these novel island saddles were termed as *induced islands*. In the presence of two baths, consider the entanglement entropy of the union of two subsystems on either bath. In the usual scenario, both these subsystems are responsible for the appearance of additional branch points on the brane. However, when the central charge of one of the CFT$_2$s is larger than the other, branch points in the gravitating manifold may emerge solely due to the subsystem in the CFT with the larger central charge. Since the

CFTs interact on the gravitating manifold, the other CFT also realizes the same branch points and perceives an induced island. Note that, as the island region is induced from the CFT with larger central charge, it bears no signature of the subsystem in the other CFT.[18] In the following we will assume $c_{\mathrm{II}} > c_{\mathrm{I}}$ without loss of generality, and hence the induced islands will only appear under the influence of the subsystem in $\mathrm{CFT}_2^{\mathrm{II}}$.

The origin of the conventional and induced islands may also be understood from the doubly holographic (three dimensional bulk) perspective. The conventional island appears in the effective intermediate picture when the RT saddle homologous to the subsystems crosses the brane only once. On the other hand for a double-crossing RT saddle homologous to the subsystem in $\mathrm{CFT}_2^{\mathrm{II}}$, we obtain an induced island in the lower dimensional perspective. In both the cases, the island region is bounded by the crossing points on the brane.

The generalized entanglement entropy for $A \cup B$ in the presence of an island $\mathrm{Is}(AB) = [-y_3, -y_1]$ may be expressed as[19] [4, 49]

$$S_{\mathrm{gen}}(AB) = \frac{\mathcal{A}\left(\partial \mathrm{Is}(AB)\right)}{4G_{\mathrm{N}}} + \lim_{n \to 1} S_{\mathrm{eff}}^{(n)}\left(AB \cup \mathrm{Is}(AB)\right) \tag{4.4}$$

$$= \Phi_0 + \lim_{n \to 1} \frac{1}{1-n} \log \left[\prod_{i=1,3} \Omega_{\mathrm{I}}(y_i)^{\Delta^{(\mathrm{I})}} \Omega_{\mathrm{II}}(y_i)^{\Delta^{(\mathrm{II})}} \tilde{G}_{\mathrm{CFT}_{\mathrm{I}}}^n G_{\mathrm{CFT}_{\mathrm{II}}}^n \right], \tag{4.5}$$

where $\Omega_{\mathrm{I,II}}(y_i) = |y_i|$ is the Weyl factor corresponding to the point y_i on the brane, $\mathrm{Is}(X)$ denotes the island region contributing to the entanglement entropy of subsystem X and $S_{\mathrm{eff}}^{(n)}$ is the effective Renyi entanglement entropy of quantum matter fields on the fixed background. In eq. (4.5), the conformal dimensions of the twist operators $\Delta^{(\mathrm{I,II})}$ are given by [52]

$$\Delta^{(k)} = \frac{c_k}{24}\left(n - \frac{1}{n}\right), \qquad k = \mathrm{I, II}. \tag{4.6}$$

The island prescription now dictates that the entanglement entropy is obtained by extremizing the generalized entropy over all possible island configurations as follows [4, 49]

$$S(AB) = \underset{\mathrm{Is}(AB)}{\mathrm{Min}}\,\mathrm{Ext}\left[S_{\mathrm{gen}}(AB)\right]. \tag{4.7}$$

Once the entanglement entropy island $\mathrm{Is}(AB)$ for $A \cup B$ is determined, the reflected entropy in the effective intermediate perspective is obtained by splitting $\mathrm{Is}(AB)$ into the respective reflected entropy islands $\mathrm{Is}_R(A)$ and $\mathrm{Is}_R(B)$ at the *island cross section* $Q = \partial \mathrm{Is}_R(A) \cap \partial \mathrm{Is}_R(B)$ as follows[20] [30, 31]

$$S_R(A:B) = \underset{Q}{\mathrm{Ext}} \left[\frac{\mathrm{Area}(Q)}{2G_{\mathrm{N}}^{(2)}} + \lim_{n \to 1} \lim_{m_e \to 1} S_R^{\mathrm{eff}}\left(A \cup \mathrm{Is}_R(A) : B \cup \mathrm{Is}_R(B)\right) \right]. \tag{4.8}$$

---

[18]See [21] for more details and the corresponding generalized island formulae.

[19]Note that the correlation functions of the twist operators, $\tilde{G}_{\mathrm{CFT}_{\mathrm{I}}}^n$ and $G_{\mathrm{CFT}_{\mathrm{II}}}^n$, generically need not have the same structure due to the presence of induced islands.

[20]Note that the above expression may intuitively be understood as the island prescription applied to $S_{vN}(\rho_{AA^\star})_{\sqrt{\rho_{AB}}}$ [30]. Similar to the case of EE islands, a gravitational replica technique featuring replica wormhole saddles to the gravitational path integral may be utilized to obtain the formula (4.8). Furthermore, eq. (4.8) may intuitively be understood in the corresponding doubly holographic formalism [32, 53] as the EWCS ending on the EOW brane precisely at the location of the QECS in the lower dimensional effective theory.

In eq. (4.8), the effective reflected entropy may be computed through its Rényi generalization as the (normalized) partition function $Z_{n,m}$ on the $m \times n$ sheeted replica manifold as follows [26]

$$
\begin{aligned}
S_R^{(m,n),\text{eff}} \left(A \cup \text{Is}_R(A) : B \cup \text{Is}_R(B) \right) &= \frac{1}{1-n} \log \left[\frac{Z_{n,m}}{(Z_{1,m})^n} \right] \\
&= \frac{1}{1-n} \log \left[\frac{\prod_i \Omega(y_i)^{\Delta_i} \tilde{G}_{\text{CFT}_\text{I}}^{m,n} G_{\text{CFT}_\text{II}}^{m,n}}{(\tilde{G}_{\text{CFT}_\text{I}}^m G_{\text{CFT}_\text{II}}^m)^n} \right] .
\end{aligned}
\tag{4.9}
$$

In the above expression, $\Omega(y_i)$ corresponds to the Weyl factor corresponding to the point y_i on the AdS$_2$ brane, $\tilde{G}_{\text{CFT}_\text{I}}^{m,n}$ and $G_{\text{CFT}_\text{II}}^{m,n}$ are appropriate correlation functions of twist operators inserted at the endpoint of the subsystems and their corresponding reflected entropy islands on the replica manifold.

4.1 Adjacent subsystems

Here we compute the entanglement entropy and reflected entropy for the configuration of adjacent subsystems $A = [\tilde{b}_1, \tilde{b}_2]_\text{I} \cup [b_1, b_2]_\text{II}$ and $B = [\tilde{b}_2, \tilde{b}_3]_\text{I} \cup [b_2, b_3]_\text{II}$ in the lower dimensional effective perspective described above, by employing the replica technique developed in [26]. To this end we first consider different saddles for the entanglement island for $A \cup B$ and subsequently discuss the phase transitions of reflected entropy between A and B within each phase of the entanglement entropy.

4.1.1 Conventional island

We begin by considering the case of conventional islands, where the entanglement entropy island $\text{Is}(AB) = [-y_3, -y_1]$ conceived on the brane depends on the degrees of freedom of the subsystems in both CFT$_2$s. In this case, the correlation functions $\tilde{G}_{\text{CFT}_\text{I}}^n$ and $G_{\text{CFT}_\text{II}}^n$ have the same large-c structure:[21]

$$
\begin{aligned}
\tilde{G}_{\text{CFT}_\text{I}}^n &= \langle \sigma_{g_n}(\tilde{b}_1) \sigma_{g_n^{-1}}(\tilde{b}_3) \sigma_{g_n}(-y_3) \sigma_{g_n^{-1}}(-y_1) \rangle \\
&\approx \langle \sigma_{g_n}(\tilde{b}_1) \sigma_{g_n^{-1}}(-y_1) \rangle \langle \sigma_{g_n^{-1}}(\tilde{b}_3) \sigma_{g_n}(-y_3) \rangle,
\end{aligned}
\tag{4.10}
$$

with a similar factorization for $G_{\text{CFT}_\text{II}}^n = \langle \sigma_{g_n}(b_1) \sigma_{g_n^{-1}}(b_3) \sigma_{g_n}(-y_3) \sigma_{g_n^{-1}}(-y_1) \rangle$. We are going to follow this convention for the rest of the article. Now from eqs. (4.2) and (4.5), we obtain

$$
S_{\text{gen}}(y_1, y_3) = \Phi_0 + \frac{c_\text{I}}{6} \log \left[\frac{(y_1 + \tilde{b}_1)^2 (y_3 + \tilde{b}_3)^2}{\epsilon^2 y_1 y_3} \right] + \frac{c_\text{II}}{6} \log \left[\frac{(y_1 + b_1)^2 (y_3 + b_3)^2}{\epsilon^2 y_1 y_3} \right] . \tag{4.11}
$$

where the constant area contribution denoted as Φ_0 is defined in eq. (4.2). On extremizing the above equation with respect to y_1 and y_3, the positions of the endpoints of the island are given by

$$
y_i^* = \frac{(c_\text{II} - c_\text{I})(b_i - \tilde{b}_i) + \sqrt{4 b_i \tilde{b}_i (c_\text{I} + c_\text{II})^2 + (c_\text{I} - c_\text{II})^2 (b_i - \tilde{b}_i)^2}}{2(c_\text{I} + c_\text{II})} , \qquad (i = 1, 3). \tag{4.12}
$$

---

[21]Note that on the right hand side, we have suppressed the subscripts $\text{CFT}_\text{I}^{\otimes n}$ for compactness of the expressions. In the following, unless specified explicitly, we will continue to adopt this simplification of notations.

The entanglement entropy for the adjacent subsystems in the effective intermediate perspective may be obtained by substituting eq. (4.12) in eq. (4.11). Utilizing eqs. (2.8) and (2.9), in the $\delta \to 0$ limit, the above expression is seen to match identically with the large tension limit of eq. (3.4). Incidentally, in the $\delta \to 0$ limit one obtains

$$\Phi_0^{(\delta)} = \frac{c_{\text{I}}}{6} \log \left[\frac{(L_{\text{I}} + L_{\text{II}})}{L_{\text{I}} \delta} \right] + \frac{c_{\text{II}}}{6} \log \left[\frac{(L_{\text{I}} + L_{\text{II}})}{L_{\text{II}} \delta} \right] + \mathcal{O}\left(\delta \right) \equiv S_{\text{int}}^{(\delta)} - \frac{c_{\text{I}} + c_{\text{II}}}{6} \log 2 \,, \quad (4.13)$$

and hence the large tension limit of the entanglement entropy obtained from eq. (3.3) also matches with eq. (4.11).

We now compute the island contributions to the reflected entropy for the configuration of two adjacent subsystems when the entanglement entropy island is conventional. We divide the entropy island $\text{Is}(A \cup B)$ into the respective reflected islands as follows: $\text{Is}_R(A) = [-y, -y_1^*]$ and $\text{Is}_R(B) = [-y_3^*, -y]$ at the island cross-section $Q = y$ such that $\text{Is}_R(A) \cup \text{Is}_R(B) = \text{Is}(A \cup B)$ [30]. The twist correlation function computing the effective reflected entropy between $A \cup \text{Is}_R(A)$ and $B \cup \text{Is}_R(B)$ is generically obtained through the six point function which is given as

$$G_{\text{CFT}_{\text{II}}}^{m,n} = \langle \sigma_{g_A}(b_1) \sigma_{g_B g_A^{-1}}(b_2) \sigma_{g_B^{-1}}(b_3) \sigma_{g_B}(-y_3^*) \sigma_{g_A g_B^{-1}}(-y) \sigma_{g_A^{-1}}(-y_1^*) \rangle \,. \quad (4.14)$$

The expression for $\tilde{G}$ is of the same form as above with coordinates b replaced by $\tilde{b}$ while points on the brane remain the same. The correlation function $G_{\text{CFT}_{\text{II}}}^m$ on the m-sheeted Riemann surface for the configuration of adjacent subsystems may be expressed as

$$G_{\text{CFT}_{\text{II}}}^m = \langle \sigma_{g_m}(b_1) \sigma_{g_m^{-1}}(b_3) \sigma_{g_m}(-y_3^*) \sigma_{g_m^{-1}}(-y_1^*) \rangle. \quad (4.15)$$

It has the same form for the CFT_{I} with b replaced by the $\tilde{b}$ coordinates. The scaling dimensions of the relevant twist operators are given as follows ($k = \text{I}, \text{II}$) [26]

$$\Delta_{\sigma_{g_A}}^{(k)} = \Delta_{\sigma_{g_A^{-1}}}^{(k)} = \Delta_{\sigma_{g_B}}^{(k)} = \Delta_{\sigma_{g_B^{-1}}}^{(k)} = \frac{n\, c_k}{12} \left(m - \frac{1}{m} \right) = n \Delta_m^{(k)}$$

$$\Delta_{\sigma_{g_A^{-1} g_B}}^{(k)} = \Delta_{\sigma_{g_B^{-1} g_A}}^{(k)} = \frac{c_k}{12} \left(n - \frac{1}{n} \right) = 2\Delta_n^{(k)}. \quad (4.16)$$

The form of the six point function in a CFT is not known explicitly, however it can be determined in the large central charge limit leading to various phases which we discuss in the following subsections.

Phase-I

We choose the size of the subsystems A and B such that both subsystems admit their own islands on the brane region. In this case, the six point twist correlator factorizes into three two point functions (cf. figure 25(a)) as

$$\begin{aligned}
G_{\text{CFT}_{\text{II}}}^{m,n} &= \langle \sigma_{g_A}(b_1) \sigma_{g_B g_A^{-1}}(b_2) \sigma_{g_B^{-1}}(b_3) \sigma_{g_B}(-y_3^*) \sigma_{g_A g_B^{-1}}(-y) \sigma_{g_A^{-1}}(-y_1^*) \rangle \\
&= \langle \sigma_{g_A}(b_1) \sigma_{g_A^{-1}}(-y_1^*) \rangle \langle \sigma_{g_B g_A^{-1}}(b_2) \sigma_{g_A g_B^{-1}}(-y) \rangle \langle \sigma_{g_B^{-1}}(b_3) \sigma_{g_B}(-y_3^*) \rangle.
\end{aligned} \quad (4.17)$$

The correlation function G^m in this phase is given by

$$G_{\text{CFT}_{\text{II}}}^m = \langle \sigma_{g_m}(b_1) \sigma_{g_m^{-1}}(-y_1^*) \rangle \langle \sigma_{g_m}(b_3) \sigma_{g_m}(-y_3^*) \rangle. \quad (4.18)$$
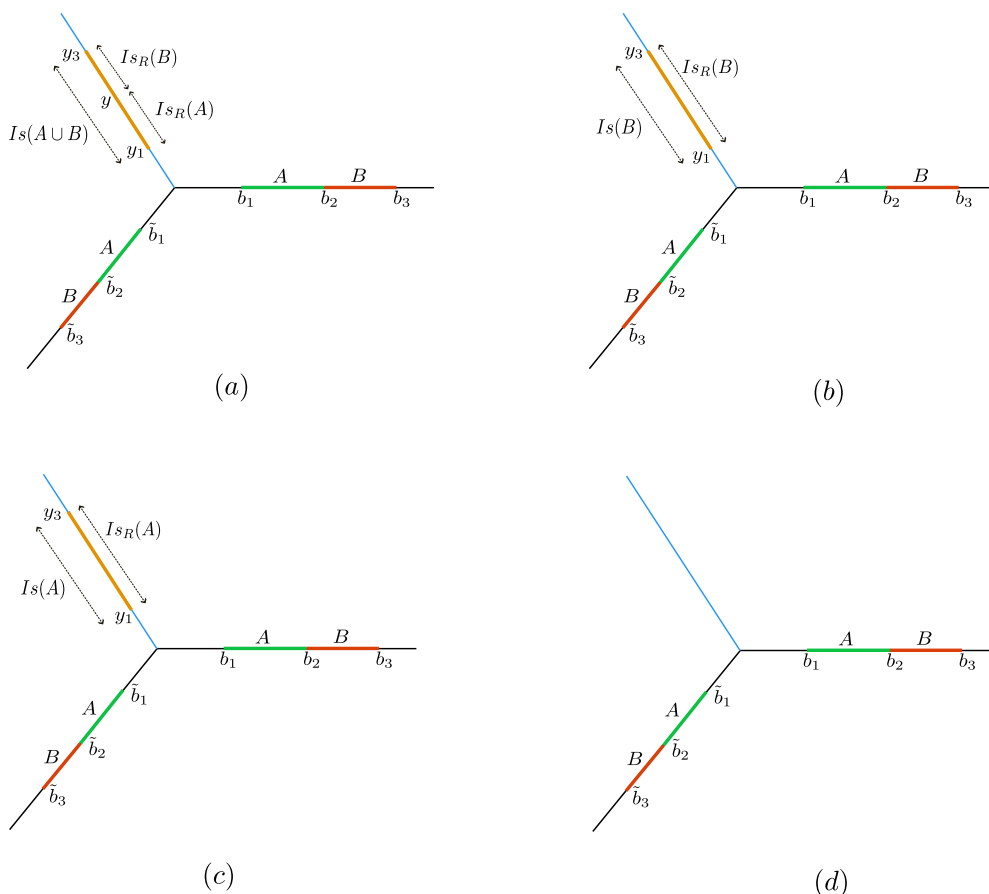
Figure 25. Various phases depicting the island contribution to the reflected entropy of adjacent subsystems. We replace y by $\bar{y}$ for the case of induced islands.

Similar factorizations occur for $\tilde{G}$ and $\tilde{G}^m$. We now utilize eqs. (4.17) and (4.18) in eq. (4.9) to obtain the generalized reflected entropy in the replica limit as

$$S_R^{\text{gen}}(y) = 2\Phi_0 + \frac{c_{\text{I}}}{3}\log\left[\frac{(y+\tilde{b}_2)^2}{\epsilon\,y}\right] + \frac{c_{\text{II}}}{3}\log\left[\frac{(y+b_2)^2}{\epsilon\,y}\right], \tag{4.19}$$

where the area term Φ_0 is defined in eq. (4.2). After extremizing the above expression with respect to y, the location of the island cross-section is given by eq. (4.12) with $i = 2$. The reflected entropy for this phase may now be obtained in the limit $\delta \to 0$ as

$$S_R(A:B) = \frac{c_{\text{I}}}{3}\log\left[\frac{(y^*+\tilde{b}_2)^2}{2y^*\,\epsilon}\right] + \frac{c_{\text{II}}}{3}\log\left[\frac{(y^*+b_2)^2}{2y^*\,\epsilon}\right] + S_{\text{int}}^{(\delta)}. \tag{4.20}$$

where $S_{\text{int}}^{(\delta)}$ is the interface entropy in the $\delta \to 0$ limit, defined in eq. (3.8). In this limit, we observe that the location of the brane crossing point y^* in the $3d$ bulk picture given in eq. (3.7) matches with the island cross-section obtained in the effective lower dimensional scenario. Furthermore, the large tension limit of the EWCS given in eq. (3.6) matches identically with half of the reflected entropy obtained in eq. (4.20).

Phase-II

In phase-II, the size of the subsystem B is much larger than A such that the entire island belongs to B and A does not have a corresponding island. This configuration is depicted in figure 25(b). Note that, there is no non-trivial island cross-section for this phase and hence no extremization is involved. The corresponding twist correlation function computing the effective reflected entropy in this phase is given by

$$G^{m,n}_{\text{CFT}_{\text{II}}} = \langle \sigma_{g_A}(b_1)\sigma_{g_B g_A^{-1}}(b_2)\sigma_{g_B^{-1}}(b_3)\sigma_{g_B}(-y_3^*)\sigma_{g_B^{-1}}(-y_1^*) \rangle$$
$$\approx \langle \sigma_{g_A}(b_1)\sigma_{g_B g_A^{-1}}(b_2)\sigma_{g_B^{-1}}(-y_1^*) \rangle \langle \sigma_{g_B^{-1}}(b_3)\sigma_{g_B}(-y_3^*) \rangle. \tag{4.21}$$

As earlier, the correlation function on the m-sheeted surface factorizes following eq. (4.18). Similar factorizations occur for the CFT_{I} correlators and the two point functions cancel from the numerator and denominator. Furthermore, note that y_1 and y_3 are fixed to the extremal values y_1^* and y_3^* respectively, by the entanglement island corresponding to the subsystem $A \cup B$. The three point function is fixed by the conformal symmetry up to an OPE coefficient which for the present case is given by [26]

$$C^{(k)}_{n,m} = (2m)^{2\Delta_n^{(k)}}. \tag{4.22}$$

Therefore, the reflected entropy may be obtained in this phase by utilizing eqs. (4.16) and (4.22) followed by taking the replica limit as

$$S_R(A:B) = \frac{c_{\text{I}}}{3}\log\left[\frac{2(\tilde{b}_2 - \tilde{b}_1)(\tilde{b}_2 + y_1^*)}{\epsilon_1(\tilde{b}_1 + y_1^*)}\right] + \frac{c_{\text{II}}}{3}\log\left[\frac{2(b_2 - b_1)(b_2 + y_1^*)}{\epsilon_2(b_1 + y_1^*)}\right], \tag{4.23}$$

where y_1^* is given in eq. (4.12). We observe that the above result matches exactly with twice the large tension limit of the EWCS in the bulk perspective, obtained in eq. (3.16).

Phase-III

As opposed to the previous case, the size of the subsystem A is much larger than that of B in this phase. Hence the entire entanglement entropy island now belongs to A and B does not posses an island as shown in figure 25(c). Similar to the previous phase, the correlation function in this phase factorizes as

$$G^{m,n}_{\text{CFT}_{\text{II}}} = \langle \sigma_{g_B g_A^{-1}}(b_2)\sigma_{g_B^{-1}}(b_3)\sigma_{g_A}(-y_3^*) \rangle \langle \sigma_{g_A}(b_1)\sigma_{g_A^{-1}}(-y_1^*) \rangle,$$
$$G^{m}_{\text{CFT}_{\text{II}}} = \langle \sigma_{g_m^{-1}}(b_3)\sigma_{g_m}(-y_3^*) \rangle \langle \sigma_{g_m}(b_1)\sigma_{g_m^{-1}}(-y_1^*) \rangle. \tag{4.24}$$

The reflected entropy in phase III may now be obtained in a similar manner to the previous phase as follows

$$S_R(A:B) = \frac{c_{\text{I}}}{3}\log\left[\frac{2(\tilde{b}_2 - \tilde{b}_3)(\tilde{b}_2 + y_3^*)}{\epsilon_1(\tilde{b}_3 + y_3^*)}\right] + \frac{c_{\text{II}}}{3}\log\left[\frac{2(b_2 - b_3)(b_2 + y_3^*)}{\epsilon_2(b_3 + y_3^*)}\right]. \tag{4.25}$$

Once again, since the $\delta \to 0$ limit of eq. (3.4) is identical to eq. (4.12), it is easy to verify that the reflected entropy obtained above matches identically with twice the corresponding large tension expression for the EWCS in the doubly holographic framework, as given in eq. (3.18).

4.1.2 Induced island

Next we consider the induced island $\overline{\mathrm{Is}}(AB) = [-\bar{y}_3, -\bar{y}_1]$ where the island region for the subsystem in $\mathrm{CFT}_2^{\mathrm{I}}$ is induced by the subsystem in $\mathrm{CFT}_2^{\mathrm{II}}$. As a result, although the $\mathrm{CFT}_2^{\mathrm{II}}$ correlator has the same structure as earlier, the $\mathrm{CFT}_2^{\mathrm{I}}$ correlator $\tilde{G}_{\mathrm{CFT_I}}^m$ has a different factorization in the large central charge limit (the island region is independent of the degrees of freedom on the $\mathrm{CFT_I}$ subsystem)

$$
\begin{aligned}
\tilde{G}_{\mathrm{CFT_I}}^n &= \langle \sigma_{g_n}(\tilde{b}_1)\sigma_{g_n^{-1}}(\tilde{b}_3)\sigma_{g_n}(-\bar{y}_3)\sigma_{g_n^{-1}}(-\bar{y}_1)\rangle \\
&\approx \langle \sigma_{g_n}(\tilde{b}_1)\sigma_{g_n^{-1}}(\tilde{b}_3)\rangle\langle \sigma_{g_n}(-\bar{y}_3)\sigma_{g_n^{-1}}(-\bar{y}_1)\rangle.
\end{aligned}
\tag{4.26}
$$

The generalized entropy may now be obtained using eqs. (4.2) and (4.5) as follows

$$
\begin{aligned}
S_{\mathrm{gen}}(\bar{y}_1, \bar{y}_3) = 2\Phi_0 &+ \frac{c_{\mathrm{I}}}{3}\log\left[\frac{\tilde{b}_3 - \tilde{b}_1}{\epsilon}\right] + \frac{c_{\mathrm{I}}}{6}\log\left[\frac{(\bar{y}_1 - \bar{y}_3)^2}{\bar{y}_1 \bar{y}_3}\right] \\
&+ \frac{c_{\mathrm{II}}}{6}\log\left[\frac{(\bar{y}_1 + b_1)^2 (\bar{y}_3 + b_3)^2}{\epsilon^2 \bar{y}_1 \bar{y}_3}\right].
\end{aligned}
\tag{4.27}
$$

Extremizing over the locations of the quantum extremal surfaces $\bar{y}_1^*$ and $\bar{y}_3^*$, we obtain

$$
c_{\mathrm{II}}\left(\bar{y}_1^* - \bar{y}_3^*\right)\left(\bar{y}_1^* - b_k\right) + c_{\mathrm{I}}\left(\bar{y}_1^* + \bar{y}_3^*\right)\left(b_k + \bar{y}_1^*\right) = 0, \qquad (k = 1, 3).
\tag{4.28}
$$

The entanglement entropy may be obtained upon substituting the physical solution to the above equations in eq. (4.27) and subsequently choosing the minimal saddle. Using the parametrization given in eq. (3.20), it is now straightforward to verify that eq. (3.24) together with the solution $\bar{y}_i^* = \frac{b_i}{k_D^*}$, conforms to the locations of the quantum extremal surfaces in the $2d$ effective theory as obtained from eq. (4.28).

In the following, we compute the induced island contributions to the reflected entropy between the adjacent subsystems A and B. Once again, we divide the induced entanglement island $\overline{\mathrm{Is}}(A \cup B)$ into the respective reflected islands $\overline{\mathrm{Is}}_R(A) = [-\bar{y}, -\bar{y}_1^*]$ and $\overline{\mathrm{Is}}_R(B) = [-\bar{y}_3^*, -\bar{y}]$ such that $\overline{\mathrm{Is}}_R(A) \cup \overline{\mathrm{Is}}_R(B) = \overline{\mathrm{Is}}(A \cup B)$. Note that, similar to the entanglement island, the reflected entropy islands for the $\mathrm{CFT}^{\mathrm{I}}$ degrees of freedom appearing on the AdS_2 brane is induced by the subsystem in $\mathrm{CFT}^{\mathrm{II}}$. As earlier, the twist correlators computing the effective reflected entropy between $A \cup \overline{\mathrm{Is}}_R(A)$ and $B \cup \overline{\mathrm{Is}}_R(B)$ are generically given by the six point function

$$
G_{\mathrm{CFT_{II}}}^{m,n} = \langle \sigma_{g_A}(b_1)\sigma_{g_B g_A^{-1}}(b_2)\sigma_{g_B^{-1}}(b_3)\sigma_{g_B}(-\bar{y}_3^*)\sigma_{g_A g_B^{-1}}(-\bar{y})\sigma_{g_A^{-1}}(-\bar{y}_1^*)\rangle,
\tag{4.29}
$$

in $\mathrm{CFT}^{\mathrm{II}}$, with a similar expression holding in $\mathrm{CFT}^{\mathrm{I}}$. Unlike the earlier phases, these correlators factorize differently in $\mathrm{CFT_I}$ and $\mathrm{CFT_{II}}$s as discussed in the following subsections.

Phase-I

In the first phase, the portions of the subsystems A and B residing in $\mathrm{CFT}^{\mathrm{II}}$ admit their own islands and correspondingly induce islands for their counterparts in $\mathrm{CFT}^{\mathrm{I}}$. The correlation function in the $\mathrm{CFT_I}$ (cf. figure 25(a)) factorizes as

$$
\begin{aligned}
\tilde{G}_{\mathrm{CFT_I}}^{m,n} &= \langle \sigma_{g_A}(\tilde{b}_1)\sigma_{g_B g_A^{-1}}(\tilde{b}_2)\sigma_{g_B^{-1}}(\tilde{b}_3)\rangle\langle \sigma_{g_B}(-\bar{y}_3)\sigma_{g_A g_B^{-1}}(-\bar{y})\sigma_{g_A^{-1}}(-\bar{y}_1^*)\rangle, \\
\tilde{G}_{\mathrm{CFT_I}}^m &= \langle \sigma_{g_m}(\tilde{b}_1)\sigma_{g_m^{-1}}(\tilde{b}_3)\rangle_{\mathrm{CFT_I^{\otimes m}}}\langle \sigma_{g_m}(-\bar{y}_3^*)\sigma_{g_m^{-1}}(-\bar{y}_1^*)\rangle_{\mathrm{CFT_I^{\otimes m}}},
\end{aligned}
\tag{4.30}
$$

while the correlator in the CFT_{II} factorizes into two point twist correlators as

$$
\begin{aligned}
G^{m,n}_{\text{CFT}_{\text{II}}} &= \langle \sigma_{g_A}(b_1) \sigma_{g_A^{-1}}(\bar{y}_1^*) \rangle \langle \sigma_{g_B g_A^{-1}}(b_2) \sigma_{g_A g_B^{-1}}(\bar{y}) \rangle \langle \sigma_{g_B^{-1}}(b_3) \sigma_{g_B}(\bar{y}_3^*) \rangle \\
G^{m}_{\text{CFT}_{\text{II}}} &= \langle \sigma_{g_m}(b_1) \sigma_{g_m^{-1}}(\bar{y}_1^*) \rangle \langle \sigma_{g_m^{-1}}(b_3) \sigma_{g_m}(\bar{y}_3^*) \rangle.
\end{aligned}
\tag{4.31}
$$

Now, the generalized reflected entropy in this phase may be obtained using eqs. (4.22), (4.30) and (4.31) in eq. (4.9) in the replica limit as follows

$$
\begin{aligned}
S_R^{\text{gen}}(A:B) = 2\Phi_0 &+ \frac{c_\text{I}}{3} \log\left[\frac{2(\tilde{b}_2 - \tilde{b}_1)(\tilde{b}_3 - \tilde{b}_2)}{\epsilon(\tilde{b}_3 - \tilde{b}_1)} \right] + \frac{c_\text{I}}{3} \log\left[\frac{2(\bar{y} - \bar{y}_1^*)(\bar{y} - \bar{y}_3^*)}{\bar{y}(\bar{y}_1^* - \bar{y}_3^*)} \right] \\
&+ \frac{c_\text{II}}{3} \log\left[\frac{(b_2 + \bar{y})^2}{\epsilon\,\bar{y}} \right].
\end{aligned}
\tag{4.32}
$$

Extremization of the above expression with respect to the (induced) island cross-section $\bar{y}$ leads precisely to eq. (3.32), where $\bar{y}_1^*$ and $\bar{y}_3^*$ are fixed according to the solution of eq. (4.28). Utilizing eq. (4.13), the reflected entropy in the effective lower dimensional perspective matches identically with twice the large tension limit of the corresponding EWCS obtained in eq. (3.31) in the doubly holographic perspective.

Phase-II

In the next phase, we consider the subsystem A to be much larger than B as described in figure 25(c), so that the entire (induced) island belongs to A. In this case, there is no non-trivial island cross section on the AdS_2 region and the following factorization occurs

$$
\begin{aligned}
\tilde{G}^{m,n}_{\text{CFT}_{\text{I}}} &= \langle \sigma_{g_A}(\tilde{b}_1) \sigma_{g_B g_A^{-1}}(\tilde{b}_2) \sigma_{g_B^{-1}}(\tilde{b}_3) \rangle \langle \sigma_{g_B}(-\bar{y}_3^*) \sigma_{g_A^{-1}}(-\bar{y}_1^*) \rangle, \\
\tilde{G}^{m}_{\text{CFT}_{\text{I}}} &= \langle \sigma_{g_A}(\tilde{b}_1) \sigma_{g_B^{-1}}(\tilde{b}_3) \rangle \langle \sigma_{g_m}(-\bar{y}_3^*) \sigma_{g_m^{-1}}(-\bar{y}_1^*) \rangle.
\end{aligned}
\tag{4.33}
$$

The correlation function in the CFT_{II} factorizes in the following way

$$
\begin{aligned}
G^{m,n}_{\text{CFT}_{\text{II}}} &= \langle \sigma_{g_B g_A^{-1}}(b_2) \sigma_{g_B^{-1}}(b_3) \sigma_{g_A}(-\bar{y}_3^*) \rangle \langle \sigma_{g_A}(b_1) \sigma_{g_A^{-1}}(-\bar{y}_1^*) \rangle, \\
G^{m}_{\text{CFT}_{\text{II}}} &= \langle \sigma_{g_m^{-1}}(b_3) \sigma_{g_m}(-\bar{y}_3^*) \rangle \langle \sigma_{g_m}(b_1) \sigma_{g_m^{-1}}(-\bar{y}_1^*) \rangle.
\end{aligned}
\tag{4.34}
$$

The reflected entropy for this phase may now be determined as follows

$$
S_R(A:B) = \frac{c_\text{I}}{3} \log\left[\frac{2(\tilde{b}_2 - \tilde{b}_1)(\tilde{b}_3 - \tilde{b}_2)}{\epsilon(\tilde{b}_3 - \tilde{b}_1)} \right] + \frac{c_\text{II}}{3} \log\left[\frac{2(b_3 - b_2)(b_2 + \bar{y}_3^*)}{\epsilon(b_3 + \bar{y}_3^*)} \right],
\tag{4.35}
$$

where $\bar{y}_3^*$ is fixed by the entanglement island of $A \cup B$, as given in eq. (4.28). This matches identically with the large tension limit of the EWCS in the doubly holographic picture, given in eq. (3.35).

Phase-III

In this phase, the subsystem B is much larger than the subsystem A as shown in figure 25(b). Hence the factorization of correlator remains same as in the previous case for CFT_{I} while for CFT_{II} we have

$$
G^{m,n}_{\text{CFT}_{\text{II}}} = \langle \sigma_{g_A}(b_1) \sigma_{g_B g_A^{-1}}(b_2) \sigma_{g_B^{-1}}(-\bar{y}_1^*) \rangle \langle \sigma_{g_B^{-1}}(b_3) \sigma_{g_B}(-\bar{y}_3) \rangle.
\tag{4.36}
$$

The reflected entropy for this phase may be obtained in a similar manner to the previous phase as follows

$$S_R(A:B) = \frac{c_I}{3} \log\left[\frac{2(\tilde{b}_2 - \tilde{b}_1)(\tilde{b}_3 - \tilde{b}_2)}{\epsilon(\tilde{b}_3 - \tilde{b}_1)}\right] + \frac{c_{II}}{3} \log\left[\frac{2(b_2 - b_1)(b_2 + \bar{y}_1^*)}{\epsilon(b_1 + \bar{y}_1^*)}\right], \qquad (4.37)$$

where $\bar{y}_1^*$ is given by eq. (4.28) and the corresponding minimal EWCS obtained in eq. (3.36) from the double holographic perspective, matches with the above expression in the limit of large brane tension.

4.1.3 No island saddle

When the sizes the subsystems A and B are small enough such that they do not posses any entanglement entropy islands as shown in figure 25(d), the corresponding entanglement entropies are computed via the usual two-point functions in either CFT [52]. The correlation function computing the reflected entropy between A and B may be written as a three point function in either CFT:

$$G_{\mathrm{CFT}_{II}}^{m,n} = \langle \sigma_{g_A}(b_1) \sigma_{g_B g_A^{-1}}(b_2) \sigma_{g_B^{-1}}(b_3) \rangle. \qquad (4.38)$$

The CFT_{II} correlator $\tilde{G}^{m,n}$ is given by a similar two point function with b replaced by $\tilde{b}$. Therefore, the reflected entropy may be obtained in a straightforward manner as follows

$$S_R(A:B) = \frac{c_I}{3} \log\left[\frac{2(\tilde{b}_2 - \tilde{b}_1)(\tilde{b}_3 - \tilde{b}_2)}{\epsilon(\tilde{b}_3 - \tilde{b}_1)}\right] + \frac{c_{II}}{3} \log\left[\frac{2(b_2 - b_1)(b_3 - b_2)}{\epsilon(b_3 - b_1)}\right], \qquad (4.39)$$

which matches identically with the corresponding EWCS in the $3d$ bulk perspective, given in eq. (3.37).

4.2 Disjoint subsystems

In this section we determine the island contributions to the reflected entropy for two disjoint subsystems $A = [b_1, b_2]_I \cup [b_1, b_2]_{II}$ and $B = [b_3, b_4]_I \cup [b_3, b_4]_{II}$ in the lower dimensional effective theory described by dynamical gravity on the AdS$_2$ manifold coupled to two flat Minkowski baths, utilizing the replica technique [26, 30].

Similar to the earlier investigation with adjacent subsystems, in the following, we will discover both conventional and induced island regions conceived in the gravitating manifold depending on the locations and (relative) sizes of the subsystems.

4.2.1 Conventional island

We begin by considering the case of the conventional entanglement island for $A \cup B$, denoted as $\mathrm{Is}(AB) = [-y_1, -y_4]$. Recall that a conventional island on the gravitational manifold depends on the degrees of freedom from the subsystems on both baths. Hence, the twist correlators computing the effective Rényi entropy corresponding to $A \cup B$ have the same kind of factorization in the large-c limit. For the present configuration of two disjoint subsystems with the corresponding conventional island $\mathrm{Is}(AB)$, the effective Rényi entropy is computed through six point correlation functions of twist operators as follows

$$G_{\mathrm{CFT}_{I/II}}^n = \langle \sigma_{g_n}(b_1) \sigma_{g_n^{-1}}(b_2) \sigma_{g_n}(b_3) \sigma_{g_n^{-1}}(b_4) \sigma_{g_n}(-y_4) \sigma_{g_n^{-1}}(-y_1) \rangle.$$

In the large central charge limit, the above twist correlator may be factorized as follows [4, 49, 54]

$$G^n_{\mathrm{CFT_{I/II}}} = \langle \sigma_{g_n^{-1}}(b_2)\sigma_{g_n}(b_3)\rangle\langle \sigma_{g_n}(b_1)\sigma_{g_n^{-1}}(-y_1)\rangle\langle \sigma_{g_n^{-1}}(b_4)\sigma_{g_n}(-y_4)\rangle .$$ (4.40)

Substituting the above correlation in eq. (4.5) and accounting for the appropriate Weyl factors for the points y_i on the AdS$_2$ region given as $\Omega(y_i) = |y_i|$, the generalized entanglement entropy may be obtained as follows

$$S_{gen}(AB) = \Phi_0 + \frac{\mathrm{c_I} + \mathrm{c_{II}}}{6}\left(2\log\left(\frac{b_3 - b_2}{\epsilon}\right) + \log\left[\frac{(b_4 + y_4)^2}{\epsilon\, y_1}\right] + \log\left[\frac{(b_4 + y_4)^2}{\epsilon\, y_4}\right]\right).$$
(4.41)

Extremizing the above expression with respect to y_i we obtain $y_i^* = b_i$ leading to the following expression for the entanglement entropy

$$S(AB) = \Phi_0 + \frac{\mathrm{c_I} + \mathrm{c_{II}}}{6}\log 2 + \frac{\mathrm{c_I} + \mathrm{c_{II}}}{6}\left[2\log\left(\frac{b_3 - b_2}{\epsilon}\right) + \log\left(\frac{2b_1}{\epsilon}\right) + \log\left(\frac{2b_4}{\epsilon}\right)\right].$$
(4.42)

In the large tension regime, utilizing eq. (4.13), the above result is seen to be an exact match of the corresponding expression obtained from the bulk geometry given in eq. (3.41).

Having obtained the entanglement entropy we now compute the reflected entropy of two disjoint subsystems for phases involving the conventional islands utilizing the replica technique developed in [26].

Phase-I

We begin by considering the configuration described by figure 26(a). The twist correlation function characterizing the reflected entropy of AB in this phase is given by $G^{m,n}_{\mathrm{CFT_{I/II}}}$ which corresponds to the following seven point correlation function

$$G^{m,n}_{\mathrm{CFT_{I/II}}} = \langle \sigma_{g_A}(b_1)\sigma_{g_A^{-1}}(b_2)\sigma_{g_B}(b_3)\sigma_{g_B^{-1}}(b_4)\sigma_{g_B}(-b_4)\sigma_{g_A g_B^{-1}}(-y)\sigma_{g_A^{-1}}(-b_1)\rangle .$$

Note that the two correlations $G^{m,n}_{\mathrm{CFT_I}}$ and $G^{m,n}_{\mathrm{CFT_{II}}}$ are identical in this case because of the symmetry of chosen configuration. Since the seven point function is hard to determine analytically even in the large-c limit, we take b_4, b_1 away from b_2, b_3 such that the following factorization occurs

$$G^{m,n}_{\mathrm{CFT_{I/II}}} = \langle \sigma_{g_A}(b_1)\sigma_{g_A^{-1}}(-b_1)\rangle\sigma_{g_B^{-1}}(b_4)\sigma_{g_B}(-b_4)\rangle\langle \sigma_{g_A^{-1}}(b_2)\sigma_{g_B}(b_3)\sigma_{g_A g_B^{-1}}(-y)\rangle .$$ (4.43)

Note that $\mathrm{CFT_{I/II}}$ on l.h.s. indicates that the structure is same for both $\mathrm{CFT_{II}}$ and $\mathrm{CFT_I}$. The corresponding correlation functions of the m-sheeted Riemann surface which for this phase are given as

$$G^m_{\mathrm{CFT_{I/II}}} = \langle \sigma_{g_m}(b_1)\sigma_{g_m^{-1}}(b_2)\sigma_{g_m}(b_3)\sigma_{g_m^{-1}}(b_4)\sigma_{g_m}(-b_4)\sigma_{g_m^{-1}}(-b_1)\rangle$$ (4.44)

$$= \langle \sigma_{g_m}(b_1)\sigma_{g_m^{-1}}(-b_1)\rangle\langle \sigma_{g_m^{-1}}(b_4)\sigma_{g_m}(-b_4)\rangle\langle \sigma_{g_m^{-1}}(b_2)\sigma_{g_m}(b_3)\rangle$$ (4.45)
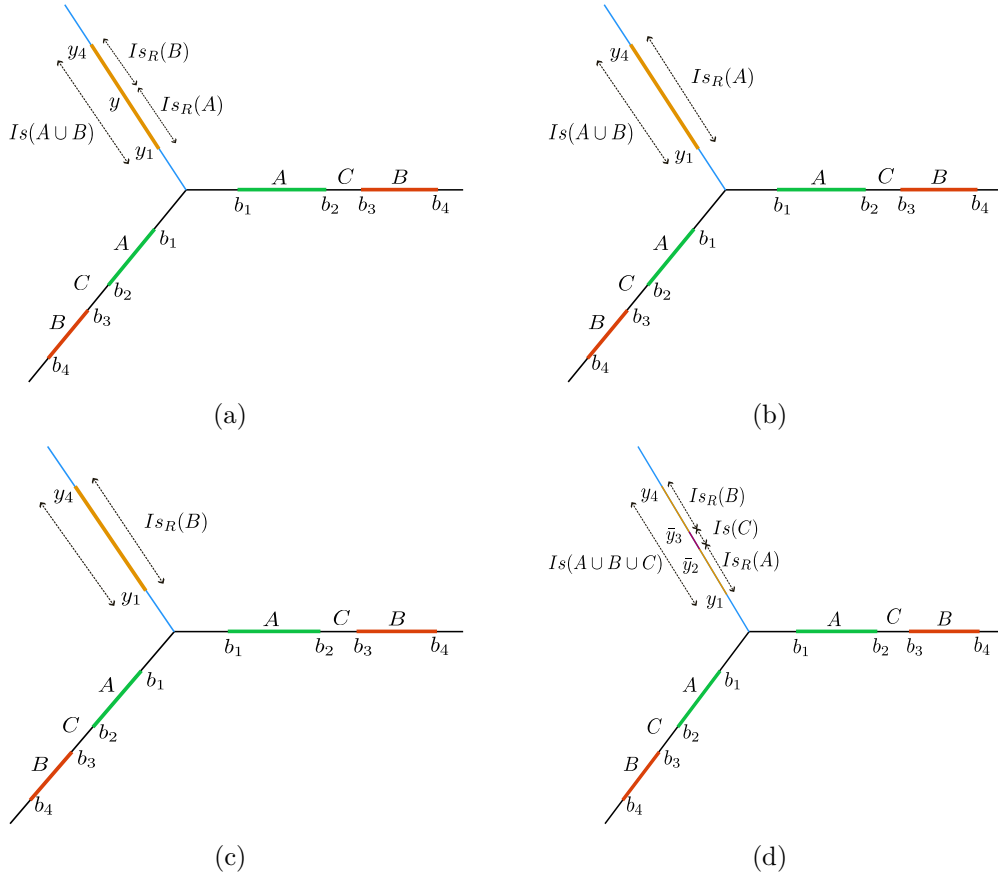
Figure 26. Various phases depicting the island contributions to the reflected entropy of disjoint intervals in a zero temperature holographic ICFT$_2$.

where the second equality comes from the factorization specific to this phase. Note that the two point functions in the numerator and denominators exactly cancel. Also the Weyl factors in the numerator and denominators cancel for all the operators except $\sigma_{g_A g_B^{-1}}(y)$. We may now obtain the generalized Renyi reflected entropy by substituting the expressions for the correlators in eqs. (4.43) and (4.45) in (4.9) as follows

$$S_R^{(m,n,\mathrm{eff})}\left(A \cup \mathrm{Is}_R(A) : B \cup \mathrm{Is}_R(B)\right)$$

$$= \frac{1}{1-n} \log \left[\frac{\Omega_{\mathrm{I}}(-y)^{\Delta_{g_A g_B^{-1}}^{(\mathrm{I})}} \langle \sigma_{g_A^{-1}}(b_2) \sigma_{g_B}(b_3) \sigma_{g_A g_B^{-1}}(-y) \rangle_{\mathrm{CFT}_{\mathrm{I}}^{\otimes mn}}}{\left(\langle \sigma_{g_m^{-1}}(b_2) \sigma_{g_m}(b_3) \rangle_{\mathrm{CFT}_{\mathrm{I}}^{\otimes m}} \right)^n} \right] + (\mathrm{I} \leftrightarrow \mathrm{II}).$$

(4.46)

The three point function is fixed by the conformal symmetry up to the OPE constant given in eq. (4.22). This leads to the following expression for the generalized reflected entropy in the replica limit

$$S_R^{\mathrm{gen}}(b_0) = 2\Phi_0 + \frac{\mathrm{c_I} + \mathrm{c_{II}}}{3} \log \left[\frac{2(y+b_2)(y+b_3)}{y(b_3 - b_2)} \right].$$

(4.47)

Extremizing the above expression over the island cross-section $Q = -y$ leads to $y = \sqrt{b_2 b_3}$ and hence we may obtain the following expression for the reflected entropy in this phase

$$S_R(A : B) = 2\left(\Phi_0 + \frac{c_\mathrm{I} + c_\mathrm{II}}{6} \log 2\right) + \frac{c_\mathrm{I} + c_\mathrm{II}}{3} \log\left(\frac{\sqrt{b_2} + \sqrt{b_3}}{\sqrt{b_3} - \sqrt{b_2}}\right). \qquad (4.48)$$

Utilizing eqs. (3.8) and (4.13), it is straightforward to verify that the above expression matches identically with twice the large tension limit of the EWCS given in eq. (3.50).

Phase-II

We now consider the reflected entropy for phase-II of the disjoint interval configuration which is described in figure 26(b). In this phase-II the subsystem-B does not posses an island and hence the entire island belongs to A. The corresponding correlation function may be factorized in the corresponding OPE channel as follows

$$\begin{aligned}
G^{m,n}_{\mathrm{CFT}_{\mathrm{I/II}}} &= \langle \sigma_{g_A}(b_1)\sigma_{g_A^{-1}}(b_2)\sigma_{g_B}(b_3)\sigma_{g_B^{-1}}(b_4)\sigma_{g_A}(-b_4)\sigma_{g_A^{-1}}(-b_1)\rangle \\
&= \langle \sigma_{g_A}(b_1)\sigma_{g_A^{-1}}(-b_1)\rangle\langle \sigma_{g_A}(-b_4)\sigma_{g_A^{-1}}(b_2)\sigma_{g_B}(b_3)\sigma_{g_B^{-1}}(b_4)\rangle.
\end{aligned} \qquad (4.49)$$

A similar factorization holds for the correlation function on m-sheeted surface. As earlier, the two point functions cancel from the numerator and the denominator which leads to the following expression for the reflected entropy

$$\begin{aligned}
&S_R^{(m,n,\mathrm{eff})}(A \cup \mathrm{Is}_R(A) : B \cup \mathrm{Is}_R(B)) \\
&= \frac{1}{1-n} \log\left[\frac{\langle \sigma_{g_A}(-b_4)\sigma_{g_A^{-1}}(b_2)\sigma_{g_B}(b_3)\sigma_{g_B^{-1}}(b_4)\rangle_{\mathrm{CFT}_\mathrm{I}^{\otimes mn}}}{\left(\langle \sigma_{g_m}(-b_4)\sigma_{g_m^{-1}}(b_2)\sigma_{g_m}(b_3)\sigma_{g_m^{-1}}(b_4)\rangle_{\mathrm{CFT}_\mathrm{I}^{\otimes m}}\right)^n}\right] + (\mathrm{I} \leftrightarrow \mathrm{II}). \qquad (4.50)
\end{aligned}$$

Note that since the subsystem B does not posses any island there is no island cross-section and hence no extremization involved in this phase. The conformal block that gives dominant contribution to the above four point function(s) is well known in the large central charge limit [26] to be of the following form

$$\log \mathcal{F}_{(k)}(n\Delta_m, 2\Delta_n | x) = -2n\Delta_m^{(k)} \log x - 2\Delta_n^{(k)} \log\left(\frac{1+\sqrt{x}}{1-\sqrt{x}}\right) \qquad (4.51)$$

where $x = \frac{b_{12}b_{34}}{b_{13}b_{24}}$ is the cross-ratio. Hence, in the replica limit the above expression directly leads to the reflected entropy as follows

$$S_R(A : B) = \frac{c_\mathrm{I} + c_\mathrm{II}}{3} \log\left[\frac{b_4^2 - b_2 b_3 + \sqrt{(b_3^2 - b_4^2)(b_2^2 - b_4^2)}}{b_4(b_3 - b_2)}\right], \qquad (4.52)$$

which matches identically with half of the corresponding EWCS in the $3d$ bulk description, given in eq. (3.55).

Phase-III

Phase-III of the disjoint interval configuration with the conventional island saddle for entanglement entropy is depicted in figure 26(c). In this phase the subsystem A does not possess any reflected entropy island whereas B does. The computation of the generalized Renyi reflected entropy proceeds similar to the previous phase and we may as well replace b_4 by b_1 in eq. (4.52) for the present case, to obtain

$$S_R(A:B) = \frac{c_{\mathrm{I}} + c_{\mathrm{II}}}{3} \log \left[\frac{b_1^2 - b_2 b_3 + \sqrt{(b_3^2 - b_1^2)(b_2^2 - b_1^2)}}{b_1(b_3 - b_2)} \right] . \tag{4.53}$$

The above expression is trivially seen to match with the corresponding EWCS in eq. (3.58).

4.2.2 Induced islands

Next we consider situation involving induced islands for various subsystems under consideration. This can be further subdivided into phases based on whether the subsystem C sandwiched between A and B in either baths claims an induced island as follows:

- The subsystem $A \cup B \cup C$ is large enough to possess an induced island. This situation arises when $\Theta_{ABC} = \frac{b_4}{b_1}$ exceeds its critical value (cf. the discussion in section 3.2.2). We simultaneously require the subsystem C to be small enough to be lacking any induced island.

- In the second case, $A \cup B \cup C$ possesses the conventional island while $\Theta_C = \frac{b_3}{b_2}$ exceeds its critical value giving access to the induced island for subsystem C.

- Both C and $A \cup B \cup C$ possess their induced islands. However, as discussed in footnote 16, we do not encounter this scenario for a large range of parameter values and hence will be omitted in the following discussion.

In the following, we will investigate each of these situations individually and discuss the phase transitions for the reflected entropy within each scenario.

A. Subsystem C lacking an island

We begin with the case where C does not have an island which results in the following expression for the correlation functions computing the Rényi entropy for $A \cup B$,

$$G^n_{\mathrm{CFT_{I/II}}} = \langle \sigma_{g_n}(b_1) \sigma_{g_n^{-1}}(b_2) \sigma_{g_n}(b_3) \sigma_{g_n^{-1}}(b_4) \rangle \langle \sigma_{g_n}(-\bar{y}_4) \sigma_{g_n^{-1}}(-\bar{y}_1) \rangle .$$

As mentioned above in the large-c limit the above correlators factorize differently in the two CFTs as follows

$$G^n_{\mathrm{CFT_I}} = \langle \sigma_{g_n}(b_1) \sigma_{g_n^{-1}}(b_4) \rangle \langle \sigma_{g_n^{-1}}(b_2) \sigma_{g_n}(b_3) \rangle \langle \sigma_{g_n}(-\bar{y}_1) \sigma_{g_n^{-1}}(-\bar{y}_4) \rangle$$

$$G^n_{\mathrm{CFT_{II}}} = \langle \sigma_{g_n}(b_1) \sigma_{g_n^{-1}}(-\bar{y}_1) \rangle \langle \sigma_{g_n^{-1}}(b_2) \sigma_{g_n}(b_3) \rangle \langle \sigma_{g_n}(-\bar{y}_4) \sigma_{g_n^{-1}}(b_4) \rangle . \tag{4.54}$$

Since the above correlation functions are expressed in terms of the two point functions completely fixed by conformal symmetry, we may readily obtain the generalized entanglement entropy from eq. (4.5) as follows

$$S_{\text{gen}}(AB) = \Phi_0 + \frac{c_{\text{I}}}{6} \log \left[\frac{(b_2 - b_3)^2 (b_1 - b_4)^2 (\bar{y}_1 - \bar{y}_4)^2}{\epsilon^4 \bar{y}_1 \bar{y}_4} \right]$$
$$+ \frac{c_{\text{II}}}{6} \log \left[\frac{(b_2 - b_3)^2 (b_1 + \bar{y}_1)^2 (b_4 + \bar{y}_4)^2}{\epsilon^4 \bar{y}_1 \bar{y}_4} \right]. \tag{4.55}$$

Extremizing the above equation w.r.t. y_1 and y_4 we get

$$c_{\text{II}} \left(\bar{y}_1 - \bar{y}_4 \right) \left(\bar{y}_1 - b_i \right) + c_{\text{I}} \left(\bar{y}_1 + \bar{y}_4 \right) \left(b_i + \bar{y}_1 \right) = 0, \qquad (i = 1, 4). \tag{4.56}$$

The above result exactly matches with the corresponding expression obtained from the bulk geometry given in eq. (3.24), together with the solution $\bar{y}_1^* = \frac{b_1}{k_{ABC}^*}$ in the large tension limit.[22] Finally, the entanglement entropy for the present configuration may be obtained by substituting the solutions $\bar{y}_1^*$ and $\bar{y}_4^*$ to the above extremization equations in the expression for the generalized entropy in eq. (4.55).

We now proceed to compute the islands contributions to the reflected entropy for phases involving induced islands for $A \cup B \cup C$. As earlier, we divide the induced entanglement island $\bar{\text{Is}}(AB) = [-\bar{y}_4^*, -\bar{y}_1^*]$ into the corresponding reflected entropy islands $\bar{\text{Is}}_R(A) = [-\bar{y}, -\bar{y}_1^*]$ and $\bar{\text{Is}}_R(B) = [-\bar{y}_4^*, -\bar{y}]$ by placing the island cross-section at $Q = -\bar{y}$. The twist correlator computing the effective Rényi reflected entropy is then given by a seven point function

$$G_{\text{CFT}_{\text{I/II}}}^{m,n} = \langle \sigma_{g_A}(b_1) \sigma_{g_A^{-1}}(b_2) \sigma_{g_B}(b_3) \sigma_{g_B^{-1}}(b_4) \sigma_{g_B}(-\bar{y}_4^*) \sigma_{g_A g_B^{-1}}(-\bar{y}) \sigma_{g_A^{-1}}(-\bar{y}_1^*) \rangle.$$

In this case, the corresponding correlation functions of both CFT$_{\text{I}}$ and CFT$_{\text{II}}$ factorize differently. These phases correspond to the double crossing geodesics in the dual bulk geometry. Note that the diagrams depicting induced island phases remain same as figure 26. The difference however is in the way correlators factorize.

Phase-I

We now compute the reflected entropy for the disjoint subsystems when both A and B admit their reflected entropy islands. In this phase depicted in figure 26(a) (replace y with $\bar{y}$ and y_i with $\bar{y}_i$) $G_{\text{CFT}_{\text{I}}}^{m,n}$, $\tilde{G}_{\text{CFT}_{\text{II}}}^{m,n}$ corresponds to the seven point correlation functions which factorize in the large-c limit as follows

$$G_{\text{CFT}_{\text{I}}}^{m,n} = \langle \sigma_{g_A}(b_1) \sigma_{g_A^{-1}}(b_2) \sigma_{g_B}(b_3) \sigma_{g_B^{-1}}(b_4) \sigma_{g_B}(-\bar{y}_1^*) \sigma_{g_A g_B^{-1}}(-\bar{y}) \sigma_{g_A^{-1}}(-\bar{y}_4^*) \rangle$$
$$= \langle \sigma_{g_A}(b_1) \sigma_{g_A^{-1}}(b_2) \sigma_{g_B}(b_3) \sigma_{g_B^{-1}}(b_4) \rangle \langle \sigma_{g_B}(-\bar{y}_1^*) \sigma_{g_A g_B^{-1}}(-\bar{y}) \sigma_{g_A^{-1}}(-\bar{y}_4^*) \rangle$$
$$G_{\text{CFT}_{\text{II}}}^{m,n} = \langle \sigma_{g_A}(b_1) \sigma_{g_A^{-1}}(b_2) \sigma_{g_B}(b_3) \sigma_{g_B^{-1}}(b_4) \sigma_{g_B}(-\bar{y}_1^*) \sigma_{g_A g_B^{-1}}(-\bar{y}) \sigma_{g_A^{-1}}(-\bar{y}_4^*) \rangle$$
$$= \langle \sigma_{g_A}(b_1) \sigma_{g_A^{-1}}(-\bar{y}_1^*) \rangle \langle \sigma_{g_A^{-1}}(b_2) \sigma_{g_B}(b_3) \sigma_{g_A g_B^{-1}}(-\bar{y}) \rangle \langle \sigma_{g_B}(-\bar{y}_4^*) \sigma_{g_B^{-1}}(b_4) \rangle. \tag{4.57}$$

---

[22]Note that in the present context, $k_D \equiv k_{ABC}$ and $\Theta_D \equiv \Theta_{ABC} = \frac{b_4}{b_1}$ in the parametrization given in eq. (3.20) (cf. footnote 17) with $i = 1, 4$.

Note that $[-\bar{y}_1^*, -\bar{y}_4^*]$ corresponds to the entanglement entropy island of AB which were obtained in eq. (4.56). Observe that in the second line we have specific factorization of the correlation function in the large-c limit in this phase. Also a similar factorization exists for the corresponding correlation functions on the m-sheeted Riemann surface which are expressed as follows

$$
\begin{aligned}
G_{\text{CFT}_\text{I}}^m &= \langle \sigma_{g_m}(b_1)\sigma_{g_m^{-1}}(b_2)\sigma_{g_m}(b_3)\sigma_{g_m^{-1}}(b_4)\sigma_{g_m}(-\bar{y}_1^*)\sigma_{g_m^{-1}}(-\bar{y}_4^*)\rangle \\
&= \langle \sigma_{g_m}(b_1)\sigma_{g_m^{-1}}(b_2)\sigma_{g_m}(b_3)\sigma_{g_m^{-1}}(b_4)\rangle \langle \sigma_{g_m}(-\bar{y}_1^*)\sigma_{g_m^{-1}}(-\bar{y}_4^*)\rangle \\
\tilde{G}_{\text{CFT}_\text{II}}^m &= \langle \sigma_{g_m}(b_1)\sigma_{g_m^{-1}}(b_2)\sigma_{g_m}(b_3)\sigma_{g_m^{-1}}(b_4)\sigma_{g_m}(-\bar{y}_1^*)\sigma_{g_m^{-1}}(-\bar{y}_4^*)\rangle \\
&= \langle \sigma_{g_m}(b_1)\sigma_{g_m^{-1}}(-\bar{y}_1^*)\rangle \langle \sigma_{g_m^{-1}}(b_2)\sigma_{g_m}(b_3)\rangle \langle \sigma_{g_m}(-\bar{y}_4^*)\sigma_{g_m^{-1}}(b_4)\rangle .
\end{aligned}
\tag{4.58}
$$

Utilizing the above expressions given by eq. (4.57), eq. (4.58) in eq. (4.9) we determine the following result for the generalized or effective reflected entropy in the replica limit

$$
\begin{aligned}
S_R(A:B) = 2\left(\Phi_0 + \frac{c_\text{I}+c_\text{II}}{6}\log 2 \right) + \frac{c_\text{I}}{3}\log\left[\frac{1+\sqrt{x}}{1-\sqrt{x}} \right] + \frac{c_\text{I}}{3}\log\left[\frac{(\bar{y}-\bar{y}_1^*)(\bar{y}_4^*-\bar{y})}{\bar{y}(\bar{y}_4^*-\bar{y}_1^*)} \right] \\
+ \frac{c_\text{II}}{3}\log\left[\frac{(\bar{y}+b_2)(\bar{y}+b_3)}{\bar{y}(b_3-b_2)} \right]
\end{aligned}
\tag{4.59}
$$

where $x = \frac{b_{12}b_{34}}{b_{13}b_{24}}$ is the cross-ratio. Extremizing the above expression w.r.t. $\bar{y}$ we obtain the following relation

$$
c_\text{I}(\bar{y}^2 - \bar{y}_1^*\bar{y}_4^*)(\bar{y}+b_2)(\bar{y}+b_3) + c_\text{II}(\bar{y}^2 - b_2 b_3)(\bar{y}-\bar{y}_1^*)(\bar{y}-\bar{y}_4^*) = 0
\tag{4.60}
$$

which is identical to its doubly holographic counterpart in eq. (3.68) in the large tension limit. Consequently upon utilizing eq. (4.13), the large tension limit of the reflected entropy matches identically with the corresponding large tension value of the EWCS given in eq. (3.69).

Phase-II

In this phase only the reflected entropy island for A receives the entire island contribution as depicted in figure 26(b) (with $y_i \to \bar{y}_i$). Hence, the required correlation function factorize in this phase as follows

$$
\begin{aligned}
G_{\text{CFT}_\text{I}}^{m,n} &= \langle \sigma_{g_A}(b_1)\sigma_{g_A^{-1}}(b_2)\sigma_{g_B}(b_3)\sigma_{g_B^{-1}}(b_4)\rangle \langle \sigma_{g_A}(-\bar{y}_1^*)\sigma_{g_A^{-1}}(-\bar{y}_4^*)\rangle \\
G_{\text{CFT}_\text{II}}^{m,n} &= \langle \sigma_{g_A}(b_1)\sigma_{g_A^{-1}}(-\bar{y}_1^*)\rangle \langle \sigma_{g_A}(-\bar{y}_4^*)\sigma_{g_A^{-1}}(b_2)\sigma_{g_B}(b_3)\sigma_{g_B^{-1}}(b_4)\rangle .
\end{aligned}
\tag{4.61}
$$

A similar factorization holds for the correlation function on m-sheeted surface. Once again the two point functions cancel from the numerator and the denominator leading to the following expression for the reflected entropy

$$
\begin{aligned}
&S_R^{(m,n,\text{eff})}\left(A\cup \text{Is}_R(A) : B\cup \text{Is}_R(B) \right) \\
&\quad = \frac{1}{1-n}\log\left[\frac{\langle \sigma_{g_A}(b_1)\sigma_{g_A^{-1}}(b_2)\sigma_{g_B}(b_3)\sigma_{g_B^{-1}}(b_4)\rangle_{\text{CFT}_\text{I}^{\otimes mn}}}{\left(\langle \sigma_{g_m}(b_1)\sigma_{g_m^{-1}}(b_2)\sigma_{g_m}(b_3)\sigma_{g_m^{-1}}(b_4)\rangle_{\text{CFT}_\text{I}^{\otimes m}} \right)^n} \right] \\
&\quad\quad + \frac{1}{1-n}\log\left[\frac{\langle \sigma_{g_A}(-\bar{y}_4^*)\sigma_{g_A^{-1}}(b_2)\sigma_{g_B}(b_3)\sigma_{g_B^{-1}}(b_4)\rangle_{\text{CFT}_\text{II}^{\otimes mn}}}{\left(\langle \sigma_{g_m}(-\bar{y}_4^*)\sigma_{g_m^{-1}}(b_2)\sigma_{g_m}(b_3)\sigma_{g_m^{-1}}(b_4)\rangle_{\text{CFT}_\text{II}^{\otimes m}} \right)^n} \right] .
\end{aligned}
\tag{4.62}
$$

Note that since the subsystem-B does not posses any island there is no island cross-section and hence no extremization involved in this phase. Now utilizing eq. (4.51), the replica limit of the above expression directly leads to the reflected entropy as follows

$$S_R(A:B) = \frac{c_I}{3} \log \left[\frac{1+\sqrt{x}}{1-\sqrt{x}} \right] + \frac{c_{II}}{3} \log \left[\frac{1+\sqrt{x_0}}{1-\sqrt{x_0}} \right], \tag{4.63}$$

where the cross ratios are given by $x = \frac{b_{12}b_{34}}{b_{13}b_{24}}$ and $x_0 = \frac{(\bar{y}_4^* + b_2)(b_3 - b_4)}{(\bar{y}_4^* + b_3)(b_2 - b_4)}$. Once again, the reflected entropy obtained above matches identically with twice the large tension limit of the bulk EWCS in eq. (3.75), obtained in the doubly holographic framework.

Phase-III

The computation of the reflected entropy in this phase proceeds exactly as the previous phase except that the subsystem-B receives the reflected island contribution whereas A does not. This phase may be described by replacing y_i with $\bar{y}_i$ in figure 26(c). As earlier, the correlation functions $G_{\text{CFT}_{I,II}}^{m,n}$ factorize as follows

$$G_{\text{CFT}_I}^{m,n} = \langle \sigma_{g_A}(b_1)\sigma_{g_A^{-1}}(b_2)\sigma_{g_B}(b_3)\sigma_{g_B^{-1}}(b_4)\rangle \langle \sigma_{g_B}(-\bar{y}_4^*)\sigma_{g_B^{-1}}(-\bar{y}_1^*)\rangle,$$
$$G_{\text{CFT}_{II}}^{m,n} = \langle \sigma_{g_B}(-\bar{y}_4^*)\sigma_{g_B^{-1}}(b_4)\rangle \langle \sigma_{g_A}(b_1)\sigma_{g_A^{-1}}(b_2)\sigma_{g_B}(b_3)\sigma_{g_B^{-1}}(-\bar{y}_1^*)\rangle, \tag{4.64}$$

leading to the following expression for the reflected entropy in the replica limit

$$S_R(A:B) = \frac{c_I}{3} \log \left[\frac{1+\sqrt{x}}{1-\sqrt{x}} \right] + \frac{c_{II}}{3} \log \left[\frac{1+\sqrt{x_1}}{1-\sqrt{x_1}} \right], \tag{4.65}$$

where $x = \frac{b_{12}b_{34}}{b_{13}b_{24}}$ and $x_1 = \frac{(b_1 - b_2)(b_3 + \bar{y}_1^*)}{(b_1 - b_3)(b_2 + \bar{y}_1^*)}$ are the corresponding cross ratios. The above expression matches with twice the EWCS obtained in eq. (3.78) in the doubly holographic perspective.

B. Subsystem C with an induced island

Next we will focus on the computations of the reflected entropy for specific configurations where $A \cup B \cup C$ possesses a conventional island $\text{Is}(A \cup B \cup C) = [-y_4^*, -y_1^*]$ and the subsystem C claims an induced island $\bar{\text{Is}}(C) = [-\bar{y}_3^*, -\bar{y}_2^*]$ (figure 26(d)). Following the extremization of eq. (4.41), we have $y_4^* = b_4$ and $y_1^* = b_1$ respectively. However for $\bar{y}_2^*$ and $\bar{y}_3^*$ we need to extremize the expression for the entanglement entropy of C which leads to a similar set of equations given in eq. (4.28) or eq. (4.56). Note that when C has an induced island of its own, the corresponding induced reflected entropy islands for A and B are disconnected as depicted in figure 26(d). This is a novel aspect of the induced islands absent in earlier investigations of reflected entropy involving islands. The relevant twist correlators for this case are given as

$$G_{\text{CFT}_{I,II}}^{m,n} = \langle \sigma_{g_A}(b_1)\sigma_{g_A^{-1}}(b_2)\sigma_{g_B}(b_3)\sigma_{g_B^{-1}}(b_4)\sigma_{g_A^{-1}}(-b_1)\sigma_{g_A}(-\bar{y}_2^*)\sigma_{g_B^{-1}}(-\bar{y}_3^*)\sigma_{g_B}(-b_4)\rangle, \tag{4.66}$$

There are three different phases I, II and III for this configuration depending on how the above correlators factorize.

Phase-IV

In this phase the subsystems A and B are comparable in size where the correlators in eq. (4.66) factorize as follows

$$G^{m,n}_{\text{CFT}_\text{I}} = \langle \sigma_{g_A}(-\bar{y}_2^*)\sigma_{g_A^{-1}}(b_2)\sigma_{g_B}(b_3)\sigma_{g_B^{-1}}(-\bar{y}_3^*)\rangle\langle \sigma_{g_A}(b_1)\sigma_{g_A^{-1}}(-b_1)\rangle\langle \sigma_{g_B^{-1}}(b_4)\sigma_{g_B}(-b_4)\rangle,$$
$$G^{m,n}_{\text{CFT}_\text{II}} = \langle \sigma_{g_A}(b_1)\sigma_{g_A^{-1}}(-b_1)\rangle\langle \sigma_{g_A}(-\bar{y}_2^*)\sigma_{g_A^{-1}}(b_2)\rangle\langle \sigma_{g_B}(b_3)\sigma_{g_B^{-1}}(-\bar{y}_3^*)\rangle\langle \sigma_{g_B}(-b_4)\sigma_{g_B^{-1}}(b_4)\rangle.$$
$$(4.67)$$

A similar factorization holds for the correlation function on the m-sheeted Riemann surface. Substituting the above expressions in eq. (4.9) and utilizing eq. (4.51) we determine the reflected entropy to be as follows

$$S_R(A:B) = \frac{c_\text{I}}{3}\log\left[\frac{1+\sqrt{w}}{1-\sqrt{w}}\right],\qquad(4.68)$$

where $w = \frac{(\bar{y}_2+b_2)(b_3+\bar{y}_3)}{(\bar{y}_2+b_3)(b_2+\bar{y}_3)}$ is the cross ratio. This matches identically with the large tension limit of twice the EWCS in the doubly holographic picture, given in eq. (3.84).

Phase-V

In phase-V, the size of the subsystem A is sufficiently large compared to the subsystem B. Here the eight point correlation function $G^{m,n}_{\text{CFT}_\text{I}}$ in eq. (4.66) factorizes into a six point function and a two point function as follows

$$G^{m,n}_{\text{CFT}_\text{I}} = \langle \sigma_{g_A}(b_1)\sigma_{g_A^{-1}}(-b_1)\rangle\langle \sigma_{g_A^{-1}}(b_2)\sigma_{g_B}(b_3)\sigma_{g_B^{-1}}(b_4)\sigma_{g_A}(-\bar{y}_2^*)\sigma_{g_B^{-1}}(-\bar{y}_3^*)\sigma_{g_B}(-b_4)\rangle.$$
$$(4.69)$$

The six point function on the r.h.s. of the above equation further factorizes into a product of two four point function in the large-c limit[23]

$$G^{m,n}_{\text{CFT}_\text{I}} = \langle \sigma_{g_A}(b_1)\sigma_{g_A^{-1}}(-b_1)\rangle\langle \sigma_{g_A^{-1}}(b_2)\sigma_{g_B}(b_3)\sigma_{g_A}(-\bar{y}_2^*)\sigma_{g_B^{-1}}(-\bar{y}_3^*)\rangle$$
$$\times\ \langle \sigma_{g_A^{-1}}(b_2)\sigma_{g_B}(b_3)\sigma_{g_B^{-1}}(b_4)\sigma_{g_B}(-b_4)\rangle.\qquad(4.70)$$

The CFT_II correlation function in eq. (4.66) on the other hand factorizes into product of two point function as follows

$$G^{m,n}_{\text{CFT}_\text{II}} = \langle \sigma_{g_A}(b_1)\sigma_{g_A^{-1}}(-b_1)\rangle\langle \sigma_{g_A}(-\bar{y}_2^*)\sigma_{g_A^{-1}}(b_2)\rangle\langle \sigma_{g_B}(b_3)\sigma_{g_B^{-1}}(-\bar{y}_3^*)\rangle\langle \sigma_{g_B}(-b_4)\sigma_{g_B^{-1}}(b_4)\rangle.$$
$$(4.71)$$

Substituting the above expressions in eq. (4.9) and utilizing eq. (4.51) we determine the reflected entropy to be as follows

$$S_R(A:B) = \frac{c_\text{I}}{3}\log\left[\frac{1+\sqrt{w_0}}{1-\sqrt{w_0}}\right] + \frac{c_\text{I}}{3}\log\left[\frac{1+\sqrt{w_1}}{1-\sqrt{w_1}}\right],\qquad(4.72)$$

---

[23]As demonstrated in [55], in the OPE channel corresponding to the present configuration the six point conformal black factorizes into two four point conformal blacks in the large central charge limit. Assuming the dominance of the $|\sigma_{g_A^{-1}g_B}\rangle$ block, the corresponding six point correlator may in turn be factorized into two four point correlators. Note that a similar factorization has been demonstrated in [56].

with cross ratios $w_0 = \frac{(b_4 - \bar{y}_3^*)(b_4 + \bar{y}_2^*)}{(b_4 + \bar{y}_3^*)(b_4 - \bar{y}_2^*)}$ and $w_1 = \frac{(b_3 - b_4)(b_2 + b_4)}{(b_2 - b_4)(b_3 + b_4)}$. Note that the reflected entropy computed in the effective lower dimensional perspective in eq. (4.72) is exactly the twice of EWCS in the large tension limit evaluated in eq. (3.89) in the context of double holography.

Phase-VI

In this phase, we observe the opposite situation compared to the previous phase, the subsystem B is larger than A. As a result, the correlator $G_{\mathrm{CFT_I}}^{m,n}$ in eq. (4.66) again factorizes into a six point function and a two point function. However, the factorization is different from the earlier case,

$$G_{\mathrm{CFT_I}}^{m,n} = \langle \sigma_{g_B}(-b_4)\sigma_{g_B^{-1}}(b_4)\rangle \langle \sigma_{g_A}(b_1)\sigma_{g_A^{-1}}(b_2)\sigma_{g_B}(b_3)\sigma_{g_A^{-1}}(-b_1)\sigma_{g_A}(-\bar{y}_2^*)\sigma_{g_B^{-1}}(-\bar{y}_3^*)\rangle. \tag{4.73}$$

As earlier the six point function on the r.h.s. of the above equation once again factorizes into a product of two four point function in the large-c limit

$$\begin{aligned} G_{\mathrm{CFT_I}}^{m,n} &= \langle \sigma_{g_B}(-b_4)\sigma_{g_B^{-1}}(b_4)\rangle \langle \sigma_{g_A}(b_1)\sigma_{g_A^{-1}}(b_2)\sigma_{g_B}(b_3)\sigma_{g_A^{-1}}(-b_1)\rangle \\ &\quad \times \langle \sigma_{g_A}(b_1)\sigma_{g_A^{-1}}(-b_1)\sigma_{g_A}(-\bar{y}_2^*)\sigma_{g_B^{-1}}(-\bar{y}_3^*)\rangle. \end{aligned} \tag{4.74}$$

The $\mathrm{CFT_{II}}$ correlation function in eq. (4.66) on the other hand factorizes into product of two point functions as in eq. (4.71). Substituting the above expressions in eq. (4.9) and utilizing eq. (4.51) we may determine the reflected entropy as

$$S_R(A:B) = \frac{c_\mathrm{I}}{3}\log\left[\frac{1+\sqrt{w_2}}{1-\sqrt{w_2}}\right] + \frac{c_\mathrm{I}}{3}\log\left[\frac{1+\sqrt{w_3}}{1-\sqrt{w_3}}\right], \tag{4.75}$$

where $w_2 = \frac{(b_3 + b_1)(b_1 - b_2)}{(b_1 - b_3)(b_1 + b_2)}$ and $w_3 = \frac{(\bar{y}_3^* + b_1)(b_1 - \bar{y}_2^*)}{(b_1 + \bar{y}_2^*)(b_1 - \bar{y}_3^*)}$ are the cross ratios. Similar to the earlier phases, the reflected entropy calculated here matches with the twice of EWCS computed in eq. (3.92).

4.2.3 No island saddle

In this phase all the subsystems A, B and C are very small in size such that neither of A, B, C and $A \cup B \cup C$ has any island. The effective Renyi reflected entropy is therefore given by

$$\begin{aligned} &S_R^{(m,n,\mathrm{eff})}(A \cup \mathrm{Is}_R(A) : B \cup \mathrm{Is}_R(B)) \\ &= \frac{1}{1-n}\log\left[\frac{\langle \sigma_{g_A}(b_1)\sigma_{g_A^{-1}}(b_2)\sigma_{g_B}(b_3)\sigma_{g_B^{-1}}(b_4)\rangle_{\mathrm{CFT_I}^{\otimes mn}}}{\left(\langle \sigma_{g_m}(b_1)\sigma_{g_m^{-1}}(b_2)\sigma_{g_m}(b_3)\sigma_{g_m^{-1}}(b_4)\rangle_{\mathrm{CFT_I}^{\otimes m}}\right)^n}\right] + (\mathrm{I} \leftrightarrow \mathrm{II}). \end{aligned} \tag{4.76}$$

Considering the contributions from both the CFTs and taking the replica limit we obtain

$$S_R(A:B) = \frac{c_\mathrm{I} + c_\mathrm{II}}{3}\log\left[\frac{1+\sqrt{x}}{1-\sqrt{x}}\right], \tag{4.77}$$

where $x = \frac{b_{12}b_{34}}{b_{13}b_{24}}$ is the cross-ratio. We observe an exact agreement between the above expression and the corresponding EWCS given in eq. (3.93).

5 Black hole evaporation: time evolution of EWCS

In this section, we study the time evolution of the EWCS dual to the reflected entropy for bipartite mixed states in the AdS/ICFT setup, in the context of the black hole information loss paradox. We will consider bipartite mixed state configurations in the thermal baths located outside an eternal black hole, where these baths collect Hawking radiation emitted from the black hole. The holographic dual of the eternal black hole in AdS$_3$ is the thermofield double (TFD) state [57], which may be obtained from the vacuum state of the ICFT$_2$ via a conformal map. As described in [20], the TFD state in the ICFT$_2$ may be prepared from a path integral on half of an infinite cylinder with a circular interface between the two CFT$_2$s dividing the cylinder into two distinct parts. Furthermore, as explained in [20], the TFD state on the cylinder may be obtained via a series of conformal transformations from the vacuum state of the ICFT on the complex plane described by $\zeta = x + it_E$. The planar interface $x_i = 0$ between the two CFT$_2$s may be mapped into a circle of length ℓ, $\tilde{x}^2 + \tilde{t}^2 = \ell^2$ by utilizing the transformation

$$p = \frac{4\ell^2}{2\ell - \zeta} - \ell \,, \tag{5.1}$$

where $p = \tilde{x} + i\tilde{t}_E$ is the complex coordinate on the plane where the CFT$_{\text{I/II}}$s are defined respectively on the interior and exterior of the circle of length ℓ centered at the origin. Subsequently, the conformal transformation

$$p = \ell\, e^{\frac{2\pi q}{\beta}} \,, \tag{5.2}$$

maps the planar geometry into the infinite cylinder with the interface mapped to a disk $\mathfrak{Re}(q) = 0$ with $q = u + iv_E$ denoting the complex coordinate on the thermal cylinder on which the TFD state is defined.

The bulk dual geometry corresponding to the ICFT defined on the plane with a circular interface will be important for computational purposes in the following. Note that the transformation in eq. (5.1) is nothing but a $SL(2, R)$ transformation[24] for which the bulk dual geometry may be easily found by looking for the AdS$_3$ isometry which maps straight lines into circles[25] [6]. The corresponding coordinate transformations are given as follows

$$\tilde{x}_i = \frac{x_i - \frac{x_i^2 + z_i^2 - t_i^2}{2\ell}}{1 - \frac{x_i}{\ell} + \frac{x_i^2 + z_i^2 - t_i^2}{4\ell^2}} + l \,, \quad \tilde{z}_i = \frac{z_i}{1 - \frac{x_i}{\ell} + \frac{x_i^2 + z_i^2 - t_i^2}{4\ell^2}} \,, \quad \tilde{t}_i = \frac{t_i}{1 - \frac{x_i}{\ell} + \frac{x_i^2 + z_i^2 - t_i^2}{4\ell^2}} \,, \quad (i = \text{I}, \text{II}) \tag{5.3}$$

where we have Wick rotated the time coordinate to $t = -it_E$. Being an isometry, the above bulk transformations do not change the metric and hence we have Poincaré AdS$_3$ on either side of the spherical EOW brane with profile

$$\tilde{x}_{\text{I}}^2 - \tilde{t}_{\text{I}}^2 + (\tilde{z}_{\text{I}} - \ell \tan \psi_{\text{I}})^2 = \ell^2 \sec^2 \psi_{\text{I}} \,,$$
$$\tilde{x}_{\text{II}}^2 - \tilde{t}_{\text{II}}^2 + (\tilde{z}_{\text{II}} + \ell \tan \psi_{\text{II}})^2 = \ell^2 \sec^2 \psi_{\text{II}} \,. \tag{5.4}$$

---

[24]In particular, it is given by a special conformal transformation followed by a translation.

[25]Alternatively, one may use the Banados formalism [58, 59].

On the cylinder, we will consider Lorentzian time evolution utilizing the Wick rotation $v = -iv_E$. Having described the required notations and conventions we will now compute the EWCS dual to the reflected entropy of the mixed state configuration involving two adjacent subsystems of an ICFT$_2$ in a TFD state. Note that unlike the vacuum case, here we will restrict ourselves to the computation for the adjacent intervals as we do not expect that the disjoint interval case will reveal any novel physical aspects that are qualitatively different from those observed in the adjacent interval scenario.

Consider the mixed state configuration of adjacent subsystems $A \cup B$ where $A = A_L \cup A_R$ and $B = B_L \cup B_R$ with

$$
\begin{aligned}
A_L &= [(u_0, v), (u_1, v)]_{\text{I}} \cup [(-u_0, v), (-u_1, v)]_{\text{II}}, \\
B_L &= [(u_1, v), (\infty, v)]_{\text{I}} \cup [(-u_1, v), (-\infty, v)]_{\text{II}}, \\
A_R &= \left[\left(u_0, -v + \frac{i\beta}{2}\right), \left(u_1, -v + \frac{i\beta}{2}\right)\right]_{\text{I}} \cup \left[\left(-u_0, -v + \frac{i\beta}{2}\right), \left(-u_1, -v + \frac{i\beta}{2}\right)\right]_{\text{II}}, \\
B_R &= \left[\left(u_1, -v + \frac{i\beta}{2}\right), \left(\infty, -v + \frac{i\beta}{2}\right)\right]_{\text{I}} \cup \left[\left(-u_1, -v + \frac{i\beta}{2}\right), \left(-\infty, -v + \frac{i\beta}{2}\right)\right]_{\text{II}}.
\end{aligned}
$$
(5.5)

The entanglement entropy for $A \cup B$ has been investigated in [20], where it was observed that in the doubly holographic picture the entanglement entropy is computed through the lengths of two competing sets of RT surfaces: the Hartman-Maldacena (HM) surfaces [57] and a pair of geodesics which cross the EOW brane. The Page time at which these two saddles change dominance, was found to be [20]

$$
v_P = \frac{\beta}{2\pi} \cosh^{-1}\left[\sinh\left(\frac{2\pi u_0}{\beta}\right) \frac{6 S_{\text{int}}}{c_{\text{I}} + c_{\text{II}}}\right],
$$
(5.6)

where S_{int} denotes the interface entropy. Within each phase of the entanglement entropy of $A \cup B$, the entanglement wedge cross section corresponding to the mixed state ρ_{AB} undergoes various phase transitions with time v. In the following, we will systematically investigate all these phases and compute the EWCS in each case.

5.1 Before Page time

Before the Page time, the RT saddle contributing to the entanglement entropy of $A \cup B$ consists of two HM surfaces which connect the endpoints of the subsystems from both copies. In the effective intermediate picture, this corresponds to the non-island phase. In this phase, the EWCS between A and B is either HM surface connecting the shared boundary of A and B on each copy or terminates on the smaller HM surface, as sketched in figure 27.

Phase-I

To compute the length of the EWCS, we employ the trick utilized in [20], namely perform the computations in the planar tilde coordinates in eq. (5.3) and finally transform back to the cylinder. From eq. (5.2) the Lorentzian trajectories of the endpoints of A and B in
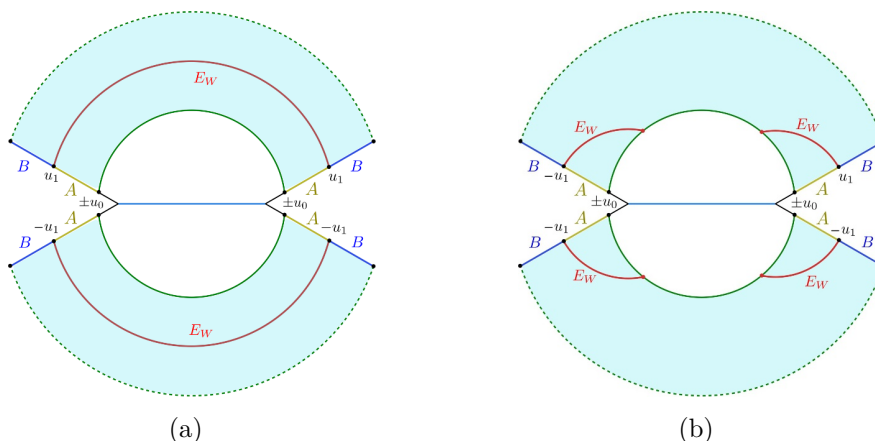
Figure 27. Phase transitions of the EWCS corresponding to two adjacent subsystems in the radiation bath, before the Page time: (a) the EWCS does not terminate on the RT of $A \cup B$, (b) EWCS terminates on the smaller HM surface.

the left copy of the ICFT are given by

$$\tilde{x}_{\mathrm{I}}(u_k, v) = \ell e^{-\frac{2\pi u_k}{\beta}} \cosh\left(\frac{2\pi v}{\beta}\right), \qquad \tilde{t}_{\mathrm{I}}(u_k, v) = \ell e^{-\frac{2\pi u_k}{\beta}} \sinh\left(\frac{2\pi v}{\beta}\right)$$

$$\tilde{x}_{\mathrm{II}}(u_k, v) = \ell e^{\frac{2\pi u_k}{\beta}} \cosh\left(\frac{2\pi v}{\beta}\right), \qquad \tilde{t}_{\mathrm{II}}(u_k, v) = \ell e^{\frac{2\pi u_k}{\beta}} \sinh\left(\frac{2\pi v}{\beta}\right), \qquad (5.7)$$

while similar expressions hold for the TFD copy with $\tilde{x}$ replaced by $-\tilde{x}$. For the present phase, as described earlier, the EWCS is a HM surface whose length has already been computed in [20]. Following this, we may write down the EWCS as follows

$$E_W(\rho_{AB}) = \frac{L_{\mathrm{I}}}{2G_{\mathrm{N}}} \log\left[\frac{2\tilde{x}_{\mathrm{I}}(u_1, v)}{\tilde{\epsilon}_{\mathrm{I}}(u_1, v)}\right] + \frac{L_{\mathrm{II}}}{2G_{\mathrm{N}}} \log\left[\frac{2\tilde{x}_{\mathrm{II}}(u_1, v)}{\tilde{\epsilon}_{\mathrm{II}}(u_1, v)}\right]$$

$$= \frac{L_{\mathrm{I}} + L_{\mathrm{II}}}{2G_{\mathrm{N}}} \log\left[\frac{\beta}{\pi\epsilon} \cosh\left(\frac{2\pi v}{\beta}\right)\right], \qquad (5.8)$$

where we have utilized the fact that the cut-off in tilde coordinates is related to the cylinder cut-off as follows (cf. eq. (5.2))

$$\tilde{\epsilon} = \left(\frac{\beta}{2\pi\ell} e^{-\frac{\pi(q+\bar{q})}{\beta}}\right) \epsilon. \qquad (5.9)$$

Phase-II

Next, we compute the lengths of the EWCS landing on the HM surfaces, utilizing the Poincaré AdS$_3$ geometry described by the tilde coordinates.

In the following, we will suppress the subscripts I, II to keep the notation simple. Due to the symmetry of the setup, the computation reduces to finding the length of a minimal surface from $(\tilde{x}_1, \tilde{t}_1)$ to the RT surface described by equation $\tilde{x}^2 + \tilde{z}^2 = \tilde{x}_0^2$ at $\tilde{t} = \tilde{t}_0$. Parametrizing a point $P : (\tilde{x}, \tilde{t}, \tilde{z}) = (\tilde{x}_0 \sin\theta, \tilde{t}_0, \tilde{x}_0 \cos\theta)$ on the RT surface, we may obtain the length of the surface from $Q = (\tilde{x}_1, \tilde{t}_1)$ as follows

$$d_{PQ} = L \cosh^{-1}\left[\frac{(\tilde{x}_0 \sin\theta - \tilde{x}_1)^2 - (\tilde{t}_0 - \tilde{t}_1)^2 + (\tilde{x}_0 \cos\theta)^2}{2\tilde{\epsilon}_1 \tilde{x}_0 \cos\theta}\right]. \qquad (5.10)$$
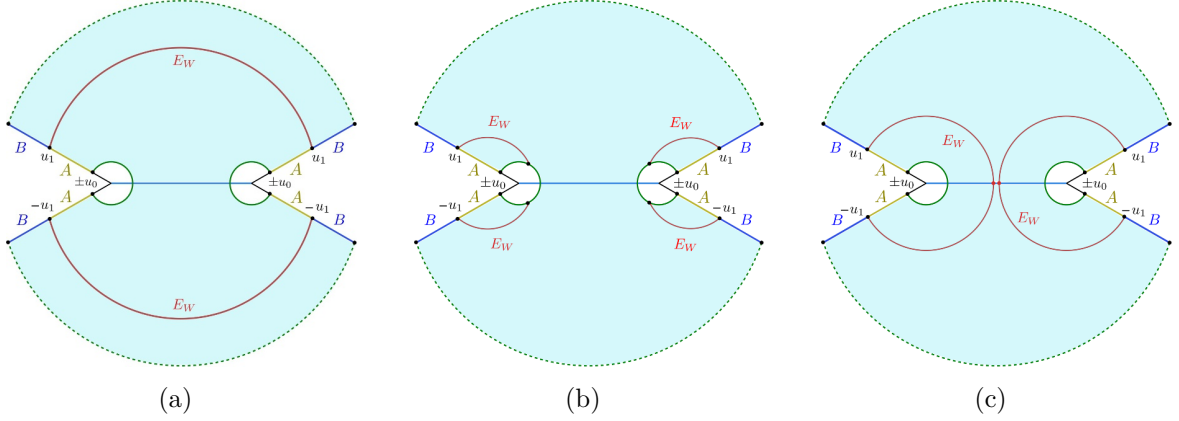
Figure 28. Phase transitions of the EWCS corresponding to two adjacent subsystems in the radiation bath, after the Page time: (a) the EWCS is a HM surface connecting the shared boundary of A and B on both copies, (b) EWCS terminates on the RT surface of $A \cup B$, (c) the EWCS crosses the brane. In the intermediate braneworld perspective, non-trivial island cross-sections for the reflected entropy appear on the brane.

Extremization with respect to the arbitrary angle θ leads to

$$\partial_\theta d_{PQ} = 0 \Rightarrow \theta = \sin^{-1}\left[\frac{2\tilde{x}_0\tilde{x}_1}{\tilde{x}_0^2 + \tilde{x}_1^2 - (\tilde{t}_0 - \tilde{t}_1)^2}\right]. \tag{5.11}$$

Substituting this back into eq. (5.10), we obtain the minimal length to be

$$d_{PQ}^{\min} = L \log\left[\frac{\sqrt{\left(\tilde{x}_0^2 + \tilde{x}_1^2 - (\tilde{t}_0 - \tilde{t}_1)^2\right)^2 - 4\tilde{x}_0^2\tilde{x}_1^2}}{\tilde{\epsilon}_1\tilde{x}_0}\right]. \tag{5.12}$$

Now restoring the subscripts I, II, utilizing eqs. (5.7) and (5.9) and accounting for the pair of geodesics for both TFD copies of the setup, we obtain the minimal EWCS for this phase to be

$$E_W(\rho_{AB}) = \frac{L_{\mathrm{I}} + L_{\mathrm{II}}}{2G_{\mathrm{N}}} \log\left[\frac{\beta\left(e^{\frac{2\pi u_1}{\beta}} - e^{\frac{2\pi u_0}{\beta}}\right)\sqrt{e^{\frac{4\pi u_0}{\beta}} + e^{\frac{4\pi u_1}{\beta}} + 2e^{\frac{2\pi(u_0+u_1)}{\beta}}\cosh\left(\frac{4\pi v}{\beta}\right)}}{2\pi\epsilon\, e^{\frac{2\pi(u_0+u_1)}{\beta}}\cosh\left(\frac{2\pi v}{\beta}\right)}\right]. \tag{5.13}$$

5.2 After Page time

After the Page time v_P, the RT saddle for $A \cup B$ crosses the EOW brane which corresponds to the appearance of an island in the intermediate braneworld picture. In this case, the minimal EWCS has three possible phases which are depicted in figure 28.

Phase-III

As shown in figure 28(a), this phase corresponds to a HM surface connecting the shared boundary of A and B on both copies, which is identical to phase-I. Hence, the EWCS is given by

$$E_W(\rho_{AB}) = \frac{L_{\mathrm{I}} + L_{\mathrm{II}}}{2G_{\mathrm{N}}} \log\left[\frac{\beta}{\pi\epsilon}\cosh\left(\frac{2\pi v}{\beta}\right)\right]. \tag{5.14}$$

Note that although the expression is identical to that of phase-I, this phase gets activated only after the Page time and hence contributes non-trivially to the Page curve of the holographic reflected entropy.

Phase-IV

In phase-IV, the EWCS terminates on the RT surfaces which cross the EOW brane. We find it easier to perform the computations in the original planar coordinates[26] (x_i, t_i, z_i) given in eq. (5.3), where the equations for the RT surfaces may be easily obtained as [7]

$$x_i^2 + z_i^2 = x_0^2, \qquad t = t_0 \,, \tag{5.15}$$

where (u_0, v) has been mapped to (x_0, t_0) utilizing the transformations in eqs. (5.2) and (5.3). In these coordinates, the task of finding the EWCS reduces to that for a minimal curve starting on the above RT surface and terminating on (x_1, t_1). We have already performed an identical computation in the tilde coordinates for phase-II. Hence, utilizing eq. (5.12) we may write down the corresponding length as follows

$$
\begin{aligned}
d_{\min} &= L \log \left[\frac{\sqrt{\left(x_0^2 + x_1^2 - (t_0 - t_1)^2\right)^2 - 4x_0^2 x_1^2}}{\epsilon(x_1, t_1) x_0} \right] \\
&= L \log \left[\frac{2\sqrt{\left((\tilde{x}_0 - \tilde{x}_1)^2 - (\tilde{t}_0 - \tilde{t}_1)^2\right)\left(\ell^4 + 2\ell^2(\tilde{t}_0\tilde{t}_1 - \tilde{x}_0\tilde{x}_1) + (\tilde{t}_0^2 - \tilde{x}_0^2)(\tilde{t}_1^2 - \tilde{x}_1^2)\right)}}{\tilde{\epsilon}_1 \left(\tilde{x}_0^2 - \tilde{t}_0^2 - \ell^2\right)} \right] ,
\end{aligned}
\tag{5.16}
$$

where in the second equality, we have used eq. (5.3) and the fact that the cut-off in tilde and non-tilde coordinates are related by

$$\epsilon(x, t) = \frac{4\ell^2 \tilde{\epsilon}}{(\tilde{x} + \ell)^2 - \tilde{t}^2} \,. \tag{5.17}$$

Finally transforming to the cylinder coordinates using eqs. (5.2) and (5.9), restoring the subscripts I, II and accounting for the pair of geodesics in both copies of the geometry, we obtain the EWCS for this phase as follows

$$E_W(\rho_{AB}) = \frac{L_{\mathrm{I}} + L_{\mathrm{II}}}{2G_{\mathrm{N}}} \log \left[\frac{\beta}{\pi\epsilon} \frac{\cosh\left(\frac{2\pi u_1}{\beta}\right) - \cosh\left(\frac{2\pi u_0}{\beta}\right)}{\sinh\left(\frac{2\pi u_0}{\beta}\right)} \right] . \tag{5.18}$$

Phase-V

In the final phase depicted in figure 28(c), the EWCS between A and B consists of two geodesics connecting the shared boundary of A and B in $\mathrm{CFT}_2^{\mathrm{I}}$ and $\mathrm{CFT}_2^{\mathrm{II}}$, which cross the EOW brane. The length of such geodesics has already been computed in [20] and hence the EWCS is given as

$$E_W(\rho_{AB}) = \frac{L_{\mathrm{I}} + L_{\mathrm{II}}}{2G_{\mathrm{N}}} \log \left[\frac{\beta}{\pi\epsilon} \sinh\left(\frac{2\pi u_1}{\beta}\right) \right] + 2S_{\mathrm{int}} \,, \tag{5.19}$$

where S_{int} is the interface entropy defined in eq. (3.50).

---

[26]Once again, owing to the symmetry of the setup, we are suppressing the subscripts I, II, which will be restored at the end of computations.

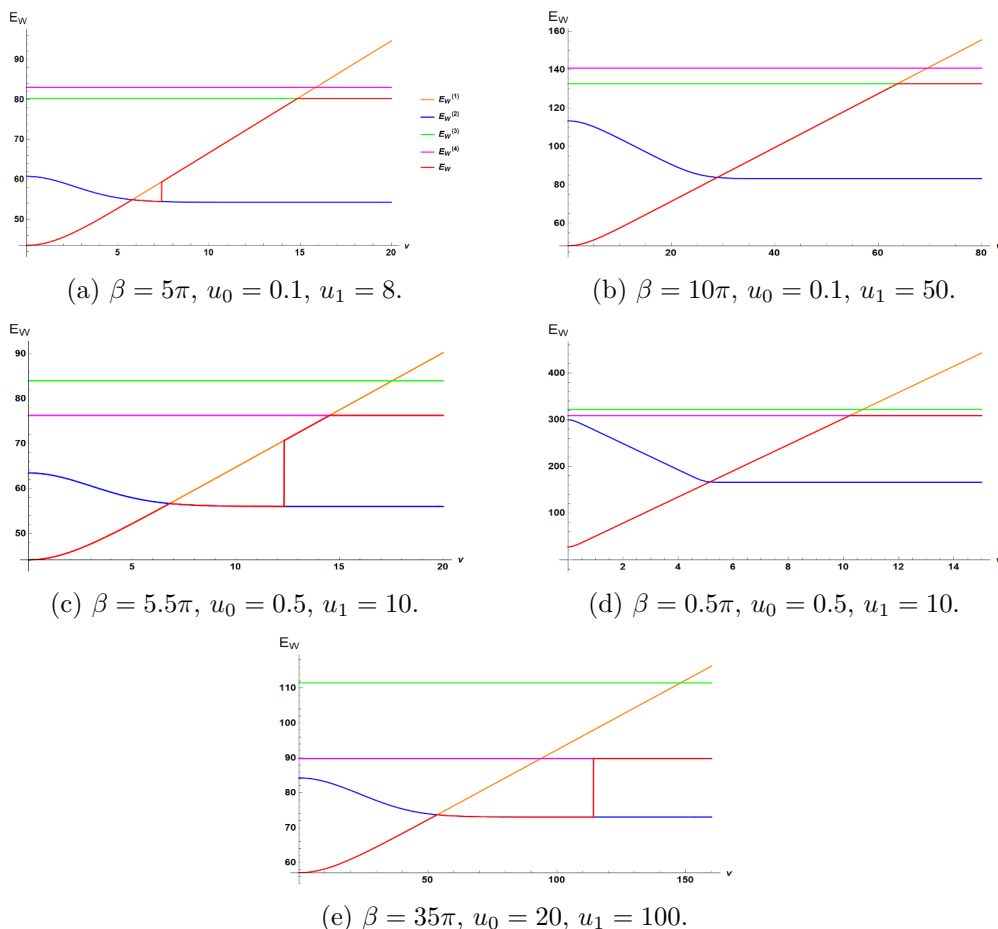(a) $\beta = 5\pi$, $u_0 = 0.1$, $u_1 = 8$.

(b) $\beta = 10\pi$, $u_0 = 0.1$, $u_1 = 50$.

(c) $\beta = 5.5\pi$, $u_0 = 0.5$, $u_1 = 10$.

(d) $\beta = 0.5\pi$, $u_0 = 0.5$, $u_1 = 10$.

(e) $\beta = 35\pi$, $u_0 = 20$, $u_1 = 100$.

Figure 29. Page curves (red): for $c_{\mathrm{I}} = 1$, $c_{\mathrm{II}} = 20$, $L_{\mathrm{I}} = 0.1$, $L_{\mathrm{II}} = 0.2$, $\epsilon = 0.01$, $\delta = 0.01$.

5.3 Page curves

In this subsection, we plot the evolution of the EWCS with time in figure 29 which correspond to the analogues of the Page curves for reflected entropy from the holographic duality mentioned earlier. We note that the EWCS between nearby radiation and distant radiation experiences two phases. At early times the entanglement entropy of $A \cup B$ is in the connected phase and correspondingly the EWCS is given by the minimum of phase-I and phase-II. On the other hand, after the Page time for $A \cup B$ given in eq. (5.6), the disconnected phase dominates and the EWCS is given by the minimum of phase-III, phase-IV and phase-V.

6 Reflected entropy from island prescription: TFD state

In this section, we compute the island contributions to the reflected entropy for the mixed state of adjacent subsystems A and B in two copies of ICFT$_2$s in a TFD state. As depicted in figure 30 we consider one of the two intervals denoted by B to be semi-infinite in order to simplify our computations. As described in section 5, the two copies of the ICFT$_2$s in a TFD state are on a cylinder which is obtained from the vacuum state on the complex plane through a series of conformal transformations. Note that on such a cylinder we denote the
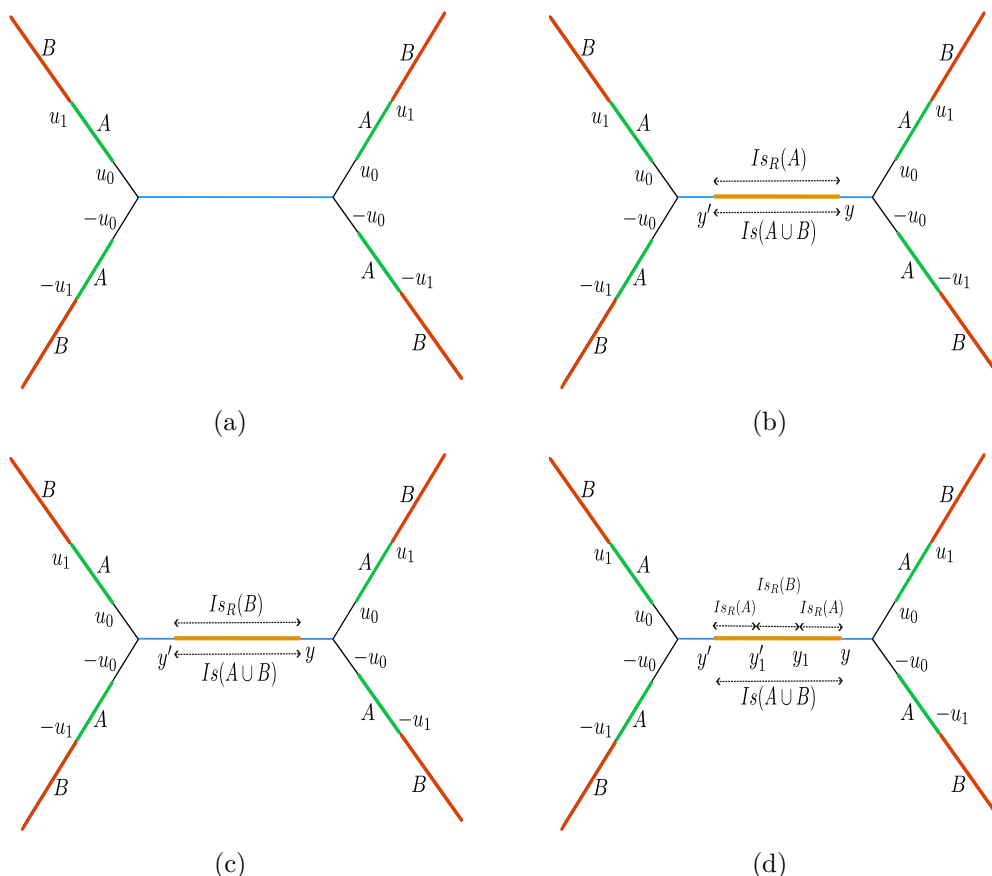
Figure 30. Schematic for a mixed state configuration involving adjacent subsystems A and B in the two copies of thermal ICFT$_2$s in a TFD state and their corresponding reflected entropy islands on the brane in the effective two dimensional theory. Note that we have denoted the points on brane in the left and the right subsystem by y' and y respectively for clarity but their numerical values are same.

complex coordinates on the two copies ICFT$_L$ and ICFT$_R$ by $\tilde{q}$ and q respectively. Since the intervals chosen in the CFT$_I$ and CFT$_{II}$ are identical, the spatial u coordinates differ only by sign whereas the temporal v coordinates are same i.e. if

$$q_i^I = u_i + iv_E, \qquad\qquad q_i^{II} = -u_i + iv_E$$
$$\tilde{q}_i^I = u_i - iv_E - \frac{i\beta}{2}, \qquad\qquad \tilde{q}_i^{II} = -u_i - iv_E - \frac{i\beta}{2} \qquad (6.1)$$

where $i = 0, 1, 2$. Note that the points on the brane are denoted by

$$q_b^I = -y + iv_E, \qquad\qquad q_b^{II} = y + iv_E$$
$$\tilde{q}_b^I = -y - iv_E - \frac{i\beta}{2}, \qquad\qquad \tilde{q}_b^{II} = y - iv_E - \frac{i\beta}{2} . \qquad (6.2)$$

When we require multiple points on the brane we will denote them as $q_a, q_b, q_c \ldots$ and $\tilde{q}_a, \tilde{q}_b, \tilde{q}_c \ldots$. At the end of computation we will analytically continue to Lorentzian coordinates by Wick rotation $v_E = -iv$. Note that in the above definitions the Roman numerals I, II in

the superscript indicate whether the coordinate is in CFT_I or CFT_II within a single copy of the ICFT_2. The two subsystems are given by $A = A_L \cup A_R$ and $B = B_L \cup B_R$ where

$$
\begin{aligned}
A_L &= [q_0^\text{I}, q_1^\text{I}] \cup [q_0^\text{II}, q_1^\text{II}], \\
B_L &= [q_1^\text{I}, q_2^\text{I}] \cup [q_1^\text{II}, q_2^\text{II}], \\
A_R &= [\tilde{q}_0^\text{I}, \tilde{q}_1^\text{I}] \cup [\tilde{q}_0^\text{II}, \tilde{q}_1^\text{II}], \\
B_R &= [\tilde{q}_1^\text{I}, \tilde{q}_2^\text{I}] \cup [\tilde{q}_1^\text{II}, \tilde{q}_2^\text{II}].
\end{aligned}
\tag{6.3}
$$

Note that we have chosen B to be semi-infinite and therefore $q_2^\text{I} = [\infty, v]$, $q_2^\text{II} = [-\infty, v]$ and $\tilde{q}_2^\text{I} = \left[\infty, -v - \frac{i\beta}{2}\right]$, $\tilde{q}_2^\text{II} = \left[-\infty, -v - \frac{i\beta}{2}\right]$. In the rest of this article we will drop the superscripts I, II for brievity. However note that there is a sign difference between the spatial coordinate depending on whether it is occuring in the correlation function of CFT_I or CFT_II. As discussed in the previous section there are two phases for the bulk entanglement wedge corresponding to the semi-infinite subsystem AB. These two phases correspond to the presence or absence of the entanglement entropy islands for AB. For each phase of the entanglement entropy there are multiple sub-phases for the reflected entropy which we describe below.

6.1 Before Page time

We begin by considering the case when the subsystem AB does not receive any island contribution as depicted in figure 30(a). When there are no island contributions the required correlation function corresponding to the reflected entropy is given by

$$
G_{\text{CFT}_\text{k}}^{m,n} = \langle \sigma_{g_A}(q_0) \sigma_{g_A^{-1} g_B}(q_1) \sigma_{g_A}(\tilde{q}_0) \sigma_{g_A^{-1} g_B}(\tilde{q}_1) \rangle
\tag{6.4}
$$

where $k = \text{I}, \text{II}$ indicates that the correlators in CFT_I and CFT_II have the same form. As earlier we have dropped the subscript $CFT_k^{\otimes mn}$ on the r.h.s. for brevity. Apart from these we would also require the following correlator which occurs in the denominator in the r.h.s. of eq. (4.9) for the effective reflected entropy

$$
G_{\text{CFT}_\text{k}}^{m} = \langle \sigma_{g_m}(q_0) \sigma_{g_m}(\tilde{q}_0) \rangle .
\tag{6.5}
$$

Phase-I

In phase-I the four point correlator above simply factorizes into product of 2 two-point correlators in the large-c limit as follows

$$
G_{\text{CFT}_\text{k}}^{m,n} = \langle \sigma_{g_A}(q_0) \sigma_{g_A}(\tilde{q}_0) \rangle \langle \sigma_{g_A^{-1} g_B}(q_1) \sigma_{g_A^{-1} g_B}(\tilde{q}_1) \rangle .
\tag{6.6}
$$

From the above result and eq. (6.5) we have all the correlation functions required to compute the reflected entropy in eq. (4.9) in terms of the two point functions. Hence substituting them in eq. (4.9), we obtain the reflected entropy to be as follows

$$
S_R(A : B) = 2 \frac{c_\text{I} + c_\text{II}}{3} \log\left[\frac{\beta}{\pi\epsilon} \cosh\left(\frac{2\pi v}{\beta}\right)\right].
\tag{6.7}
$$

Note that the above result for the reflected entropy exactly matches with twice the area of EWCS in the bulk geometry given in eq. (5.8) upon utilizing the Brown-Henneaux relation.

Phase-II

In this phase, the size of the subsystem A is considered to be small compared to that of B and in the large-c limit the four point function in eq. (6.4) receives maximum contribution from the block corresponding to the operator σ_{g_B} ($|\sigma_{g_B}\rangle\langle\sigma_{g_B}|$) which leads to the following factorization[27]

$$G^{m,n}_{\mathrm{CFT_k}} = \langle\sigma_{g_A}(q_0)\sigma_{g_A^{-1}g_B}(q_1)\sigma_{g_B}(\tilde{q}_0)\rangle\langle\sigma_{g_B}(q_0)\sigma_{g_A}(\tilde{q}_0)\sigma_{g_A^{-1}g_B}(\tilde{q}_1)\rangle$$
$$G^{m}_{\mathrm{CFT_k}} = \langle\sigma_{g_m}(q_0)\sigma_{g_m}(\tilde{q}_0)\rangle\,. \tag{6.8}$$

Since the form of the three point correlators are fixed by conformal symmetry we obtain the following expression for the reflected entropy

$$S_R(A:B) = 2\frac{c_{\mathrm{I}} + c_{\mathrm{II}}}{3}\log\left[\frac{\beta\left(e^{\frac{2\pi u_1}{\beta}} - e^{\frac{2\pi u_0}{\beta}}\right)\sqrt{e^{\frac{4\pi u_0}{\beta}} + e^{\frac{4\pi u_1}{\beta}} + 2e^{\frac{2\pi(u_0+u_1)}{\beta}}\cosh\left(\frac{4\pi v}{\beta}\right)}}{2\pi\epsilon\, e^{\frac{2\pi(u_0+u_1)}{\beta}}\cosh\left(\frac{2\pi v}{\beta}\right)}\right]\,. \tag{6.9}$$

Once again this precisely matches with twice the EWCS given in eq. (5.13) verifying the holographic duality between the two.

6.2 After Page time

We now proceed to compute the reflected entropy for phases in which the subsystem-AB possesses an entanglement entropy island.

Phase-III

The island phase for the entanglement entropy of the subsystem-AB leads to three sub-phases for the reflected entropy (phase III, phase IV and phase V). In phase III, the subsystem-A is so large that the entire entanglement entropy island belongs to the reflected entropy island of A as depicted in the above figure 30(b). The correlator required to determine the reflected entropy is given as

$$G^{m,n}_{\mathrm{CFT_k}} = \langle\sigma_{g_A}(q_0)\sigma_{g_A^{-1}g_B}(q_1)\sigma_{g_A^{-1}}(q_b)\sigma_{g_A^{-1}}(\tilde{q}_b)\sigma_{g_A}(\tilde{q}_0)\sigma_{g_A^{-1}g_B}(\tilde{q}_1)\rangle \tag{6.10}$$

$$G^{m}_{\mathrm{CFT_k}} = \langle\sigma_{g_m}(q_0)\sigma_{g_m^{-1}}(q_b)\sigma_{g_m^{-1}}(\tilde{q}_b)\sigma_{g_m}(\tilde{q}_0)\rangle\,. \tag{6.11}$$

In the large-c limit, each six point correlator in eq. (6.10) factorizes into the product of a two point correlator of the composite operator $\sigma_{g_A^{-1}g_B}$ and a four point correlator of non-composite operators. The four point function of non-composite operators further factorizes into a product of 2 two-point correlators which leads to the following result

$$G^{m,n}_{\mathrm{CFT_k}} = \langle\sigma_{g_A}(q_0)\sigma_{g_A^{-1}}(q_b)\rangle\langle\sigma_{g_A^{-1}}(\tilde{q}_b)\sigma_{g_A}(\tilde{q}_0)\rangle\langle\sigma_{g_A^{-1}g_B}(q_1)\sigma_{g_A^{-1}g_B}(\tilde{q}_1)\rangle \tag{6.12}$$

$$G^{m}_{\mathrm{CFT_k}} = \langle\sigma_{g_m}(q_0)\sigma_{g_m^{-1}}(q_b)\rangle\langle\sigma_{g_m^{-1}}(\tilde{q}_b)\sigma_{g_m}(\tilde{q}_0)\rangle\,. \tag{6.13}$$

---

[27]Note that this phase corresponds to the channel in which the operators $\sigma_{g_A^{-1}g_B}$ and σ_{g_B} come close by. Since the leading operator in their OPE expansion is σ_{g_B}, it provides the dominant contribution in the large-c limit.

Since the full correlator is now expressed in terms of the two point correlators, we obtain the following expression for the reflected entropy

$$S_R(A:B) = 2\frac{c_{\mathrm{I}} + c_{\mathrm{II}}}{3} \log\left[\frac{\beta}{\pi\epsilon}\cosh\left(\frac{2\pi v}{\beta}\right)\right]. \tag{6.14}$$

Observe that this is exactly equal to twice the EWCS in the bulk 3D geometry obtained in eq. (5.14) which once again verifies the holographic duality between the two.

Phase-IV

In phase IV, the subsystem-A is so small that the entire entanglement entropy island belongs the reflected entropy island of B as depicted in the above figure 30(c). The correlation function required to determine the reflected entropy is given as

$$G^{m,n}_{\mathrm{CFT_k}} = \langle \sigma_{g_A}(q_0)\sigma_{g_A^{-1}g_B}(q_1)\sigma_{g_B^{-1}}(q_b)\sigma_{g_B^{-1}}(\tilde{q}_b)\sigma_{g_A}(\tilde{q}_0)\sigma_{g_A^{-1}g_B}(\tilde{q}_1)\rangle \tag{6.15}$$

$$G^{m}_{\mathrm{CFT_k}} = \langle \sigma_{g_m}(q_0)\sigma_{g_m^{-1}}(q_b)\sigma_{g_m^{-1}}(\tilde{q}_b)\sigma_{g_m}(\tilde{q}_0)\rangle. \tag{6.16}$$

In the large-c limit the above correlation functions factorizes as follows

$$G^{m,n}_{\mathrm{CFT_k}} = \langle \sigma_{g_A}(q_0)\sigma_{g_A^{-1}g_B}(q_1)\sigma_{g_B^{-1}}(q_b)\rangle\langle \sigma_{g_B^{-1}}(\tilde{q}_b)\sigma_{g_A}(\tilde{q}_0)\sigma_{g_A^{-1}g_B}(\tilde{q}_1)\rangle. \tag{6.17}$$

Utilizing the conformal transformation from the cylinder to the plane (where the form of the three point functions is known) and introducing the appropriate Weyl Factors for points on the brane, we may compute the Renyi reflected entropy by substituting the above correlators in eq. (4.9). This leads to the following result for reflected entropy upon taking the replica limit

$$S_R(A:B) = 2\frac{c_{\mathrm{I}} + c_{\mathrm{II}}}{3} \log\left[\frac{\beta}{\pi\epsilon}\frac{\cosh\left(\frac{2\pi u_1}{\beta}\right) - \cosh\left(\frac{2\pi u_0}{\beta}\right)}{\sinh\left(\frac{2\pi u_0}{\beta}\right)}\right]. \tag{6.18}$$

which precisely matches with twice the corresponding EWCS given in eq. (5.18) upon using Brown Henneaux relations for the central charges of the two CFTs.

Phase-V

In this phase both the subsystems A and B posses their respective reflected entropy islands as depicted in the figure 30(d) above. In this case we require the following correlators to compute the reflected entropy

$$G^{m,n}_{\mathrm{CFT_k}} = \langle \sigma_{g_A}(q_0)\sigma_{g_A^{-1}g_B}(q_1)\sigma_{g_{AB^{-1}}}(q_a)\sigma_{g_A^{-1}}(q_b)\sigma_{g_A^{-1}}(\tilde{q}_b)\sigma_{g_{AB^{-1}}}(\tilde{q}_a)\sigma_{g_A}(\tilde{q}_0)\sigma_{g_A^{-1}g_B}(\tilde{q}_1)\rangle$$
$$G^{m}_{\mathrm{CFT_k}} = \langle \sigma_{g_m}(q_0)\sigma_{g_m^{-1}}(q_b)\sigma_{g_m^{-1}}(\tilde{q}_b)\sigma_{g_m}(\tilde{q}_0)\rangle. \tag{6.19}$$

In the large-c limit, the above correlation functions factorize as follows

$$G^{m,n}_{\mathrm{CFT_k}} = \langle \sigma_{g_A}(q_0)\sigma_{g_A^{-1}}(q_b)\rangle\langle \sigma_{g_A^{-1}g_B}(q_1)\sigma_{g_{AB^{-1}}}(q_a)\rangle\langle \sigma_{g_A}(\tilde{q}_0)\sigma_{g_A^{-1}}(\tilde{q}_b)\rangle\langle \sigma_{g_{AB^{-1}}}(\tilde{q}_a)\sigma_{g_A^{-1}g_B}(\tilde{q}_1)\rangle$$
$$G^{m}_{\mathrm{CFT_k}} = \langle \sigma_{g_m}(q_0)\sigma_{g_m^{-1}}(q_b)\rangle\langle \sigma_{g_m^{-1}}(\tilde{q}_b)\sigma_{g_m}(\tilde{q}_0)\rangle. \tag{6.20}$$

Substituting the above correlators in eq. (4.9) and adding the area term in eq. (4.2) to it, followed by an extremization similar to that in [20], we obtain the following expression for the reflected entropy

$$S_R(A:B) = 2\frac{c_{\mathrm{I}} + c_{\mathrm{II}}}{3} \log\left[\frac{2\beta}{\pi\epsilon}\sinh\left(\frac{2\pi u_1}{\beta}\right)\right] + 2\Phi_0. \tag{6.21}$$

Utilizing eq. (4.13) it is straightforward to verify that the above expression for the reflected entropy is exactly twice the large tension limit of the EWCS given in eq. (5.19) which validates the holographic duality between the two.

7 Summary

To summarize, in this article we investigated the mixed state entanglement structure for various bipartite states in such theories through the bulk EWCS. In this connection, we considered adjacent and disjoint subsystems (spanning over both CFT_I and CFT_II) in the vacuum state of the ICFT_2 and constructed appropriate entanglement wedges by identifying all possible RT saddles, depending on the relative sizes and locations of the subsystems with respect to the interface. We were able to demonstrate that the smoothness of RT surfaces across the brane naturally follows from an extremization of their total length. As discussed in [20], certain RT saddles inevitably cross the interface brane more than once. Consequently, we observed novel phases of the EWCS with probe the geometry behind the brane. Subsequently, we also considered the TFD state of the ICFT_2 defined on half of a thermal cylinder with a circular interface, obtained through a series of conformal maps from the vacuum state. The entanglement entropy of semi-infinite subsystems in the dual eternal black string geometry endowed with an interface brane had already been investigated in [20]. We considered the time evolution of the EWCS for two adjacent subsystems before and past the Page time and obtained the analogues of the Page curve.

Interestingly, our bulk computations of the EWCS may be re-interpreted as an investigation of higher-point correlation functions of heavy operators in an ICFT_2, in the geodesic approximation. Due to lack of conformal symmetry, the coordinate dependence of such correlation functions of primary operators are not necessarily fixed by symmetry (unless, of course, the operators are placed symmetrically across the conformal interface and the folding trick may be applied [20, 60]). However, as described in [20] for the case of the two-point function, our results (viewed as saddle-point approximations in the worldline formalism) resemble the geodesic Witten diagrams [61] describing the large central charge structure of higher-point correlation functions.

The effective intermediate picture consists of dynamical gravity on a AdS_2 brane coupled to two flat non-gravitating CFT_2 reservoirs, with transparent boundary conditions for the $\mathrm{CFT}_{\mathrm{I,II}}$ degrees of freedom at the interface [20]. Interestingly, the effective theory may be obtained in the large tension limit $T \to T_{\max}$ of the interface brane upon integrating out the bulk degrees of freedom and consists of two copies of the Polyakov action describing two CFT_2s coupled to the weakly fluctuating AdS_2 metric. In this context, we investigated the island contributions to the reflected entropy for bipartite mixed states in the bath CFT_2s. Similar to [21], when the size of the subsystem in the CFT_2 with a larger central charge exceeds a certain critical value, we observed the dominance of certain novel replica

wormhole saddles to the gravitational path integral which gives rise to induced islands for the entanglement entropy. Correspondingly, the reflected entropy islands were determined through an extremization over the induced island cross-section. Remarkably, in the limit of large brane tension, the island cross-sections were in perfect agreement with the locations where the bulk EWCS crosses the interface brane in the doubly holographic perspective. We have also investigated the reflected entropy for various bipartite states in the effective lower dimensional perspective obtained from a dimensional reduction of the eternal black string geometry. As the black string horizon crosses the interface brane, the gravitational theory on the brane inherits a lower dimensional black hole and consequently the flat CFT_2s act as reservoirs for the Hawking radiation emitted by this black hole. Once again, we observed a rich phase structure of the reflected entropy between subsystems in the radiation baths. Remarkably, our field theoretic computations including the island contributions matched exactly with the corresponding bulk EWCS in the limit of a large brane tension, providing a non-trivial consistency check of the applicability of the island prescription in such scenarios.

Several possible interesting directions may be explored in the near future. It would be exciting to explore the rich phase structure of entanglement negativity in the AdS/ICFT framework utilizing the holographic proposals described in [62–64] and the corresponding island formulation [53, 65–67]. It would also be interesting to compare the behaviour of the reflected entropy to other quantum information theoretic measures with holographic description such as the entanglement of purification [25], the odd entanglement entropy [68], and the balanced partial entanglement [69, 70]. Furthermore it would be fascinating to explore how the rich phase structure of the reflected entropy and other such measures are useful in the information recovery from the Hawking radiation emitted during the black hole evaporation process. We hope to come back to these exciting issues soon.

Acknowledgments

References

[1] G. Penington, *Entanglement Wedge Reconstruction and the Information Paradox*, *JHEP* **09** (2020) 002 [arXiv:1905.08255] [inSPIRE].

[2] A. Almheiri, N. Engelhardt, D. Marolf and H. Maxfield, *The entropy of bulk quantum fields and the entanglement wedge of an evaporating black hole*, *JHEP* **12** (2019) 063 [arXiv:1905.08762] [inSPIRE].

[3] A. Almheiri, R. Mahajan, J.M. Maldacena and Y. Zhao, *The Page curve of Hawking radiation from semiclassical geometry*, *JHEP* **03** (2020) 149 [arXiv:1908.10996] [INSPIRE].

[4] A. Almheiri, R. Mahajan and J.M. Maldacena, *Islands outside the horizon*, arXiv:1910.11077 [INSPIRE].

[5] A. Almheiri, T. Hartman, J.M. Maldacena, E. Shaghoulian and A. Tajdini, *The entropy of Hawking radiation*, *Rev. Mod. Phys.* **93** (2021) 035002 [arXiv:2006.06872] [INSPIRE].

[6] T. Takayanagi, *Holographic Dual of BCFT*, *Phys. Rev. Lett.* **107** (2011) 101602 [arXiv:1105.5165] [INSPIRE].

[7] M. Fujita, T. Takayanagi and E. Tonni, *Aspects of AdS/BCFT*, *JHEP* **11** (2011) 043 [arXiv:1108.5152] [INSPIRE].

[8] H.Z. Chen, R.C. Myers, D. Neuenfeld, I.A. Reyes and J. Sandor, *Quantum Extremal Islands Made Easy. Part I. Entanglement on the Brane*, *JHEP* **10** (2020) 166 [arXiv:2006.04851] [INSPIRE].

[9] H.Z. Chen, R.C. Myers, D. Neuenfeld, I.A. Reyes and J. Sandor, *Quantum Extremal Islands Made Easy. Part II. Black Holes on the Brane*, *JHEP* **12** (2020) 025 [arXiv:2010.00018] [INSPIRE].

[10] F. Deng, J. Chu and Y. Zhou, *Defect extremal surface as the holographic counterpart of Island formula*, *JHEP* **03** (2021) 008 [arXiv:2012.07612] [INSPIRE].

[11] G. Grimaldi, J. Hernandez and R.C. Myers, *Quantum extremal islands made easy. Part IV. Massive black holes on the brane*, *JHEP* **03** (2022) 136 [arXiv:2202.00679] [INSPIRE].

[12] J. Chu, F. Deng and Y. Zhou, *Page curve from defect extremal surface and island in higher dimensions*, *JHEP* **10** (2021) 149 [arXiv:2105.09106] [INSPIRE].

[13] K. Suzuki and T. Takayanagi, *BCFT and Islands in two dimensions*, *JHEP* **06** (2022) 095 [arXiv:2202.08462] [INSPIRE].

[14] A. Karch and L. Randall, *Locally localized gravity*, *JHEP* **05** (2001) 008 [hep-th/0011156] [INSPIRE].

[15] H. Geng and A. Karch, *Massive islands*, *JHEP* **09** (2020) 121 [arXiv:2006.02438] [INSPIRE].

[16] H. Geng et al., *Information Transfer with a Gravitating Bath*, *SciPost Phys.* **10** (2021) 103 [arXiv:2012.04671] [INSPIRE].

[17] H. Geng, S. Lüst, R.K. Mishra and D. Wakeham, *Holographic BCFTs and Communicating Black Holes*, *JHEP* **08** (2021) 003 [arXiv:2104.07039] [INSPIRE].

[18] H. Geng et al., *Entanglement phase structure of a holographic BCFT in a black hole background*, *JHEP* **05** (2022) 153 [arXiv:2112.09132] [INSPIRE].

[19] H. Geng, *Revisiting Recent Progress in the Karch-Randall Braneworld*, arXiv:2306.15671 [INSPIRE].

[20] T. Anous, M. Meineri, P. Pelliconi and J. Sonner, *Sailing past the End of the World and discovering the Island*, *SciPost Phys.* **13** (2022) 075 [arXiv:2202.11718] [INSPIRE].

[21] M. Afrasiar, D. Basu, A. Chandra, V. Raj and G. Sengupta, *Islands and dynamics at the interface*, *JHEP* **11** (2023) 192 [arXiv:2306.12476] [INSPIRE].

[22] P. Hayden, M. Lemm and J. Sorce, *Reflected entropy: Not a correlation measure*, *Phys. Rev. A* **107** (2023) L050401 [arXiv:2302.10208] [INSPIRE].

[23] J.K. Basak, D. Giataganas, S. Mondal and W.-Y. Wen, *Reflected entropy and Markov gap in noninertial frames*, *Phys. Rev. D* **108** (2023) 125009 [arXiv:2306.17490] [INSPIRE].

[24] A.C. Wall, *Maximin Surfaces, and the Strong Subadditivity of the Covariant Holographic Entanglement Entropy*, *Class. Quant. Grav.* **31** (2014) 225007 [arXiv:1211.3494] [INSPIRE].

[25] T. Takayanagi and K. Umemoto, *Entanglement of purification through holographic duality*, *Nat. Phys.* **14** (2018) 573 [arXiv:1708.09393] [INSPIRE].

[26] S. Dutta and T. Faulkner, *A canonical purification for the entanglement wedge cross-section*, *JHEP* **03** (2021) 178 [arXiv:1905.00577] [INSPIRE].

[27] P. Hayden, O. Parrikar and J. Sorce, *The Markov gap for geometric reflected entropy*, *JHEP* **10** (2021) 047 [arXiv:2107.00009] [INSPIRE].

[28] Y. Zou, K. Siva, T. Soejima, R.S.K. Mong and M.P. Zaletel, *Universal tripartite entanglement in one-dimensional many-body systems*, *Phys. Rev. Lett.* **126** (2021) 120501 [arXiv:2011.11864] [INSPIRE].

[29] J. Basak Kumar, D. Basu, V. Malvimat, H. Parihar and G. Sengupta, *Reflected entropy and entanglement negativity for holographic moving mirrors*, *JHEP* **09** (2022) 089 [arXiv:2204.06015] [INSPIRE].

[30] V. Chandrasekaran, M. Miyaji and P. Rath, *Including contributions from entanglement islands to the reflected entropy*, *Phys. Rev. D* **102** (2020) 086009 [arXiv:2006.10754] [INSPIRE].

[31] T. Li, J. Chu and Y. Zhou, *Reflected Entropy for an Evaporating Black Hole*, *JHEP* **11** (2020) 155 [arXiv:2006.10846] [INSPIRE].

[32] T. Li, M.-K. Yuan and Y. Zhou, *Defect extremal surface for reflected entropy*, *JHEP* **01** (2022) 018 [arXiv:2108.08544] [INSPIRE].

[33] Y. Lu and J. Lin, *The Markov gap in the presence of islands*, *JHEP* **03** (2023) 043 [arXiv:2211.06886] [INSPIRE].

[34] Y. Kusuki, *Reflected entropy in boundary and interface conformal field theory*, *Phys. Rev. D* **106** (2022) 066009 [arXiv:2206.04630] [INSPIRE].

[35] Q. Tang, Z. Wei, Y. Tang, X. Wen and W. Zhu, *Universal entanglement signatures of interface conformal field theories*, *Phys. Rev. B* **109** (2024) L041104 [arXiv:2308.03646] [INSPIRE].

[36] J.D. Brown and M. Henneaux, *Central Charges in the Canonical Realization of Asymptotic Symmetries: An Example from Three-Dimensional Gravity*, *Commun. Math. Phys.* **104** (1986) 207 [INSPIRE].

[37] N. Engelhardt and A.C. Wall, *Decoding the Apparent Horizon: Coarse-Grained Holographic Entropy*, *Phys. Rev. Lett.* **121** (2018) 211301 [arXiv:1706.02038] [INSPIRE].

[38] N. Engelhardt and A.C. Wall, *Coarse Graining Holographic Black Holes*, *JHEP* **05** (2019) 160 [arXiv:1806.01281] [INSPIRE].

[39] H.-S. Jeong, K.-Y. Kim and M. Nishida, *Reflected Entropy and Entanglement Wedge Cross Section with the First Order Correction*, *JHEP* **12** (2019) 170 [arXiv:1909.02806] [INSPIRE].

[40] Y. Kusuki and K. Tamaoka, *Entanglement Wedge Cross Section from CFT: Dynamics of Local Operator Quench*, *JHEP* **02** (2020) 017 [arXiv:1909.06790] [INSPIRE].

[41] C. Akers, T. Faulkner, S. Lin and P. Rath, *The Page curve for reflected entropy*, *JHEP* **06** (2022) 089 [arXiv:2201.11730] [INSPIRE].

[42] B. Czech, J.L. Karczmarek, F. Nogueira and M. Van Raamsdonk, *The Gravity Dual of a Density Matrix*, *Class. Quant. Grav.* **29** (2012) 155009 [`arXiv:1204.1330`] [ɪɴSPIRE].

[43] M. Headrick, V.E. Hubeny, A. Lawrence and M. Rangamani, *Causality & holographic entanglement entropy*, *JHEP* **12** (2014) 162 [`arXiv:1408.6300`] [ɪɴSPIRE].

[44] P. Nguyen, T. Devakul, M.G. Halbasch, M.P. Zaletel and B. Swingle, *Entanglement of purification: from spin chains to holography*, *JHEP* **01** (2018) 098 [`arXiv:1709.07424`] [ɪɴSPIRE].

[45] A. Lewkowycz and J.M. Maldacena, *Generalized gravitational entropy*, *JHEP* **08** (2013) 090 [`arXiv:1304.4926`] [ɪɴSPIRE].

[46] X. Dong, *The Gravity Dual of Renyi Entropy*, *Nat. Commun.* **7** (2016) 12472 [`arXiv:1601.06788`] [ɪɴSPIRE].

[47] S. Ryu and T. Takayanagi, *Holographic derivation of entanglement entropy from AdS/CFT*, *Phys. Rev. Lett.* **96** (2006) 181602 [`hep-th/0603001`] [ɪɴSPIRE].

[48] S. Fallows and S.F. Ross, *Islands and mixed states in closed universes*, *JHEP* **07** (2021) 022 [`arXiv:2103.14364`] [ɪɴSPIRE].

[49] A. Almheiri, T. Hartman, J.M. Maldacena, E. Shaghoulian and A. Tajdini, *Replica Wormholes and the Entropy of Hawking Radiation*, *JHEP* **05** (2020) 013 [`arXiv:1911.12333`] [ɪɴSPIRE].

[50] G. Penington, S.H. Shenker, D. Stanford and Z. Yang, *Replica wormholes and the black hole interior*, *JHEP* **03** (2022) 205 [`arXiv:1911.11977`] [ɪɴSPIRE].

[51] X. Dong, X.-L. Qi, Z. Shangnan and Z. Yang, *Effective entropy of quantum fields coupled with gravity*, *JHEP* **10** (2020) 052 [`arXiv:2007.02987`] [ɪɴSPIRE].

[52] P. Calabrese and J.L. Cardy, *Entanglement entropy and quantum field theory*, *J. Stat. Mech.* **0406** (2004) P06002 [`hep-th/0405152`] [ɪɴSPIRE].

[53] Y. Shao, M.-K. Yuan and Y. Zhou, *Entanglement Negativity and Defect Extremal Surface*, `arXiv:2206.05951` [ɪɴSPIRE].

[54] T. Hartman, *Entanglement Entropy at Large Central Charge*, `arXiv:1303.6955` [ɪɴSPIRE].

[55] P. Banerjee, S. Datta and R. Sinha, *Higher-point conformal blocks and entanglement entropy in heavy states*, *JHEP* **05** (2016) 127 [`arXiv:1601.06794`] [ɪɴSPIRE].

[56] D. Basu, H. Chourasiya, V. Raj and G. Sengupta, *Reflected entropy in BCFTs on a black hole background*, `arXiv:2311.17023` [ɪɴSPIRE].

[57] J.M. Maldacena, *Eternal black holes in anti-de Sitter*, *JHEP* **04** (2003) 021 [`hep-th/0106112`] [ɪɴSPIRE].

[58] M. Banados, *Three-dimensional quantum geometry and black holes*, *AIP Conf. Proc.* **484** (1999) 147 [`hep-th/9901148`] [ɪɴSPIRE].

[59] T. Shimaji, T. Takayanagi and Z. Wei, *Holographic Quantum Circuits from Splitting/Joining Local Quenches*, *JHEP* **03** (2019) 165 [`arXiv:1812.01176`] [ɪɴSPIRE].

[60] C. Bachas, J. de Boer, R. Dijkgraaf and H. Ooguri, *Permeable conformal walls and holography*, *JHEP* **06** (2002) 027 [`hep-th/0111210`] [ɪɴSPIRE].

[61] E. Hijano, P. Kraus, E. Perlmutter and R. Snively, *Witten Diagrams Revisited: The AdS Geometry of Conformal Blocks*, *JHEP* **01** (2016) 146 [`arXiv:1508.00501`] [ɪɴSPIRE].

[62] P. Chaturvedi, V. Malvimat and G. Sengupta, *Holographic Quantum Entanglement Negativity*, *JHEP* **05** (2018) 172 [`arXiv:1609.06609`] [ɪɴSPIRE].

[63] V. Malvimat, S. Mondal, B. Paul and G. Sengupta, *Holographic entanglement negativity for disjoint intervals in AdS_3/CFT_2*, *Eur. Phys. J. C* **79** (2019) 191 [`arXiv:1810.08015`] [INSPIRE].

[64] J. Kudler-Flam and S. Ryu, *Entanglement negativity and minimal entanglement wedge cross sections in holographic theories*, *Phys. Rev. D* **99** (2019) 106014 [`arXiv:1808.00446`] [INSPIRE].

[65] J. Kumar Basak, D. Basu, V. Malvimat, H. Parihar and G. Sengupta, *Islands for entanglement negativity*, *SciPost Phys.* **12** (2022) 003 [`arXiv:2012.03983`] [INSPIRE].

[66] J. Kumar Basak, D. Basu, V. Malvimat, H. Parihar and G. Sengupta, *Page curve for entanglement negativity through geometric evaporation*, *SciPost Phys.* **12** (2022) 004 [`arXiv:2106.12593`] [INSPIRE].

[67] D. Basu, H. Parihar, V. Raj and G. Sengupta, *Defect extremal surfaces for entanglement negativity*, *Phys. Rev. D* **108** (2023) 106005 [`arXiv:2205.07905`] [INSPIRE].

[68] K. Tamaoka, *Entanglement Wedge Cross Section from the Dual Density Matrix*, *Phys. Rev. Lett.* **122** (2019) 141601 [`arXiv:1809.09109`] [INSPIRE].

[69] Q. Wen, *Balanced Partial Entanglement and the Entanglement Wedge Cross Section*, *JHEP* **04** (2021) 301 [`arXiv:2103.00415`] [INSPIRE].

[70] D. Basu, J. Lin, Y. Lu and Q. Wen, *Ownerless island and partial entanglement entropy in island phases*, *SciPost Phys.* **15** (2023) 227 [`arXiv:2305.04259`] [INSPIRE].